DEPARTMENT OF TRANSPORTATION

Toward the development of pavement-specific structural synthetic fibers

Manik Barman Principal Investigator
Department of Civil Engineering
University of Minnesota, Duluth

June 2024

Final Report NRRA202403

NRRA National Road Research Alliance

To request this document in an alternative format, such as braille or large print, call 651-366-4718 or 1-800-657-3774 (Greater Minnesota) or email your request to ADArequest.dot@state.mn.us. Please request at least one week in advance.

Technical Report Documentation Page

1. Report No. NRRA202403	2.	3. Recipients Accession No.	
4. Title and Subtitle Toward the development of pavement-specific structural synthetic fibers		5. Report Date June 2024	
		6.	
7. Author(s) Manik Barman, Rohith Sabu, Pranav Sharma, and Austin Janson		8. Performing Organization Report No.	
9. Performing Organization Name and Address Department of Civil Engineering University of Minnesota - Duluth Minnesota 55812		10. Project/Task/Work Unit No. #2021035	
		11. Contract (C) or Grant (G) No. (c) 1036342 (wo) 5	
12. Sponsoring Organization Name and Address Minnesota Department of Transportation Office of Research & Innovation 395 John Ireland Boulevard, MS 330 St. Paul, Minnesota 55155-1899		13. Type of Report and Period Covered Final Report	
		14. Sponsoring Agency Code	
15. Supplementary Notes http://mdl.mndot.gov/			

16. Abstract

Thin fiber reinforced concrete (FRC) pavements and overlays can be economical for low- and moderate-traffic volume roads. Due to insufficient concrete cover thickness, thin concrete pavements or overlays cannot accommodate dowel bars that are typically used in conventional thick concrete pavements. The critical distress for such applications is the transverse joint faulting because of the lack of joint load transfer between the concrete slabs. The currently available synthetic structural fibers can contribute to joint performance to a certain extent. However, as pavements experience significant slab contraction and expansion and carry both wheel and environmental loads, there is a need to design and develop fibers that will provide high joint performance and help mitigate transverse joint faulting when used at an affordable dosage. The overall goal of this study is to develop pavement-specific fibers that will yield the needed joint performance benefits to achieve the intended design life. The study is being conducted in two phases. This report is written for Phase 1 of the study. The study started with a literature review, followed by a finite element analysis, falling weight deflectometer (FWD) data analysis, and laboratory testing of fiber reinforced concrete and individual fibers embedded in concrete. The finite element results and FWD data were amalgamated to quantify the possible joint load transfer of the base layer and foundation, aggregate interlocking, and the needed contribution from the structural fibers. A procedure was established to account for the contribution of the fibers. A new parameter, namely, modulus of fiber support, was introduced to evaluate the stiffness of the fibers that participate in joint load transfer. Notably, a laboratory approach is identified to determine the modulus of fiber support, which can help determine the optimum fiber dosages as well as design and test the pavement-specific fibers in the future phase of the study.

17. Document Analysis/Descriptors Concrete pavements, Concrete overlays, Pavement joints, Performance, Faulting, Fibers, Load transfer, Falling weight deflectometers		18. Availability Statement No restrictions. Document available from: National Technical Information Services, Alexandria, Virginia 22312	
19. Security Class (this report) Unclassified	20. Security Class (this page) Unclassified	21. No. of Pages 120	22. Price

Toward the development of pavement-specific structural synthetic fibers

Final Report

Prepared by:

Dr. Manik Barman
Rohith Sabu
Pranav Sharma
Austin Janson
Department of Civil Engineering
University of Minnesota, Duluth

June 2024

Published by:

Minnesota Department of Transportation
Office of Research & Innovation
395 John Ireland Boulevard, MS 330
St. Paul, Minnesota 55155-1899

Acknowledgments

The authors of this report sincerely acknowledge the financial support provided by the National Road Research Alliance (NRRA) for conducting this important research. The financial support provided by the University of Minnesota Duluth in the form of graduate student teaching assistantships and in-kind matching is highly appreciated. The contributions of industry partners, FORTA Corporation for providing fibers and Vigilant Enterprise LLC for providing consultation, are also gratefully acknowledged.

The authors would like to express their sincere gratitude to the project's technical liaison, Mr. David Lim, P.E., of the California Department of Transportation (Caltrans). The kind contribution of Mr. Tom Burnham, P.E., of the Minnesota Department of Transportation (MnDOT), who provided helpful suggestions throughout the project duration, is also highly appreciated.

The research team is grateful to all members of this project's Technical Advisory Panel (TAP) for their suggestions either during the TAP meeting or in reviewing the task reports. Special thanks go to the Project Coordinators Mr. Leif Halverson and Hafiz Munir and to CTS colleagues, especially Elizabeth Andrews, for their time and administrative support.

The research team sincerely acknowledges the contribution of several graduate and undergraduate students, faculty members, laboratory staff, and the Sponsored Projects Administration (SPA) staff at the University of Minnesota Duluth (UMD), who helped the research team at different phases of this project.

TAP members

1. Tim Andersen, MnDOT
2. Tom Burnham, MnDOT
3. Rob Golish, MnDOT
4. David Lim, Caltrans (TL)
5. Maria Masten, MnDOT
6. Angel Mateos, UC-Berkley
7. Somayeh Nassiri, UC Davis
8. Mike Radler, Dow Chemical Company
9. Peter Taylor, Iowa State CP Tech Center

Industry Support

1. Clifford N. MacDonald, Vigilant Enterprise LLC.
2. Gerald J. Welch, FORTA Corporation

Table of Contents

Chapter 1: INTRODUCTION 1

1.1 Organization of the report 2

Chapter 2: LITERATURE REVIEW 3

2.1 Major distresses in thin concrete pavements 3

2.2 Pavement concrete mix design 5

2.3 Types of fibers 6

2.4 Behavior of fiber reinforced concrete 8

2.4.1 Flexural behavior 9

2.4.2 Joint performance 12

2.5 Benefits of fibers in concrete pavements 14

2.6 Behavior of individual fibers 15

2.7 Finite element modeling (FEM) of pavements 19

Chapter 3: JOINT PERFORMANCE MODELLING 27

3.1 Pavement structure and materials 27

3.2 Loads 30

3.3 Transverse and longitudinal joints 30

3.4 Slab and base layer interface 31

3.5 Joint performance evaluation parameters 32

3.6 Effect of various parameters on the joint performance 32

3.6.1 Effect of joint stiffness on joint performance 32

3.6.2 Effect of pavement structure on joint performance 33

3.6.3 Effect of daily temperature cycle on joint performance 35

3.6.4 Effect of season on joint performance 36

Chapter 4: DESIRED JOINT PERFORMANCE 39

4.1 Critical distress, terminal IRI, and transverse joint faulting 39
4.2 Desired joint load transfer from the structural fibers 41
4.3 Joint load transfer from aggregate interlock and base layer 43
Chapter 5: ACCOUNTING FOR THE CONTRIBUTION OF FIBERS 46
5.1 Modulus of fiber support K_f through FEM 46
5.2 Modulus of fiber support K_f from FWD data 47
5.3 Laboratory test method to determine K_f 51
Chapter 6: SINGLE FIBER PULLOUT TEST 58
6.1 Single fiber pullout test method 58
6.2 Single fiber pullout test, Phase 1 61
6.2.1 Influence of curing age 61
6.2.2 Influence of fiber type, aggregate type, and cement content 62
6.2.3 Failure modes of fibers 67
6.3 Single fiber pullout test, Phase 2 76
Chapter 7: Conclusions 86
References 88
Appendix A

List of Figures

Figure 2.1 Transverse crack (left) and Longitudinal crack (right) (Harrington et al., 2018). 3
Figure 2.2 Diagonal cracking (Harrington et al., 2018). 4
Figure 2.3 Joint Faulting in thin pavement (left) and slab shattering in ultra-thin fiber reinforced pavement(right) (Barman et al., 2021). 4
Figure 2.4 Tarantula Curve (Taylor et al., 2014) 6

Figure 2.5 Photographs of steel fiber types (Dinh, 2010) 7

Figure 2.6 Photographs macro-fibers (left) and micro-fibers (right) 7

Figure 2.7 Fibers bridging a crack and providing post-crack performance (Gaddam, 2016)..... 8

Figure 2.8 An example of load versus deflection curves (4-point bending test) of plain concrete and FRC. 9

Figure 2.9 Residual load characteristics of different shaped structural synthetic fibers (after Bordelon, 2005) 11

Figure 2.10 Residual load capacities of FRC versus fiber volume fraction for straight synthetic fibers (after Bordelon, 2005) 11

Figure 2.11 A typical example of load and displacement profiles achieved from a joint performance test. 13

Figure 2.12 Correlation between the beam LTE and slab LTE (Barman, 2014). 13

Figure 2.13 Influence of fiber on cracking in FRC Pavement (Chanvillard et al., 1989). 14

Figure 2.14 Influence of fiber on transverse joint faulting of FRC pavement (Barman, 2021). 15

Figure 2.15 Typical load-displacement curve for steel fiber (Abbas and Khan, 2016) 16

Figure 2.16 Steel fiber pullout test setup (Abbas and Khan, 2016) 16

Figure 2.17 Schematic diagram and actual specimen (Abbas and Khan, 2016) 17

Figure 2.18 Varying indentations of polypropylene fibers (Singh et al., 2004) 18

Figure 2.19 Pullout load of the fibers (Singh et al., 2004) 18

Figure 2.20. Pullout load vs. curing age (Singh et al., 2004) 18

Figure 2.21 Finite element solution validation by Westergaard's equation (Tabatabaie et al., 1978). 20

Figure 2.22 FEM solution validation with FWD data (Uddin et al., 1995). 20

Figure 2.23 Finite element interlocking between joints (Maitra et al., 2010). 21

Figure 2.24 LTE vs modulus of interlocking joint (Maitra et al., 2010). 21

Figure 2.25 FEM model of JPCP (Sadeghi et al., 2018)..... 22

Figure 2.26 LTE vs different pavement parameters (Sadeghi et al., 2018). 23

Figure 2.27 Influence of different pavement parameter on the temperature related stress (Masad et al., 1996). 25

Figure 2.28 FEM Model of FRC overlay over HMA layer (Barman et al., 2014). 26

Figure 3.1 Key forces on the transverse joints of a thin FRC pavement (a) downward curling, (b) upward curling. 27

Figure 3.2 Six-slab FEM model of the thin concrete pavement (slab size: 6 ft x 6 ft; D1 and D2: locations of deflection calculated). 28

Figure 3.3 Modelling of the joints of thin FRC pavements 31

Figure 3.4 Effect of joint stiffness on joint performance parameters (LTE, DD and D_{max}). 33

Figure 3.5 Effect of the thicknesses of the slab and base layer on the joint performance parameters..... 34

Figure 3.6 LTE vs. K_z for different pavement structures (for a given K_z value, the first three structures have 8-inch base layer and variable slab thickness; the next four structures have a 4-inch slab and variable base layer thicknesses). 35

Figure 3.7 Effect of temperature gradient on LTE (early spring). 36

Figure 3.8 Effect of seasonal conditions on joint performance parameters (4" slab, 6" Base). 37

Figure 3.9 Effect of seasonal conditions on joint performance parameters (4" slab, 11" Base). 38

Figure 3.10 Effect of seasonal conditions on joint performance parameters (6" slab, 6" Base) 38

Figure 4.1: IRI of the MnROAD Cells 506 (plain concrete) and 806 (FRC with 11.7 lb/yd^3 fiber dosage). .. 40

Figure 4.2: Faulting of the MnROAD Cells 506 (plain concrete) and 806 (FRC with 11.7 lb/yd^3 fiber dosage)..... 40

Figure 4.3: Relationship between faulting and IRI for thin concrete pavements. 41

Figure 4.4: Joint load transfer of Cells 506 and 806. 42

Figure 4.5: Maximum slab deflection under FWD load for Cells 506 and 806. 42

Figure 4.6: LTE vs. joint stiffness for various designs in the early spring season. 43

Figure 4.7: LTE vs. joint stiffness for various designs in the winter season. 44

Figure 4.8: LTE contribution of base, aggregate interlocking and fibers. 44

Figure 4.9: LTE vs vertical joint stiffness from aggregate interlock and fibers (Kz) 45

Figure 5.1: LTE vs joint stiffness from FEM analysis. 47

Figure 5.2: Joint stiffness, Kz of Cells 506 and 806 vs. ESALs 49

Figure 5.3: Modulus of fiber support, K_f vs. ESALs. 49

Figure 5.4: LTE vs joint stiffness from FWD data analysis. 50

Figure 5.5 UMD's joint load transfer test setup (originally developed at the University of Pittsburgh). 51

Figure 5.6: LTE vs. crack width for concrete with different fiber volume fractions (lab test result). 53

Figure 5.7: Comparison of the joint stiffness vs. crack width relationships between plain concrete (same as Cell 506) and FRC with 0.75% V_f fibers (same as Cell 806). 54

Figure 5.8: K_f vs. crack width relations for FRC with 0.75% V_f fibers (same as Cell 806). 54

Figure 5.9: Crack width movement of Cell 806 (Barman et al., 2021). 55

Figure 5.10: LTE vs K_f for various crack widths (laboratory data). 56

Figure 5.11: Comparison of LTE vs K_f correlations between the FEM, FWD, and laboratory test results. 57

Figure 6.1: Plastic mold arranged for the single fiber pullout test sample preparation. 58

Figure 6.2: Casting platform with cylinders installed. 59

Figure 6.3: Embedded fibers in fresh concrete cylinders. 60

Figure 6.4: Single fiber pullout test in progress. 60

Figure 6.5: Effects of curing age on toughness. 62

Figure 6.6: Effects of curing age on peak load 62

Figure 6.7: Average peak load by fiber type. 63

Figure 6.8: Peak load vs. fiber type (all mixes) *(Note: A, B, and C are the aggregate class; 480, 550, and 620 are cement contents in lb/yd^3).* 64

Figure 6.9: Average peak load vs. aggregate class. 64

Figure 6.10: Average peak load vs. cement content (pcy = lb/yd^3). 65

Figure 6.11: Load-displacement curves for concrete batch (Class A aggregate, cement content 480 lb/yd^3, fibers 1, 2, 4). 66

Figure 6.12: Average toughness by fiber type. 66

Figure 6.13: Fiber 1 (failed fibers vs new fiber). 68

Figure 6.14: Load vs. Displacement Curves (Fiber 1) *(Note: A, B, and C are the aggregate class; 480, 550, and 620 are cement contents in lb/yd^3, and numbers in the parenthesis are sample numbers)*. 68

Figure 6.15: Fiber 2 (failed fibers vs new fiber) 69

Figure 6.16: Fiber 2 (failure at grip interface) 70

Figure 6.17: Fiber 2 (failure at concrete interface) 70

Figure 6.18: Load vs. displacement curves (Fiber 2) 71

Figure 6.19: Fiber 3 (failed fibers vs new fiber) 72

Figure 6.20: Load vs. displacement curves (Fiber 3) *(Note: A, B, and C are the aggregate class; 480, 550, and 620 are cement contents in lb/yd^3, and numbers in the parenthesis are sample numbers)*. 72

Figure 6.21: Fiber 4 (failed fibers vs new fiber). 74

Figure 6.22: Fiber 4 (failed fibers compared to original fiber). 74

Figure 6.23: Fiber 4 (failure at the concrete interface). 75

Figure 6.24: Load vs. displacement curves (Fiber 4) *(Note: A, B, and C are the aggregate class; 480, 550, and 620 are cement contents in lb/yd^3, and numbers in the parenthesis are sample numbers)*. 76

Figure 6.25: Loading behavior of Fiber 1 (Sample 1). 77

Figure 6.26: Loading behavior of Fiber 1 (Sample 2). 77

Figure 6.27: Loading behavior of Fiber 1 (Sample 3). 78

Figure 6.28: Loading behavior of Fiber 1 (Sample 4). 78

Figure 6.29: Loading behavior of Fiber 2 (Sample 1). 79

Figure 6.30: Loading behavior of Fiber 2 (Sample 2). 79

Figure 6.31: Loading behavior of Fiber 2 (Sample 3). 80

Figure 6.32: Loading behavior of Fiber 2 (Sample 4). 80

Figure 6.33: Loading behavior of Fiber 3 (Sample 1). 81

Figure 6.34: Loading behavior of Fiber 3 (Sample 2). 81

Figure 6.35: Loading behavior of Fiber 3 (Sample 3). 82

Figure 6.36: Loading behaviour of Fiber 3 (Sample 4). 82

Figure 6.37: Loading behaviour of Fiber 4 (Sample 1). 83

Figure 6.38: Loading behaviour of Fiber 4 (Sample 2). 84

Figure 6.39: Loading behaviour of Fiber 4 (Sample 3). 84

Figure 6.40: Loading behaviour of Fiber 4 (Sample 4). 85

List of Tables

Table 2-1 PCC Joint Spacing/Dowel Bars (MnDOT, 2019). 5

Table 2-2 Properties of structural synthetic fibers and FRC in Roesler et al. (2008) study. 10

Table 2-3 Volume fraction and dosages of two selected fibers in Barman (2014) study 12

Table 3-1 Summary of pavement design, material, and other variables 29

Table 3-2 Selected material properties for three seasons. 37

Table 5-1 Joint performance test details 52

Table 5-2 Base mixture design for joint performance beam samples 52

Table 6-1: Failure type of each fiber 67

Executive Summary

Thin fiber reinforced concrete (FRC) pavements and overlays can be economical for low- and moderate-traffic volume roads because of the low maintenance cost. New pavements are constructed over the granular aggregate base layer. Overlays are constructed on old, distressed concrete or asphalt pavements. The thickness of the slabs for such applications varies between 4 and 6 inches and is usually constructed with short-size slabs, e.g., 6ft x 6ft. Due to insufficient concrete cover thickness, thin concrete pavements or overlays cannot accommodate dowel bars that are typically used in conventional thick concrete pavements.

One of the critical distresses of thin concrete pavements and overlays is the transverse joint faulting that can shorten their service lives. The poor joint performance or load transfer between the thin slabs is one of the primary reasons for transverse joint faulting. The aggregate interlock, which is a key load transfer mechanism for un-dowelled concrete pavements, is less in thin concrete pavements and overlays because of the smaller area of aggregate interlocking underneath the sawed joints. Several field and laboratory research studies have shown that structural fibers, when added sufficiently, can improve the load transfer between concrete slabs and mitigate joint faulting. However, there is a strong need for improvement of the joint performance of the thin concrete pavements and overlays to yield a good service life. As the thickness of the slabs below the saw cut is only about 2.5 to 4 inches for the thin concrete pavements and overlays, joint load transfer from the aggregate interlock may not be significantly improved. On the other hand, fibers at the concrete pavement joints are affected by seasonal slab contraction and expansion, dynamic wheel loads, and environmental loads, such as curling and warping.

The overall goal of this study is to design and develop pavement-specific fibers that will provide the needed joint performance to mitigate transverse joint faulting and achieve the intended design life. The study is being conducted in two phases. This report is written for Phase 1. The objectives of this phase are to (i) investigate the factors that influence joint performance of the fiber reinforced concrete pavements, and (ii) identify the properties of the fibers or concrete that may easily be changed to improve the joint performance to mitigate the faulting of the transverse joints.

First, relevant literature in the area of fiber reinforced concrete and concrete pavements and overlays were reviewed. Then, a finite element analysis was conducted to understand the effect of joint stiffness, pavement structure, and vehicular and environmental loads on the joint performance parameters, such as load transfer efficiency (LTE), differential displacement (DD) between the adjoining slabs at the transverse joints, and maximum slab displacement ($D_{max)}$ under the load. Transverse and longitudinal joints were modeled considering the contribution from both aggregate interlock and structural fibers. Pavement variables, such as slab and base layer thicknesses, joint stiffnesses in vertical and transverse directions, temperature gradient, and season, etc. were considered.

The falling weight deflectometer (FWD) and international roughness index (IRI) data of the thin FRC projects constructed at Minnesota Road Research facility (MnROAD) were analyzed. The finite element

method (FEM) results and FWD data were used to quantify the possible load transfer contributions of the base layer, aggregate interlocking, and the needed contribution from the structural fibers. The key findings from the Phase 1 study are listed below.

- The LTE, DD, D_{max} of thin FRC pavements largely depend on the vertical stiffness of the joints, which is achieved by the base layer, aggregate interlocking and fibers lateral stiffness.

- The aggregate interlock in the thin FRC pavement is not significant because of the limitation in the thickness of the slabs. A vertical joint stiffness of about 250 lb/inch^3 can be achieved from aggregate interlocking, which can provide about 15 to 20% LTE. The base layer can provide 30 to 40% LTE and the remaining 30 to 40% LTE shall be achieved from structural fibers. As the thickness of the slabs in the thin concrete pavements is limited, achieving load transfer from fibers is the feasible approach to improve the overall performance of the pavement.

- This study introduced a procedure to characterize the fibers' contribution toward the joint load transfer. A new parameter, namely, the modulus of fiber support (K_f), was introduced. The minimum value of K_f is suggested as 3,000 lb/inch^3 for a 30 to 40% LTE required from the fibers. The laboratory joint performance testing is recommended to be conducted at 0.06 inches crack width while determining the K_f.

- Fiber pullout tests were conducted on four different types of fibers. Based on the test results, it was found that fibers with indentation on the fiber geometry help increase the peak load and toughness. The less indented fibers and smooth and brittle fibers performed on average less than the fibers with higher lateral stiffness and more indentation on the geometry. The findings from the single fiber pullout test will help develop the pavement-specific fiber.

- It may be noted that the joint load transfer test used in the laboratory takes a considerable amount of time. This test is helpful in determining the joint load transfer, but the testing is quite complicated and may not be a good candidate for a simple screening test. Also, because of the limited size of the project, a large data setup could not be developed to perform any reliability analysis. The field study included only one type of fiber; therefore, the conclusions drawn in this study should be verified for other types of fibers as well.

Chapter 1: INTRODUCTION

Thin fiber reinforced concrete (FRC) pavements and overlays can be economical for low- and moderate-traffic volume roads because of low maintenance cost. New pavements can be constructed over the granular aggregate base layer and the overlays can be constructed on the old pavements depending on the level of distress and structural strength of the old pavement layer. The thickness of the slabs for such applications varies between 4 and 6 inches and is usually constructed with short-size slabs, e.g., 6ft x 6ft. Due to insufficient concrete cover thickness, thin concrete pavements or overlays cannot accommodate dowel bars that are typically used in conventional concrete pavements.

The distress pattern of the thin concrete pavement and overlay projects constructed at Minnesota Road Research facility (MnROAD) and other locations in the last few decades revealed that transverse joint faulting is one of the critical distresses that can shorten their service lives (Burnham et al., 2016; Barman et al., 2021). The poor joint performance or slab-to-slab load transfer of the thin concrete slabs is one of the primary reasons for transverse joint faulting. The other reason for faulting is the erosion and/or settlement of the underlying layer. The aggregate interlock, which is a key load transfer mechanism for un-dowelled concrete pavements, is less in thin concrete pavements or overlays because of the smaller area of aggregate interlocking underneath the sawed joints. Previous research studies have shown that structural fibers, when added sufficiently, are capable of improving the load transfer between concrete slabs and decreasing transverse joint faulting (Burnham et al., 2016; Barman et al., 2021).

The application of fibers in concrete pavements is not new; several research works have been conducted on the behavior of fibers and fiber reinforced concretes. Research studies are available on the plastic and hardened properties of fiber reinforced concrete, including the post-crack properties of structural fibers (Zollo, 1984; Ludirdja et al., 1992; Barman et al., 2018; Barman et al., 2021). Field studies, including the distress comparison of the companion plain and FRC thin pavements and overlays, have been conducted to understand the contribution of structural fibers (Barman et al., 2021). Currently available synthetic fibers used in concrete pavements are mainly polypropylene-based. From the recently completed National Road Research Alliance (NRRA) funded study on fiber reinforced thin concrete pavements and overlays (Barman et al., 2021), it has been found that currently available synthetic structural fibers can contribute to joint performance to a certain extent. However, as pavements experience significant slab contraction and expansion in winter and summer, respectively, and carry both wheel and environmental loads, there is a need to design and develop fibers that will address the joint performance issue and help mitigate transverse joint faulting.

The overall goal of this study is to develop pavement-specific fibers that will yield the needed joint performance benefits to achieve the intended design life. The study is being conducted in two phases. This report is written for Phase 1 of the study. The primary objectives of this phase are to (i) investigate the factors that influence the joint performance of the fiber reinforced concrete pavements, and (ii) identify the properties of the fibers or concrete that may easily be changed to improve the joint performance to mitigate the faulting of the transverse joints.

In Phase 1, first, a literature review was conducted to understand the critical distress in thin concrete pavements and overlays. Then, a finite element analysis was conducted for thin FRC pavement. A six-slab thin concrete pavement model was developed to analyze the effect of joint stiffness, and vehicular and environmental loads on the joint performance parameters, such as load transfer efficiency (LTE), differential displacement (DD) between the adjoining slabs at the transverse joints, and maximum slab displacement (D_{max}) under the load. Transverse and longitudinal joints were modeled considering the contribution from both aggregate interlock and structural fibers. Pavement variables, such as slab and base layer thicknesses, joint stiffnesses in vertical and transverse directions, temperature gradient, season, etc. were considered.

The falling weight deflectometer (FWD) and international roughness index (IRI) data of the thin FRC projects constructed at MnROAD were analyzed. The FEM results and FWD data were amalgamated to quantify the possible joint load transfer of the base layer and foundation, aggregate interlocking, and the needed contribution from the structural fibers. A procedure was established to account for the contribution of the fibers. A new parameter, namely, modulus of fiber support, was introduced to evaluate the stiffness of the fibers that participate in joint load transfer. Notably, a laboratory approach is identified to determine the modulus of fiber support, which can help determine the optimum fiber dosages as well as design and develop and test the pavement-specific fibers in the future.

The study also investigated the load-displacement behavior of the various fibers. A single fiber pullout test was conducted for this purpose. This testing was able to identify the favorable geometry of the fibers as well as the elastic limit of the fibers beyond which the effectiveness of the fibers decrease.

1.1 Organization of the report

This report has seven chapters. The first chapter presents the introduction to the study. The second chapter summarizes the literature relevant to the area of study. Chapter 3 presents the finite element modeling of thin concrete pavement. The desired joint performance for thin concrete pavements is discussed in Chapter 4. The method to account for the contribution of fibers toward increasing the joint performance is established in Chapter 5. The results of the single fiber pullout test are presented in Chapter 6, and the conclusions of the study are presented in Chapter 7.

Chapter 2: LITERATURE REVIEW

The study begins with a literature review. This chapter summarizes the findings of the literature review. Literature on distresses of thin concrete overlays and pavements, concrete pavement mixture design, fibers and fiber reinforced concrete, finite element modeling of concrete pavement, etc. are discussed.

2.1 Major distresses in thin concrete pavements

Distresses that commonly occur in thin concrete pavements or overlays include fatigue cracking, transverse cracking, longitudinal cracking, corner cracking, and transverse joint faulting. The two main dominant distresses of thin concrete pavements and overlays are fatigue cracks and transverse joint faulting. Fatigue cracks generally occur in three directions – transverse direction (transverse to traffic flow), longitudinal direction (parallel to traffic flow), and diagonally at the corner of the slab (Vandenbossche, 2003), as shown in Figure 2.1 and Figure 2.2. Fatigue cracking is caused by repeated traffic loading, shrinkage (due to season change), and curling (due to daily temperature change) of the concrete slab, or a combination of the three. Due to daily temperature changes, positive and negative temperature gradients form in the concrete slab, and these temperature gradients accelerate fatigue damage.

Figure 2.1 Transverse crack (left) and Longitudinal crack (right) (Harrington et al., 2018).

Figure 2.2 Diagonal cracking (Harrington et al., 2018).

Faulting is defined as the elevation difference between an approach slab and a leave slab across a transverse joint or crack (Khazanovich et al., 2004); Figure 2.3 illustrates joint faulting. The most common reason for faulting is the pumping of fines from the base layer due to the water accumulation under the slab. Permanent settlement of the base layer or underlying old layer is also a reason for the joint faulting. Poor drainage and low joint load transfer within the concrete layer increase the chance of faulting (Huang, 2004; Barman, 2014). Joint spacing is one of the critical components that can significantly influence distresses (Harrington et al., 2018). The MnDOT pavement design manual (MnDOT, 2019) recommends the locations for transverse and longitudinal joints and the diameter of dowel and tie bars based on the slab thickness, as shown in Table 2-1.

Figure 2.3 Joint Faulting in thin pavement (left) and slab shattering in ultra-thin fiber reinforced pavement(right) (Barman et al., 2021).

Table 2-1 PCC Joint Spacing/Dowel Bars (MnDOT, 2019).

PCC Thickness (inches)	Longitudinal Joint Spacing (Panel width)	Transverse Joint Spacing (Panel Length)	Dowel Bar Diameter	All Longitudinal Joints
>=10.5	12'-14'	15'	1.5"	No.5 tie bars(36" long)
8-10	12'-14'	15'	1.25"	No.4 tie bars(30" long)
7&7.5	12'-14'	15'	1"	No.4 tie bars(30" long)
6&6.5	6'-8'	6'	None	No.4 tie bars(30" long)
4-5.5	6'-8'	6'	None	None

(Note: Figure 510.4 is related to the PCC overlay wider than the existing pavement and the outside edge of the existing pavement is not under the new driving lane).

For conventional concrete pavements, the joint load transfer for concrete pavements is achieved by aggregate interlocking and by installing dowel bars. Because of the limited cover, dowel bars are however not recommended for slabs thinner than 7 inches (MnDOT, 2019). Structural fibers have been found to help achieve joint load transfer in thin concrete overlays and pavements. Apart from the two major distresses discussed, reflective cracking and slab shattering have also been observed. Reflective cracks occur directly on top of the cracks or joints in the underlying layer (Sachs et al., 2016; Barman and Vandenbossche, 2010). Slab shattering was found to occur in ultrathin concrete pavement, shown in Figure 2.3, (Barman et al., 2021).

2.2 Pavement concrete mix design

The primary methods of concrete mixture design are based on the prescriptive-based specifications that come from the slump cone test and pressure meter test, which were developed in 1922 and 1949, respectively (Taylor et al., 2014). Most of the concrete pavements in the country were designed based on this prescriptive-based specifications. The pavement industry is recently moving forward to adopt Performance Engineered Mixture (PEM) design method to produce durable concrete pavements. It is expected that the thin fiber reinforced concrete pavements and overlays will also be constructed with PEM-based mixture design method. The PEM method relies on performance-based specifications that focus on tests that simulate real-world concerns with concrete. One important piece of the PEM design method is the use of the Tarantula curve (Figure 2.4) to achieve the optimized aggregate gradation. The Tarantula curve ensures optimal strength, workability, and homogeneity of an aggregate blend used in a concrete mix. In the PEM method, several pavement-specific tests are conducted, such as the Super Air

Meter (SAM), box, and V-Kelly tests. Barman et al. (2022) conducted a study that determined the allowable values of the test parameters for fiber reinforced concrete designed in the PEM platform.

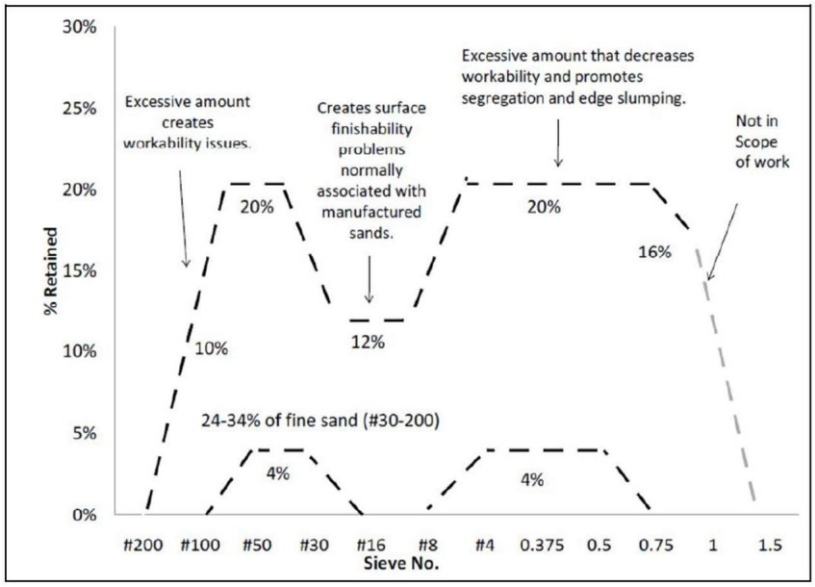

Figure 2.4 Tarantula Curve (Taylor et al., 2014)

The inclusion of fibers in a concrete mix can improve the ductility of a concrete slab. However, a big concern with FRC is it reduces the workability of the concrete mix. One way to improve the workability is to replace a portion of the cement with fly ash in a concrete mix. When class F fly ash (ASTM C618) is used to replace a portion of cement, the resulting concrete often has improved ultimate compressive strength, workability, and pore structure, increased resistance to alkali-silica reaction (ASR) and sulfate attack, while also reducing costs and carbon dioxide emissions (Sobolev et al., 2017). The ASR resistance is especially important for pavements in cold climates, where larger amounts of salt and other deicers are used. MnDOT currently allows a fly ash replacement of up to 30% (MnDOT, 2020).

2.3 Types of fibers

According to ASTM C1116, fibers used in FRC can be classified as one of four types. They are Type I (steel), Type II (glass), Type III (synthetic), and Type IV (natural). ASTM A820 classifies 5 distinct types of steel fibers which include Type I (cold-drawn wire), Type II (cut sheet), Type III (melt-extracted), Type IV (mill cut), and Type V (modified cold-drawn wire). Steel fibers are often crimped, or have hooked or flattened ends, which increases the load required to pull them out of concrete. An example of available steel fiber types can be found in Figure 2.5. While steel fibers have a high tensile strength, just 6% of FRC pavements were constructed using steel fibers due to corrosion and durability concerns, along with mixing and workability difficulty (Barman and Hansen, 2018). Natural fiber types tend to decay quickly because they absorb water. Glass fibers are another option for use in FRC. These fibers are rarely used

in concrete pavements because of their long-term durability concerns. They become brittle when exposed to the highly alkalic environment of cement paste during the curing phase. Glass fibers also tend to fail at a lower amount of strain than other fiber types (ACI, 2009).

Synthetic fibers are by far the most used fibers in FRC pavement. Almost 94% of the FRC overlays in the country were constructed using synthetic fibers (Barman and Hansen, 2018). Polypropylene synthetic fibers are popular because they are chemically inert, non-absorbent, and lightweight, as well as being cheaper than most other fiber types. Polypropylene synthetic fibers can be of different geometries and diameters. According to Barborak (2011), fibers can be broken down into two categories, micro and macro. Micro-fibers are thin and small. They are considered non-structural fibers because they are not designed to carry loads or replace traditional reinforcements, such as wire mesh or rebar using concrete. They are used to minimize early-age cracking but provide little post-crack strength. Macro fibers are considered structural fibers because they are intended to replace partially or fully traditional reinforcement and carry loads in post-crack concrete. They are larger in diameter and are typically longer than 1.25 inches. Polypropylene macro and micro synthetic fibers are shown side by side in Figure 2.6.

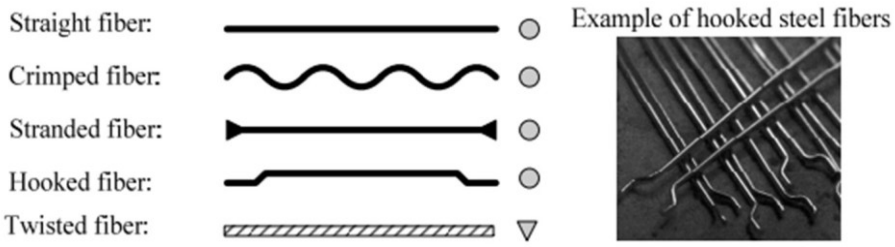

Figure 2.5 Photographs of steel fiber types (Dinh, 2010)

Figure 2.6 Photographs macro-fibers (left) and micro-fibers (right)

2.4 Behavior of fiber reinforced concrete

As depicted in Figure 2.7, structural fibers improve the post-crack performance of concrete by bridging cracks and increasing the toughness, residual strength (RS) and residual strength ratio (RSR) (Roesler et al., 2008; ACI 544.1R, 2009), load transfer efficiency (LTE) (Barman, 2014), and fatigue resistance (Rollings, 1986) of concrete. Based on full-scale slab studies, Beckett (1990) and Falkner et al. (1995) showed that structural fibers (steel or polymeric) increased the flexural and ultimate load carrying capacity of concrete slabs; the magnitude of the increase was related to the fiber volume and aspect ratio. Roesler (2003) stated that discrete synthetic fibers improved the load-deformation characteristics of concrete slabs. Figure 2.8 shows an example of load versus deflection curves (4-point bending test) of plain concrete and FRC specimens. This figure demonstrates the post-peak-load contribution of fibers. FRC can hold some amount of load even after the crack development, which is referred to as the residual load. The residual load can be a function of the fiber properties such as length, geometry, material composition, aspect ratio, and dosage.

Figure 2.7 Fibers bridging a crack and providing post-crack performance (Gaddam, 2016).

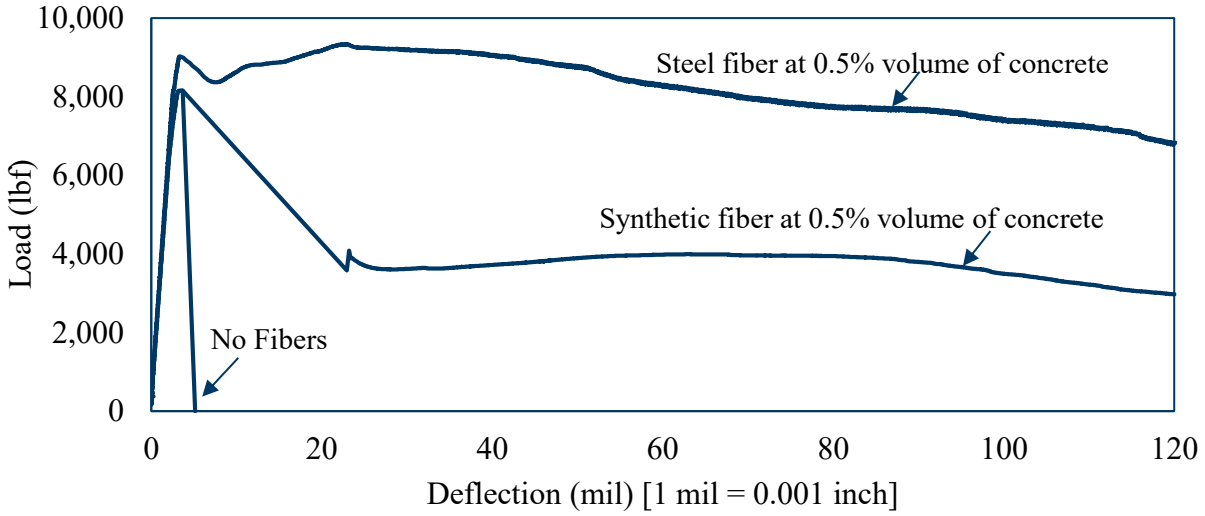

Figure 2.8 An example of load versus deflection curves (4-point bending test) of plain concrete and FRC.

2.4.1 Flexural behavior

Several synthetic FRC related research studies (Isaa, 2017; Bordelon, 2011; Roesler et al., 2008; Bordelon, 2005) were conducted in Illinois. Several factors that affect the performance of FRCs were considered, including shape (e.g., straight, crimped and twisted), type, dosage, length, diameter, and aspect ratio (length of fiber/effective diameter of fiber) of the fibers. Table 2-2 presents the properties of fibers and a few hardened concrete test results for the FRCs prepared with three different synthetic fibers in the Roesler et al. (2008) study. The peak flexural load and modulus of rupture (MOR) slightly varied with the dosage rate, shape, and aspect ratio of the fiber, but a certain trend was not observed. The R^2 for the correlation between the volume fraction of fiber (V_f) (volume of fiber/ total volume of concrete x 100%) and MOR was 0.14 for the data included in Figure 2.9, which indicated that the MOR is not significantly influenced by the properties of structural synthetic fibers.

The load-deflection vs V_f relationships for straight fibers in Bordelon (2005) study is shown in Figure 2.10. The RSR, which is also termed as 'equivalent flexural strength ratio' in ASTM C1609, is determined by a four-point bending test using beam specimens. RSR is expressed using the following equation:

$$\mathbf{RSR} = \mathbf{100}*\frac{\mathrm{fe,3}}{\mathrm{MOR}} \qquad (1)$$

Where, $f_{e,3}$ is the residual strength at mid-span for a deflection up to (span)/150 of a 24-inch (or 22-inch) x 6-inch x 6-inch beam. The span is equal to 18 inches; therefore, the residual strength is measured at a 0.12-inch deflection. It can be seen that the residual load capacity increases with the increase in fiber V_f. Figure 2.10 shows that FRC with 0.58% fiber volume fraction resulted in a greater residual load capacity (and RSR) as compared to the FRCs with 0.26% volume fraction.

Table 2-2 Properties of structural synthetic fibers and FRC in Roesler et al. (2008) study.

Fiber type	**Straight synthetic**				**Twisted synthetic**		**Crimped synthetic**
Cross section	Rectangular				Rectangular		Rectangular
Length (in)	1.57				2.13		2.00
Thickness (in)	0.004				NA		0.03
Width (in)	0.05				NA		0.05
Aspect ratio	90				NA		46
Specific gravity	0.92				0.91		0.91
Volume fraction in the mix (%)	0.19	0.26	0.29	0.58	0.30	0.50	0.40
Dosages used (lb/yd3)	3.00	4.00	4.50	8.90	4.60	7.70	6.10
Peak flexural load (lb)	6623	5472	9276	8939	8101	6487	8160
Modulus of rupture (psi)	556	456	733	745	675	541	673
Testing age (days)	14	14	14	14	14	14	14

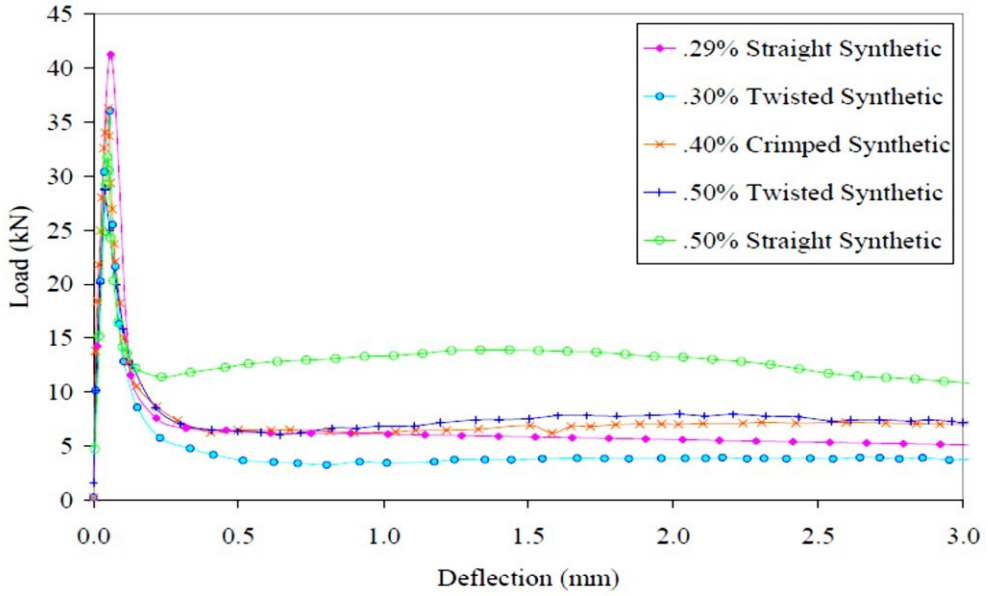

Figure 2.9 Residual load characteristics of different shaped structural synthetic fibers (after Bordelon, 2005)

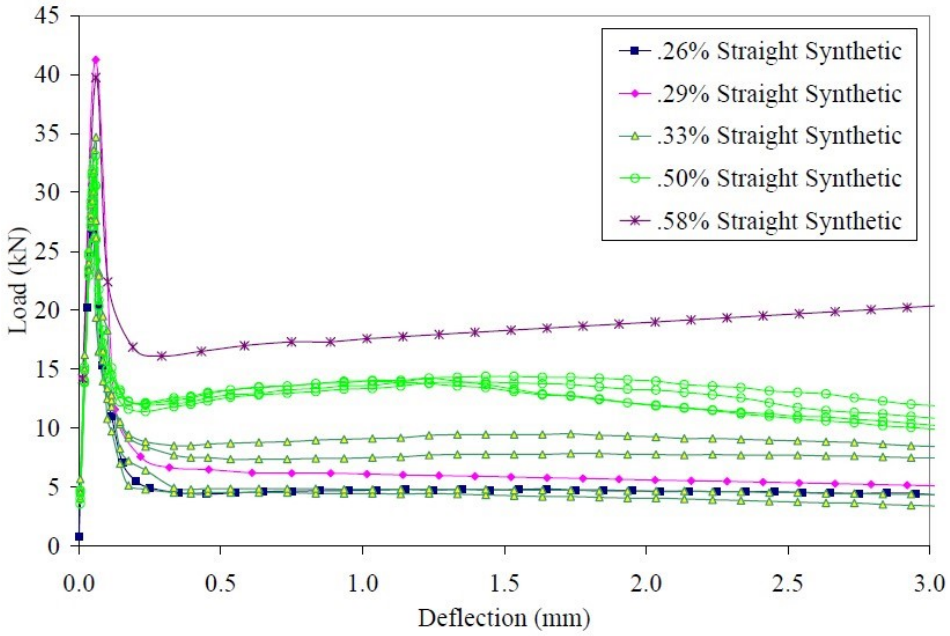

Figure 2.10 Residual load capacities of FRC versus fiber volume fraction for straight synthetic fibers (after Bordelon, 2005)

2.4.2 Joint performance

To understand the contribution of structural fibers in increasing LTE, a comprehensive laboratory study was conducted by Barman and Vandenbossche (Barman, 2014). A small-scale LTE test procedure was developed with a vision to make the LTE evaluation task simple so that the test can be conducted using readily available laboratory resources at a marginal cost. In the small-scale procedure, the LTE of concrete can be evaluated by using conventional 24-inch x 6-inch x 6-inch beam specimens. The test setup was designed to replicate the abrasive action that occurs on the joints of in-service concrete pavements loaded with an 18-kip single axle load. The loading configuration in the small-scale test procedure was established using a finite element analysis. The small-scale test results were validated by comparing them with the LTE results from a large-scale study in which full-size slabs were used to test the LTE. The LTE of plain and fiber reinforced concretes were compared in the laboratory study. Two types of structural synthetic fibers were used in that study: (i) straight synthetic fibers, and (ii) crimped synthetic fibers. Fiber dosages were selected based on the 20% residual strength ratio criteria as suggested in the Roesler et al. (2008) study. The volume fraction and dosages of the two fibers mentioned above is provided in Table 2-3. The LTE test results indicated that the straight synthetic and crimped synthetic fibers exhibited somewhat similar LTE versus crack width relationships. Overall, based on the laboratory test, it was found that the structural fibers could increase the LTE of the concrete. FRC prepared with 5.25 to 6.5 lb/yd^3 of structural synthetic fibers was able to provide about 20% more load transfer than their plain concrete counterparts.

Table 2-3 Volume fraction and dosages of two selected fibers in Barman (2014) study

Straight synthetic, 1.55-inch long		**Crimped synthetic, 2-inch long**	
Volume fraction (percent)	Dosage (lb/yd^3)	Volume fraction (percent)	Dosage (lb/yd^3)
0.36	5.25	0.43	6.20

An example of primary output from joint performance testing can be seen in Figure 2.11 and includes load, loaded side displacement, and unloaded side displacement. This figure shows load and displacement profiles for one load cycle. The peak values of the loaded side displacement and unloaded side displacement occurred at the same time were used for evaluating the joint performance in terms of LTE. The LTE was calculated as the ratio of unloaded side peak displacement and loaded side peak displacement, as shown in Equation 2 (AASHTO, 1993). LTE was calculated separately for the tension load and compression load; the average of the two was reported as the LTE for a given crack width. It shall also be noted that the average LTEs of five nearby load cycles was considered for calculating the LTE.

$$LTE = \frac{du}{dl} * 100\ \% \qquad (2)$$

Where d_l is the loaded beam's peak displacement; d_u is the unloaded beam's peak displacement.

Figure 2.12 shows that the LTE measured using beam test setup was comparable with the LTE measured using full-size slabs. It can be seen that the LTE results of 5 beams and one slab were quite similar.

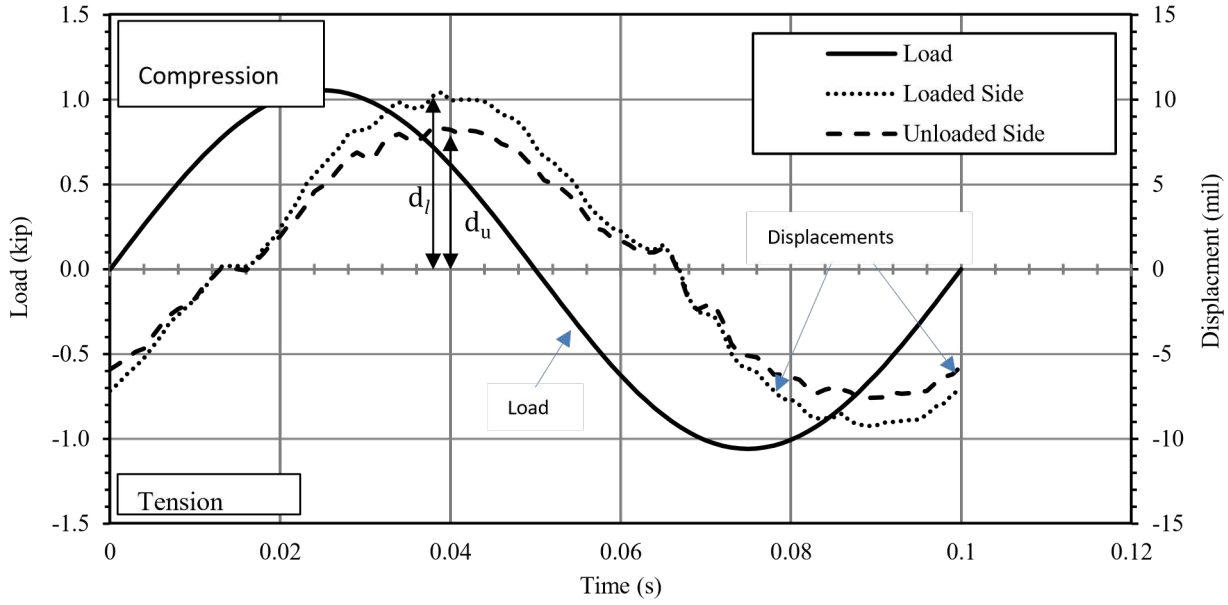

Figure 2.11 A typical example of load and displacement profiles achieved from a joint performance test.

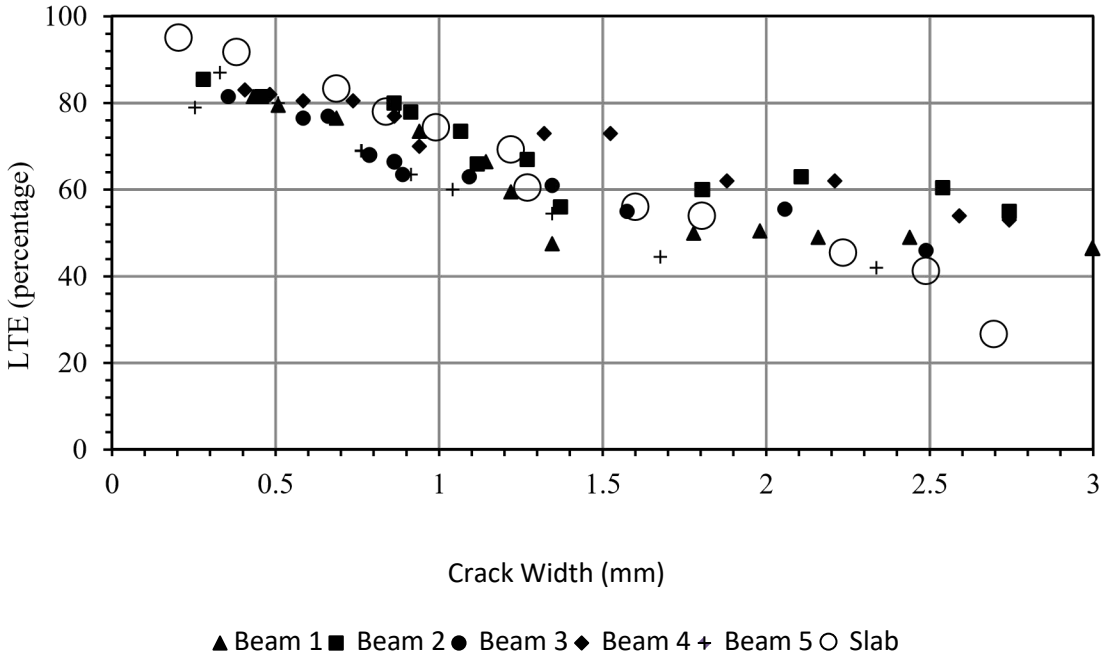

Figure 2.12 Correlation between the beam LTE and slab LTE (Barman, 2014).

2.5 Benefits of fibers in concrete pavements

The use of fibers as a reinforced material started in the early 1970s. In 1971, the first fiber-reinforced concrete pavement was constructed at a truck weigh station in Ohio (Daniel et al., 2009). Steel structural fibers were introduced first, then synthetic fibers. However, synthetic fibers have gained popularity during the past few decades as they are easier to handle than steel fibers and offer higher resistance to corrosion. In recent times, steel and synthetic fibers have been combined and employed in concrete pavement projects (Davenport et al., 2014).

Numerous laboratory, field, and analytical experiments were conducted that demonstrated the structural behavior of various fibers in concrete pavement or overlay over time (Barman, 2014; Barman et al., 2018; Roesler et al., 2008; Gaddam, 2016; Jang et al., 2014). A field investigation was carried out 1989 on three types of concrete overlay: plain concrete overlay, concrete overlay containing 0.28% volume fraction steel fiber (22 kg/m^3 or 37 lb/yd^3), and concrete overlay containing 0.44% volume fraction steel fiber (34 kg/m^3 or 57 lb/yd^3) (Chanvillard et al., 1989). Figure 2.13 shows that the use of fiber in concrete decreases the cracking in concrete pavement and increases the life of the pavement. Also, fiber helps FRC pavement hold cracks together and distribute wheel load between adjacent slabs.

Figure 2.14 shows the contribution of fibers in decreasing transverse joint faulting in some test sections constructed in MnROAD in 2017 (Barman, 2021). Different ultrathin and thin concrete pavement test cells with varying fiber dosages were constructed. Transverse joint faulting was found to be reduced by approximately 63% in the cell with 11.7 lb/yd^3 fiber dosage when compared to the cell with no fiber, after 2 years (accelerated study, ~2 million ESALs).

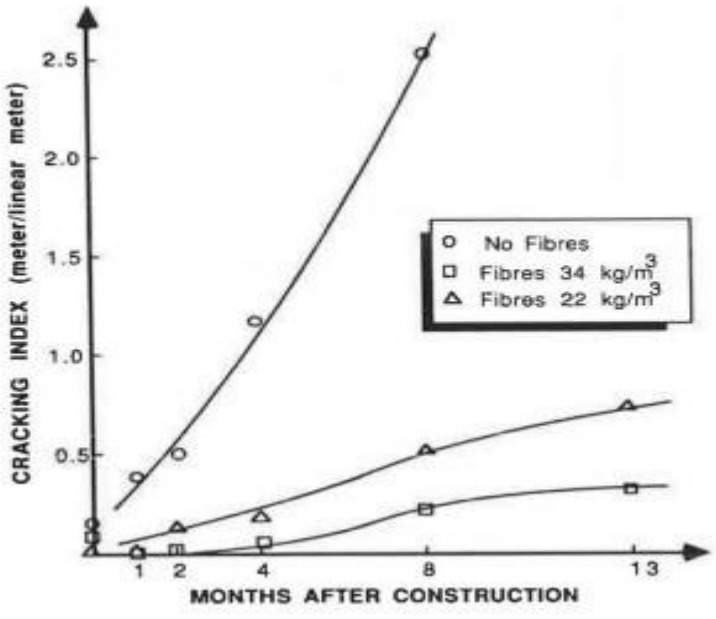

Figure 2.13 Influence of fiber on cracking in FRC Pavement (Chanvillard et al., 1989).

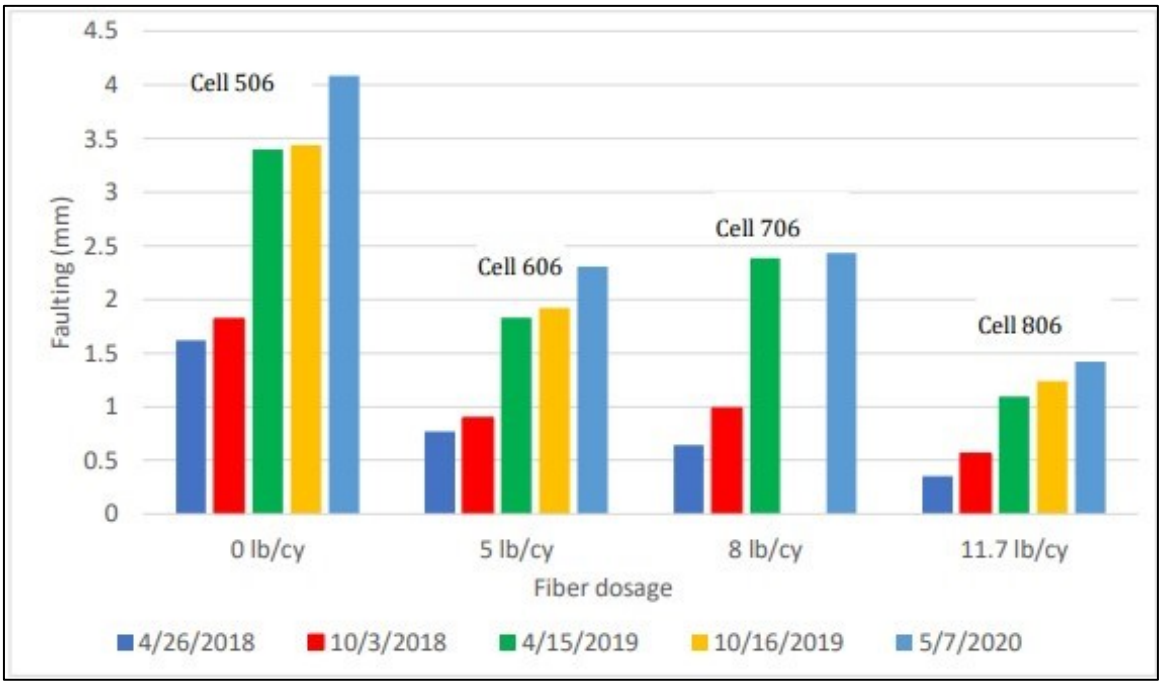

Figure 2.14 Influence of fiber on transverse joint faulting of FRC pavement (Barman, 2021).

2.6 Behavior of individual fibers

The behavior of individual fibers in FRC was also studied in various research works, typically using single-fiber pullout tests. There is no universal standard for conducting this test, so different strategies were used by different researchers. A typical load-displacement curve for a steel fiber in a single fiber pullout test is shown in Figure 2.15. A recent study used the test setup shown in Figure 2.16 to investigate the effects of embedment depth and fiber diameter on the interfacial behavior of hooked-end steel fibers (Abbas and Khan, 2016). A diagram of a concrete specimen is shown in Figure 2.17. Increasing the embedment depth from 6 mm to 30 mm has been shown to increase the load by nearly double the required to pullout the fiber. Increasing the fiber diameter from 0.625 mm to 0.750 mm also increased the resistance to pulling out, although the load difference decreased between the two diameters as the embedment depth increased (Abbas and Khan, 2016).

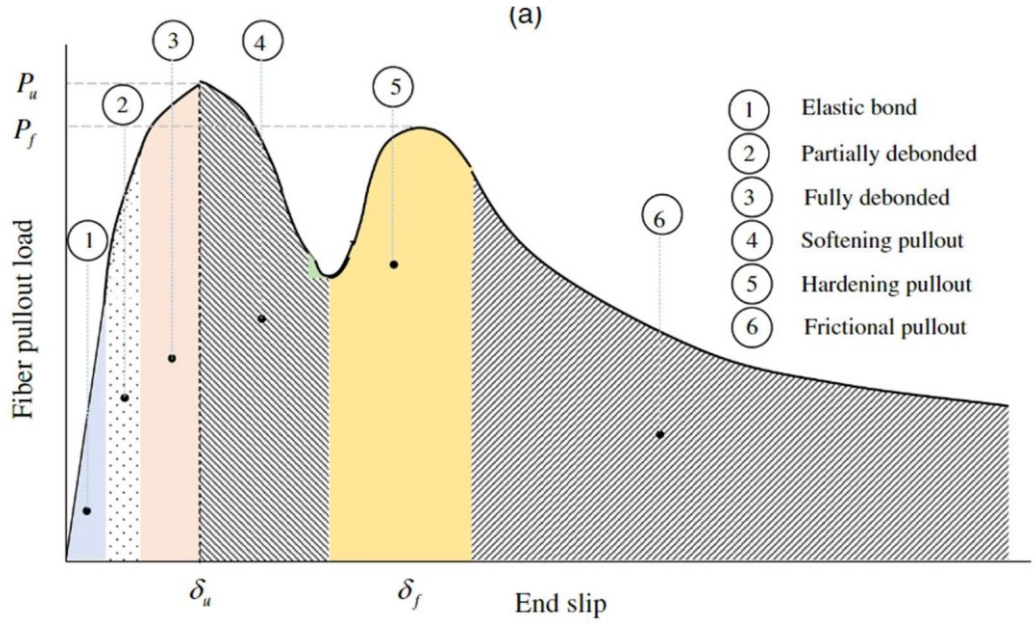

Figure 2.15 Typical load-displacement curve for steel fiber (Abbas and Khan, 2016)

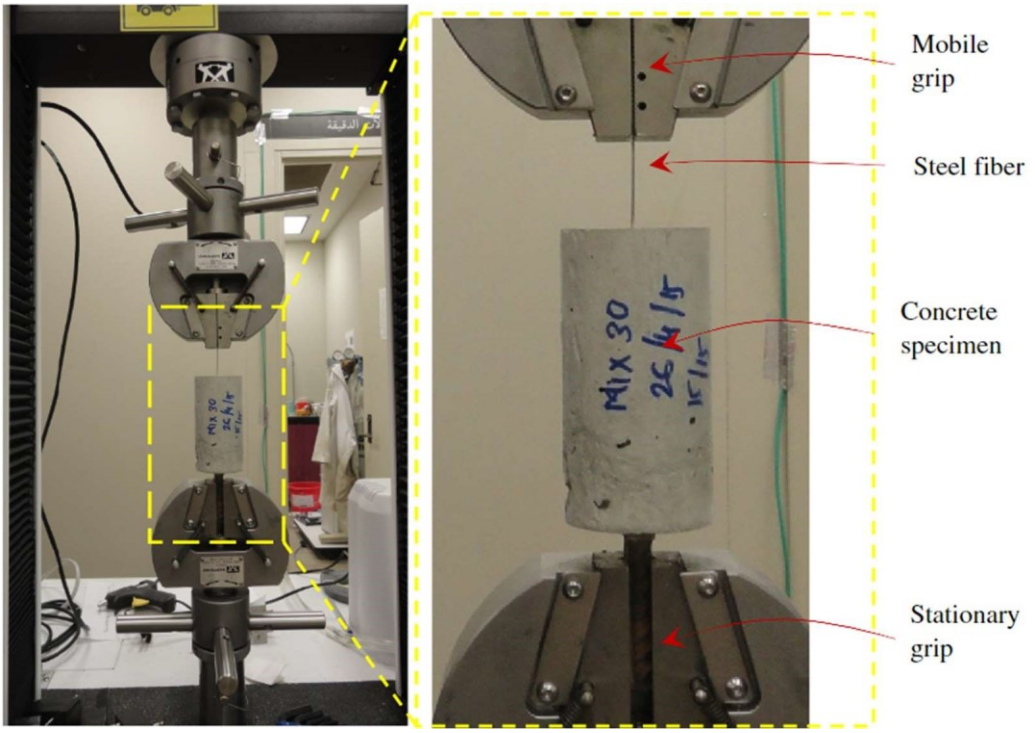

Figure 2.16 Steel fiber pullout test setup (Abbas and Khan, 2016)

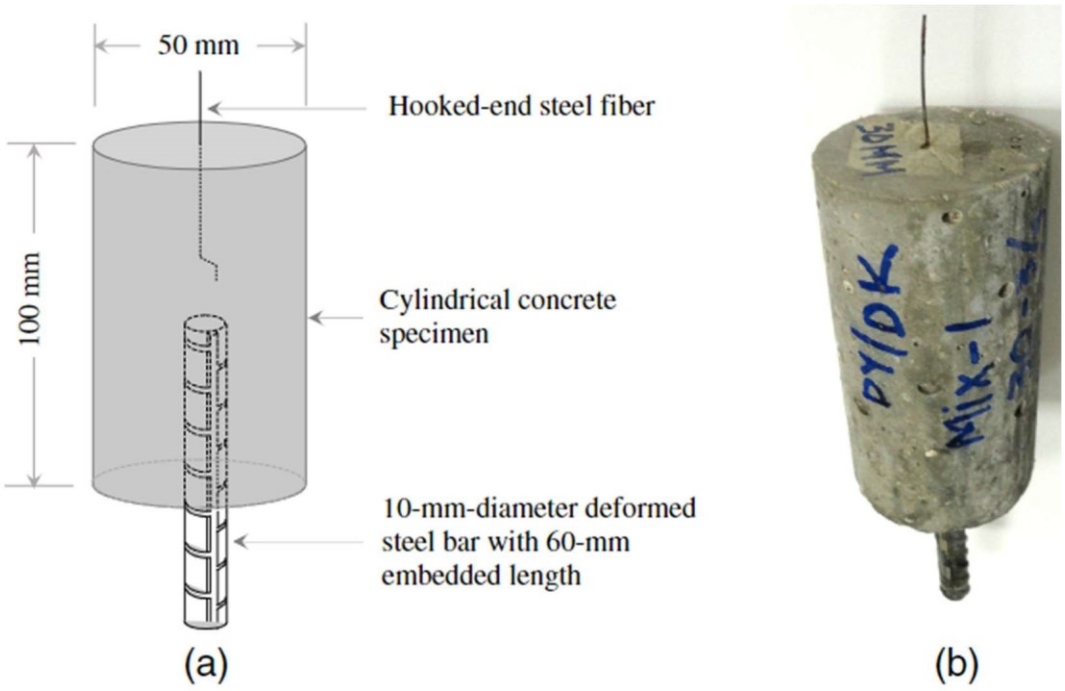

Figure 2.17 Schematic diagram and actual specimen (Abbas and Khan, 2016)

Polypropylene fibers behave in a comparable way. Typically, polypropylene macro fibers pull out before they rupture. Because polypropylene is chemically inert, there is a poor interfacial bond with the concrete matrix. Singh et al. (2004) showed that increasing the indentation of the fiber surface can improve the interfacial bond while also increasing the pullout load (Figure 2.18 and Figure 2.19). The pullout load of the most indented fiber (Fiber D) was nearly four times higher than the smooth fiber (Fiber A). Concrete continues to cure if there are hydration reactants available. The total time taken to cure can vary based on the curing method, but 28 days (an arbitrary length of time) is typically when concrete is considered fully cured. Singh et al. (2004) determined that after about three days of curing, the pullout load did not continue to increase (Figure 2.20).

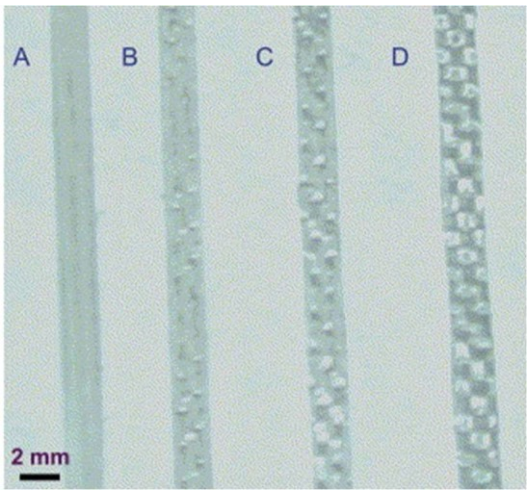

Figure 2.18 Varying indentations of polypropylene fibers (Singh et al., 2004)

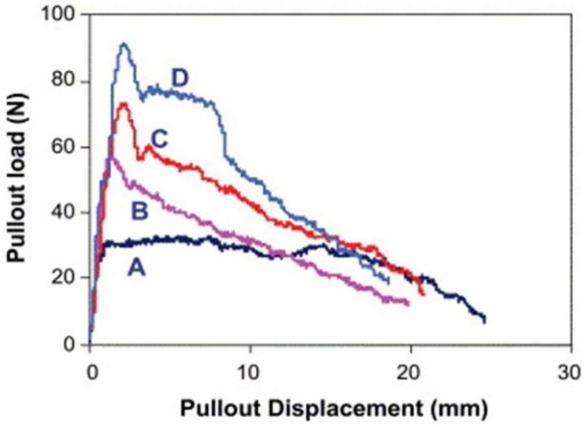

Figure 2.19 Pullout load of the fibers (Singh et al., 2004)

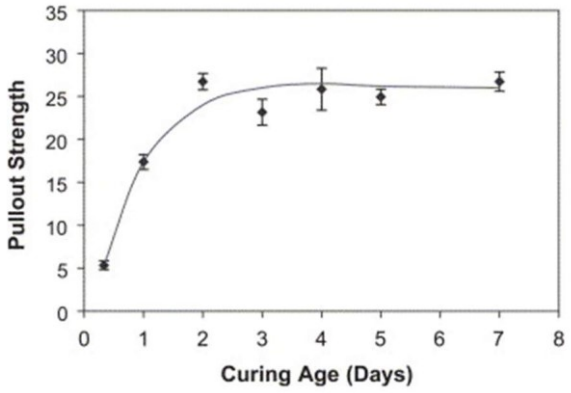

Figure 2.20. Pullout load vs. curing age (Singh et al., 2004)

The pullout load of fibers is an indirect result of the interfacial bond performance between the fiber and the concrete matrix. The strength of a concrete mixture has an impact on the interfacial bond. Studies indicated that pullout resistance for straight and hooked-end steel fibers was increased as the concrete matrix strength increased (Yoo et al., 2017; Beglarigale and Yazici, 2014). The strength of a concrete mixture is influenced by the water-cement ratio (w/c) and cementitious materials content. A lower w/c ratio increases the toughness and the peak load required for straight and hooked-end steel fibers in high-performance fiber reinforced cementitious composites (Yoo et al., 2017). In addition, a lower w/c ratio has been shown to increase the toughness and the peak load required for straight and hooked-end steel fibers in ordinary mortar (OM) and reactive powder concrete (Beglarigale and Yazici, 2014).

2.7 Finite element modeling (FEM) of pavements

The current study includes a finite element analysis of thin concrete pavement. Several studies were conducted using finite element analysis to model concrete pavements and analyze their performance. FEM can help to study the structure's physical responses, including stress, strain, temperature distribution, and other significant responses (Salman et al., 2014). All components of a model should have proper mesh sizes for efficient modeling (Spyrakos, 1994).

The behavior of concrete pavements changes throughout the course of their life span due to variations in moisture content, precipitation, frost actions, strength gain, creep, built-in warp and curl, etc. FEM has been found effective in studying these changes in concrete pavement behavior. Figure 2.21 shows the validation of the finite element analysis solution by Westergaard's theoretical equation for conventional concrete pavement. The comparison of theoretical and FE solutions validated both interior and edge deflection, and interior and edge stress solutions (Tabatabaie et al., 1978; Mahboub et al., 2004). Also, another study validated finite element solutions by using falling weight deflectometer (FWD) data. This model was developed using ABAQUS software. The comparison of solutions and field data validates the FEM analysis, as shown in Figure 2.22 (Uddin et al., 1995).

Previously, many researchers used FEM tools to examine the linear and nonlinear responses of pavement to loads imposed by traffic and environmental conditions. Some of the studies have examined a range of topics like joint load transfer, back-calculation of modulus, dynamic analysis, and responses to nonlinear temperature gradients (Maitra et al., 2009; Maitra et al., 2010; Hansen et al., 1998). Figure 2.23 shows the mechanism of aggregate interlocking between the loaded and unloaded slabs. This aggregate interlocking is represented by the linear elastic spring stiffness known as the modulus of interlocking joint (K_j) (Brink et al., 2005). The value of the modulus of interlocking joint (K_j) is represented by (MPa/mm) or (psi/inch) indicating that K_j is the stiffness of each spring per square area. The graph shown in Figure 2.24 for a 300 mm (11.8 inches) concrete slab shows the relation between LTE and K_j; as the K_j increases, the LTE also increases (Maitra et al., 2010).

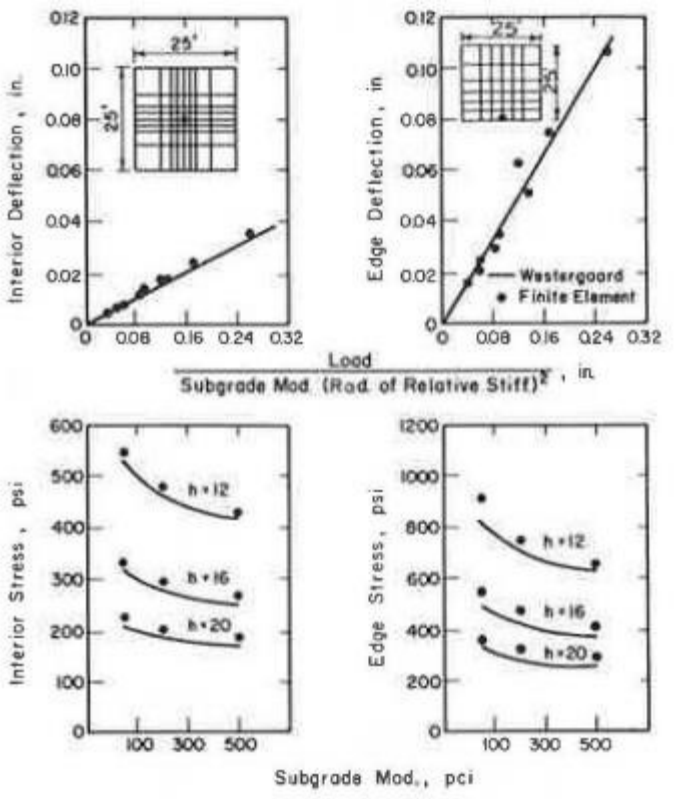

Figure 2.21 Finite element solution validation by Westergaard's equation (Tabatabaie et al., 1978).

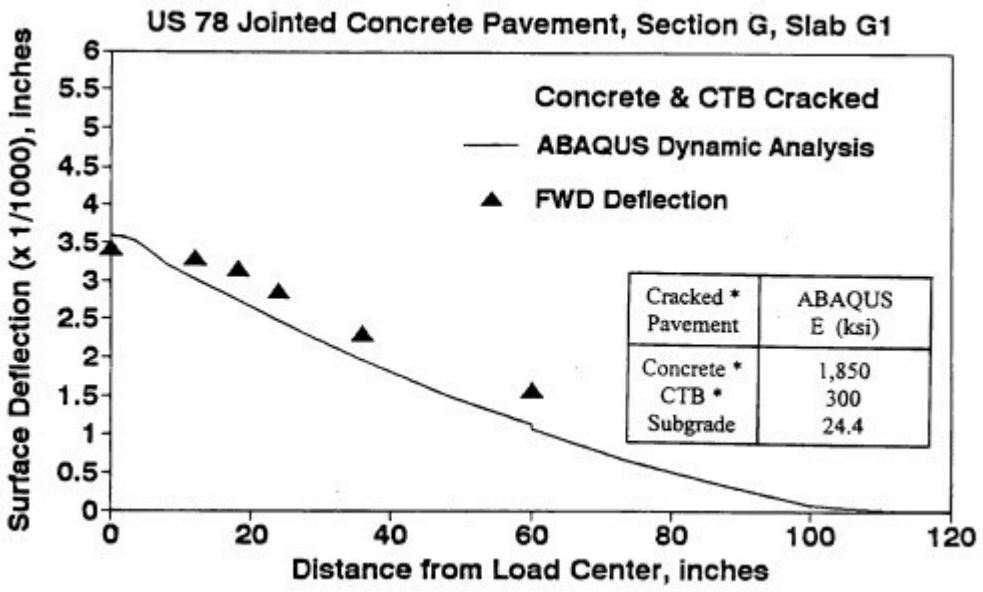

Figure 2.22 FEM solution validation with FWD data (Uddin et al., 1995).

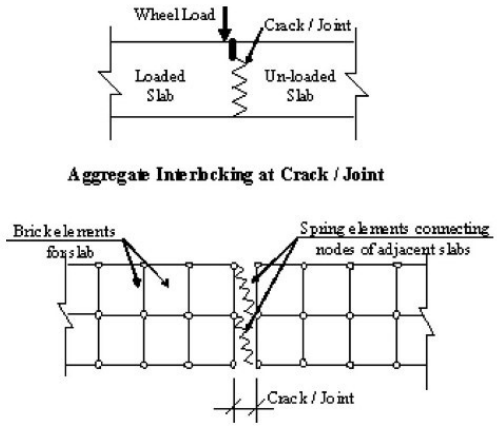

Figure 2.23 Finite element interlocking between joints (Maitra et al., 2010).

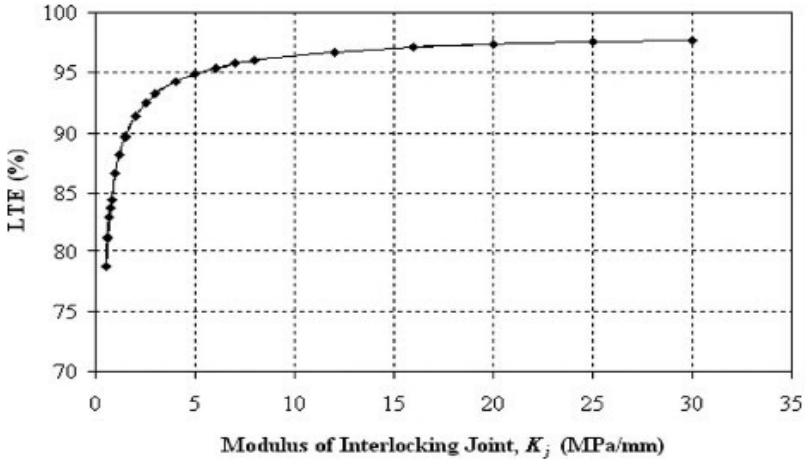

Figure 2.24 LTE vs modulus of interlocking joint (Maitra et al., 2010).

Three-dimensional FE analysis on jointed plain concrete pavement shows the effect of stress concentration on the transverse joint. Davids et al. (2003) found that poor joint interlocking can lead to higher stress concentration in the slab, thus the LTE decreases. To achieve higher LTE and smoother riding quality, the LTE should be maximized, and faulting at the joint and transverse crack should be minimized. Furthermore, higher modulus of elasticity and pavement structure thickness improve load transfer efficiency but not significantly. Figure 2.25 shows a FEM model developed for jointed plain concrete pavement (JPCP) for studying the effect of different parameters on LTE (Sadeghi et al., 2018). The findings of this study show that the effect of modulus of elasticity of concrete, modulus of elasticity of base layer, thickness of concrete slab, wheel load magnitude, and frictional force between base layer and concrete slab does not affect the LTE significantly. Moreover, by increasing the magnitude of all these parameters, the structure can only achieve an increase in LTE by 2%, which is shown in Figure 2.26 below (Sadeghi et al., 2018).

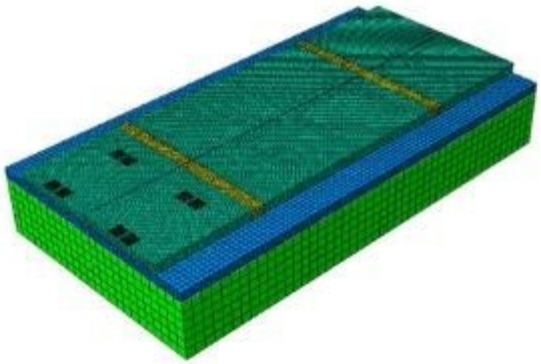

Figure 2.25 FEM model of JPCP (Sadeghi et al., 2018).

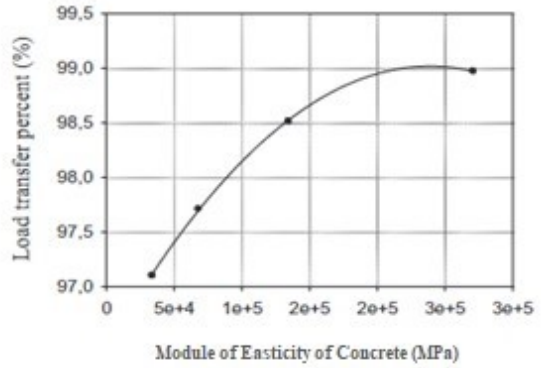

(a)

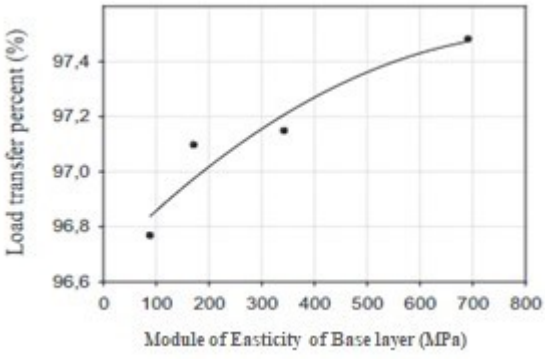

(b)

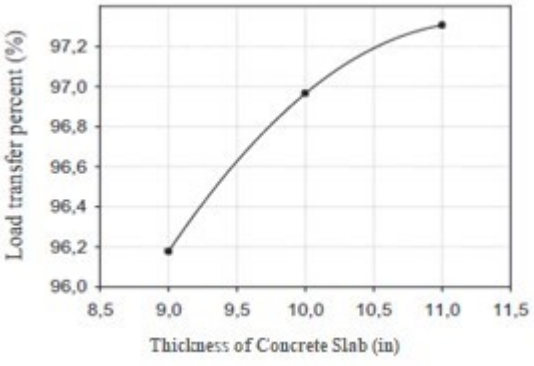

(c)

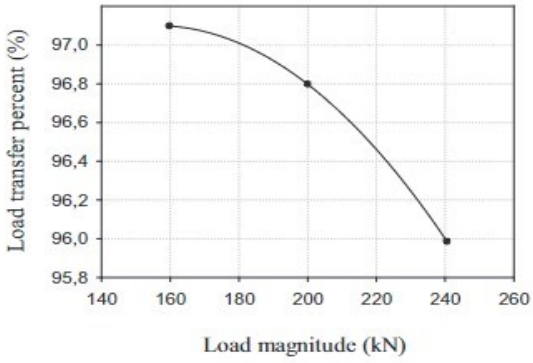

(d)

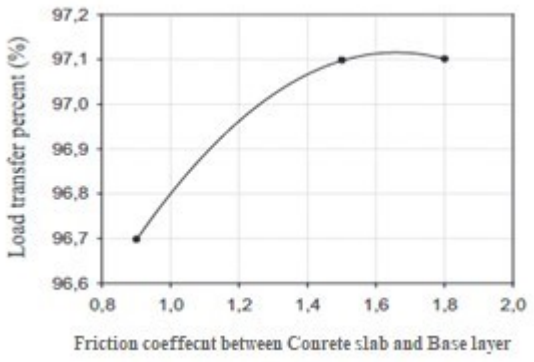

(e)

Figure 2.26 LTE vs different pavement parameters (Sadeghi et al., 2018).

Thermal stresses are caused by the curling of a concrete slab because of the temperature variation. Figure 2.27 shows the trend of maximum stress due to the effect of temperature or curling on plain jointed concrete pavement. Figure 2.27 (a) and (b) shows if the length of the slab is longer, then the maximum stress will be high for a positive temperature gradient, whereas, for a negative temperature gradient changing the length of the slab does not affect the maximum stress significantly. Figure 2.27 (c) and (d) show that increasing the slab thickness increases the maximum stress with both positive and negative temperature gradients. Tensile stresses caused by positive temperature gradients were approximately 85-90% of those caused by negative temperature gradients at the same values, shown in Figure 2.27 (e) and (f). Furthermore, the effect of friction factor on curling stresses was found to be negligible. Figure 2.27 (g) and (h) show the effect of concrete slab geometry on thermal expansion stress. It can be seen that by increasing the length of the slab and uniform temperature change the thermal stress increases. However, slab thickness does not affect the maximum tensile stress for the same uniform change in temperature. Figure 2.27 (i) shows the influence of a friction factor on maximum tensile stress for different uniform temperature changes. According to the data, tensile stresses increase with an increase in the friction factor and a uniform change in temperature. Although the change in stress is not significant, it can slide the slab if the slab is free to move (Masad et al., 1996).

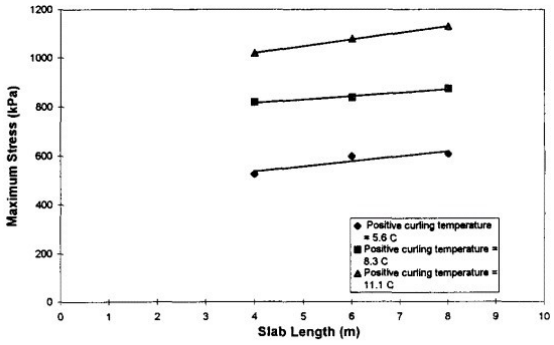

Effect of Slab Length on Positive Curling Stresses

(a)

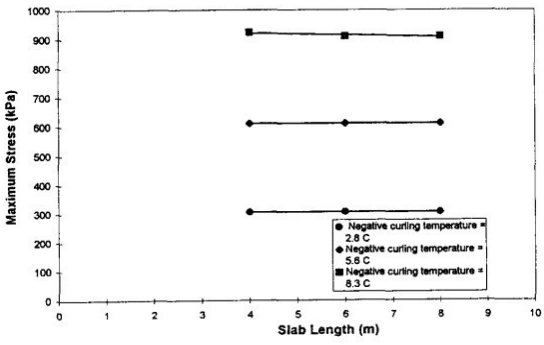

Effect of Slab Length on Negative Curling Stresses

(b)

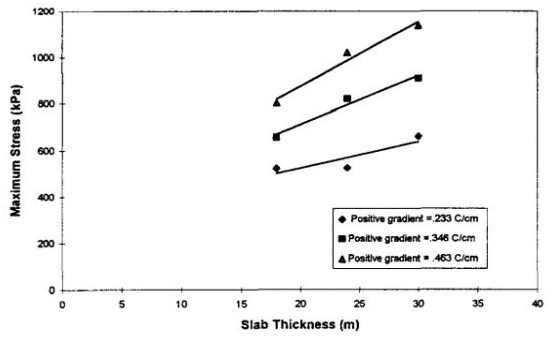

Effect of Slab Thickness on Positive Curling Stresses

(c)

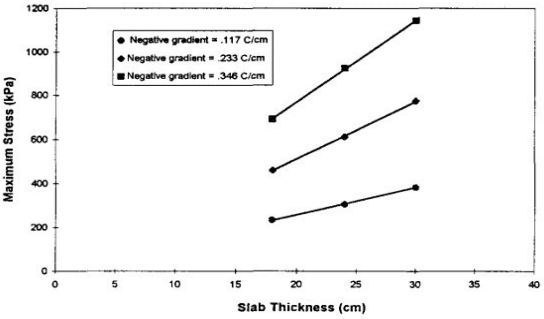

Effect of Slab Thickness on Negative Curling Stresses

(d)

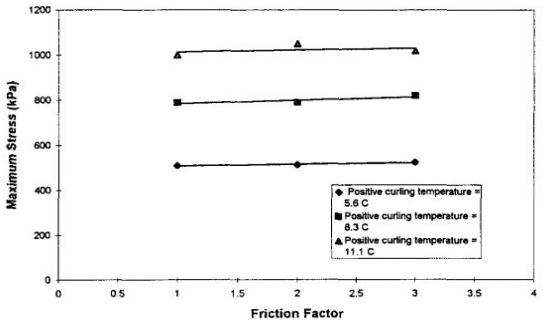

Effect of Friction on Curling Stresses due to Positive Temperature Gradients

(e)

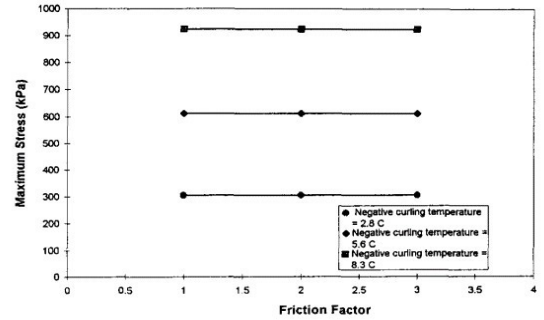

Effect of Friction on Curling Stresses due to Negative Temperature Gradients

(f)

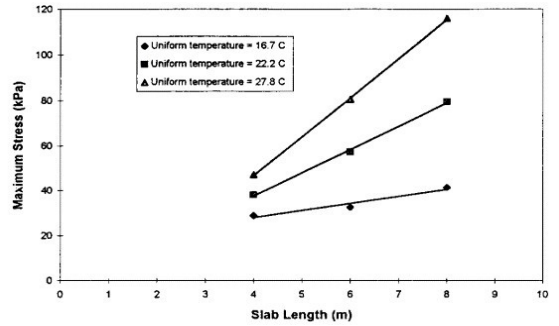

Effect of Slab Length on Thermal-Expansion Stresses due to Uniform Changes in Temperature

(g)

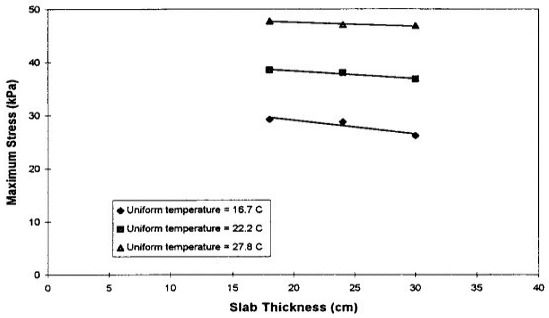

Effect of Slab Thickness on Thermal-Expansion Stresses due to Uniform Changes in Temperature

(h)

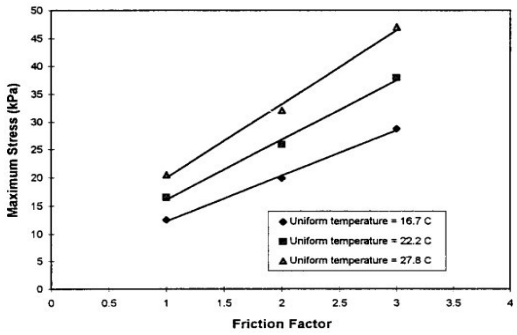

Effect of Friction on Thermal-Expansion Stresses due to Uniform Changes in Temperature

(i)

Figure 2.27 Influence of different pavement parameter on the temperature related stress (Masad et al., 1996).

At the University of Pittsburgh, bonded concrete overlay on asphalt was analyzed using finite element analysis and laboratory tests, as shown in Figure 2.28 (Barman, 2014). The study found that the thin overlay of fiber reinforced concrete improved load transfer efficiency and increased the stress distribution area. This research found that using fiber reinforced concrete reduces debonding stress by 50 to 70 percent compared to plain concrete. Furthermore, at any given crack width, load-related stresses are found to be decreased by approximately 6%.

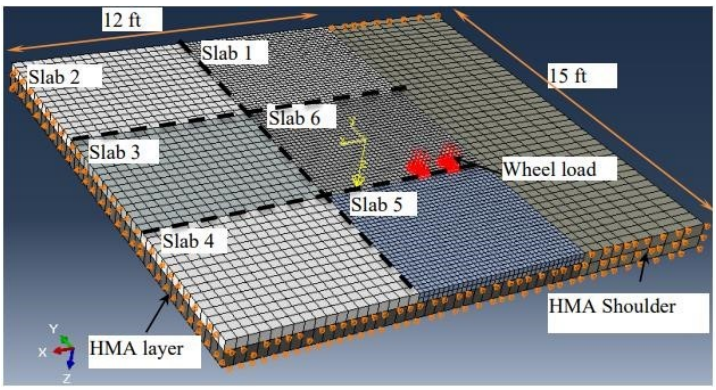

Figure 2.28 FEM Model of FRC overlay over HMA layer (Barman et al., 2014).

Chapter 3: JOINT PERFORMANCE MODELLING

This chapter focused on modeling of fiber-reinforced concrete pavement with an emphasis on the transverse joints performance. All the possible forces that affect the stiffness of the transverse and longitudinal joints are considered in the FEM model. As the transverse joints are critical to causing joint faulting, the joint performance was studied only at the transverse joints, even though both transverse and longitudinal joints were modeled identically. Figure 3.1 shows a schematic of the thin concrete pavement indicating different forces that potentially influence the transverse joints and, in other words, influence the contribution of the structural fibers that bridge the joint. The main force that influences the joints is the vehicle wheel load. Temperature and moisture gradients create downward and upward curling, which builds up stresses in the concrete slab and influences the transverse joints and the stresses in the fibers. The seasonal temperature change that expands and contracts the slabs also influences the stiffness of the transverse joints. In addition to the abovementioned forces, the frictional force between the slab and the vehicle tires, as depicted in Figure 3.1, is another force that can impact the transverse joints, especially because of the small-size slabs, which are lighter than conventional pavement slabs.

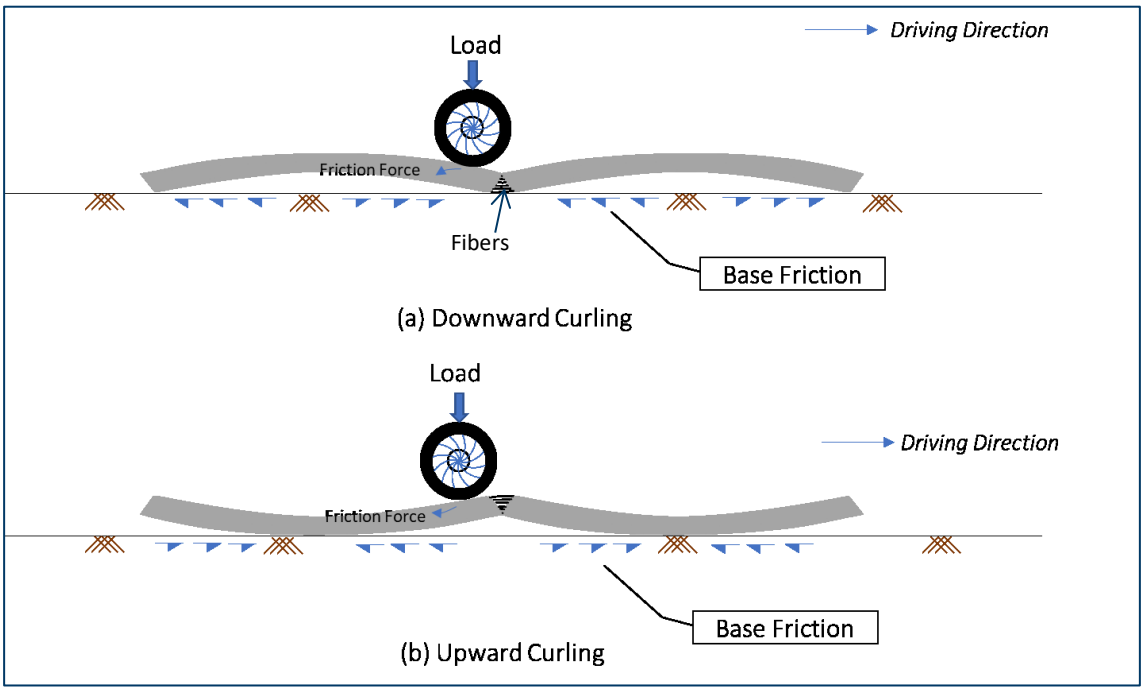

Figure 3.1 Key forces on the transverse joints of a thin FRC pavement (a) downward curling, (b) upward curling.

3.1 Pavement structure and materials

Figure 3.2 shows a screenshot of the six-slab model developed in this study. The modeling was performed using the FEM software ANSYS®. The mesh size for the concrete slabs was 1-inch x 1-inch x 1-inch. The slabs and base layer were free to move in the vertical direction. In the horizontal direction, the

boundary conditions were set in a way that the slab could expand and contract with the uniform temperature change. Rotation was set free in all three directions to allow upward and downward curling of the slabs because of the temperature gradient. Both the concrete slab and base layer materials were modeled using the Solid-186 element, as shown in Figure 3.2. This element has 20 nodes; each node has three degrees of freedom and can translate in nodal x, y, and z directions. This element can model different behaviors of material such as plasticity, creep, stress stiffening, large deflection, and strain. This element can act as incompressible elastoplastic material and fully incompressible hyper-elastic material or both and can model the curling of the concrete slabs.

The study considered different variables related to pavement structure and materials. Table 3-1 provides the list of different variables and their values. Three slab thicknesses (4 to 6 inches) and four base layer thicknesses (4 to 11 inches) were considered. As macro synthetic fibers do not significantly affect the modulus elasticity and Poisson's ratio of concrete, for the typical fiber dosages used in the pavements (Barman, 2014; Barman, et al., 2015), these parameters were kept constants for all cases as 4,300,000 psi and 0.2, respectively. The thermal conductivity of the concrete was assumed as 0.31223 BTU/sec-inch-oF for all cases.

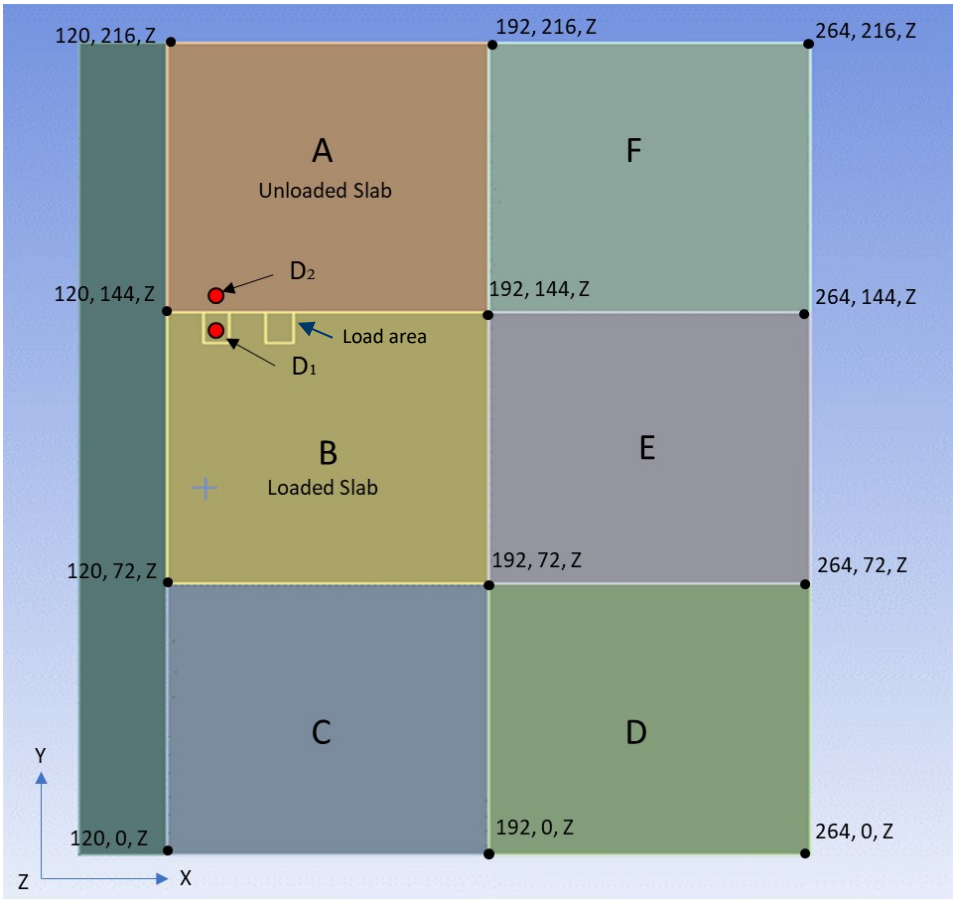

Figure 3.2 Six-slab FEM model of the thin concrete pavement (slab size: 6 ft x 6 ft; D1 and D2: locations of deflection calculated).

Base and subgrade layer materials are sensitive to the season because of the change in the moduli with the moisture content. A total of three seasons (early spring, summer, and winter) were considered in this study to accommodate the various conditions of the base and subgrade layers. The base modulus and the modulus of subgrade reaction are the lowest in early spring because of the thawing of the ice and the highest in the winter because of the freezing. The base modulus varied from 9,000 to 50,000 psi, and the modulus of the subgrade reaction varied from 138 to 768 psi/in. These values were collected from the MnDOT Pavement Manual (MnDOT, 2019). In this study, an elastic foundation was considered to represent the modulus of subgrade reaction, similar to Winkler's foundation, in which the contact pressure at any point is assumed to be proportional to the deflection at that point and independent of the deflection at other locations.

Table 3-1 Summary of pavement design, material, and other variables

Slab thickness (inches)	4, 5, and 6.
Base layer thicknesses (inches)	4, 6, 8, and 11.
Slab modulus of elasticity (psi)	4.3 x 106
Base layer modulus of elasticity (psi)	Early spring: 9,000; summer: 30,000; winter: 50,000.
Modulus of subgrade reaction (psi/in)	Early spring: 138; summer: 461; winter: 768.
Poisson's ratio of concrete	0.2
Thermal conductivity	0.31223 BTU/sec-inch-°F
Temperature gradient (Day) (°F/in)	Early spring: 5.35; summer: 4.71; winter: 4.48.
Temperature gradient (Night) (°F/in)	Early spring: -2.15; summer: -2.92; winter; -2.56.
Wheel load pressure (psi) and road surface- tire friction pressure (psi)	93.75 and 14.10 psi
Joint stiffness in the vertical direction (lbf/ inch^3)	0, 50, 400, 800, 1000, 1500, 2000, 2500, 5000, 15000, 25,000.
Joint stiffness in the horizontal direction (lbf/inch^3)	0, 500, 1500, 2000, 2500.

3.2 Loads

A dual-wheel assembly was used as the vehicular load. As shown in Figure 3.2, the load was applied on the outer wheel path in the form of a uniform pressure (93.75 psi) on two 6-inch x 8-inch rectangular load areas. The outer load area is 12 inches away from the outer edge of the slab. The center-to-center distance between the two load areas is 14 inches.

The study considered the curling-induced force. During the day, due to direct sun exposure, the temperature remains high at the top of the slab and low at the bottom; slabs curl in a downward direction. The opposite occurs during the night. To consider the effect of the curling-induced force on joint performance, temperature data collected from MnROAD's thin FRC cells (Barman et al., 2021) were referred to. The highest day- and night-temperature gradients for three seasons were considered. The temperature gradient data considered in the finite element analysis are provided in Table 3-1. It may be noted that the above-mentioned MnROAD test cells were constructed in 2017 under an NRRA-funded research project.

The study also considered the frictional force at the interface of the pavement surface and vehicle tires. When the vehicle accelerates in the driving direction, a frictional force acts in the opposite direction. Generally, the effect of this frictional force is less or negligible on large thick concrete slabs (e.g., 12ft x 12ft). However, the same can have more of an effect on the thin concrete slabs; the slab movement in the backward direction may affect the joint stiffness. To understand the effect of this frictional force, a horizontal shear pressure was applied on the pavement surface at the location of the wheel load areas. Considering a friction coefficient of 0.15, the frictional pressure is calculated as 14.10 psi.

3.3 Transverse and longitudinal joints

Figure 3.3 shows a photograph of a joint of fiber reinforced concrete specimen and a screenshot of the joint that is modeled in the FEM analysis. The thin FRC concrete pavement joints are expected to transfer wheel loads through aggregate interlock and fibers' stiffness. These load transfer mechanisms were modeled using the spring element, MATRIX27, an elastic kinematic response that can be defined by stiffness coefficients (K) in matrix form, which relates two nodes, each with six degrees of freedom per node: translations in the nodal x, y, and z directions and rotations about the nodal x, y, and z axes.

The joint stiffness coefficient in the vertical direction (z-axis), which is provided by the aggregate interlock and fibers' lateral stiffness, is denoted by Kz. Fibers' lateral stiffness is the stiffness which fibers (embedded in the concrete) offer in the vertical direction at the joints, also referred to as the modulus of fiber support in the following chapters. The joint stiffness coefficients in the x and y directions, which are provided only by the longitudinal stiffness of fibers (see Figure 3.3), are denoted by Kx and Ky, and they are assumed to be equal. Kx and Ky depend only on the contribution of the fibers (embedded in concrete), not on the aggregate interlock. It may be noted that all the transverse and longitudinal joints are assumed to have a one inch saw cut, and hence, MATRIX27 elements were not assigned at the top one inch of the joints. The magnitude of the joint stiffness varies with the joint conditions, including

crack width and concrete properties. The unit of the joint stiffness coefficients is lbf/inch/inch^2 or lbf/inch^3 as the size of the meshes is 1-inch x 1-inch x 1-inch and only one spring exists in a one-inch square area (only corner nodes of the slab elements are connected). The magnitudes of the joint stiffness values considered in this analysis are provided in Table 3-1. These values were determined by performing several initial trials so that a range of possible LTEs are considered in the analysis. It was found that the LTE maxes at around 2,500 lbf/inch^3 joint stiffness (vertical direction) after which LTE increase is minimal with the increase in joint stiffness.

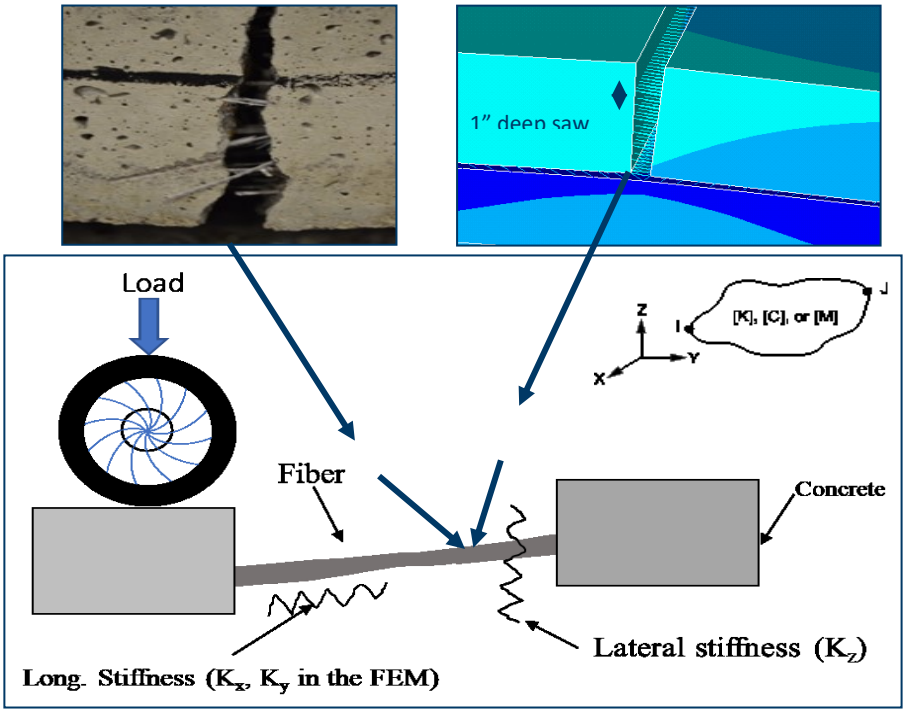

Figure 3.3 Modelling of the joints of thin FRC pavements

3.4 Slab and base layer interface

In the thin FRC pavement on the granular base layer, the FRC slab and the base layer are not bonded. However, in bonded concrete overlays on cement concrete or asphalt concrete, the slabs are assumed to remain bonded with the underlying layer. In this study, the MATRIX27 element was used at the slab-base interface, with a very low value of stiffness coefficients in the vertical direction as 50 lbf/inch^3. The stiffness in the horizontal directions (x and y) was kept at 2,000 lbf/inch^3. This element and the stiffness magnitudes helped slabs against sliding and its low stiffness in the vertical direction represented a weak slab-base interface bonding, a conservative assumption, or a worst-case scenario.

3.5 Joint performance evaluation parameters

The joint performance was studied in terms of load transfer efficiency (LTE), differential displacement (DD), and maximum slab displacement (D_{max}). LTE is defined as the ratio of displacement of the unloaded slab to the displacement of the loaded slab, expressed in percentage. In this study, the loaded and unloaded slab displacements were computed at a location one inch away from the transverse joint along the wheel path. The differential displacement is the absolute difference between the loaded slab displacement and unloaded slab displacement. The maximum slab displacement is the maximum displacement of the loaded slab, underneath the load.

3.6 Effect of various parameters on the joint performance

The effects of various factors on the abovementioned joint performance parameters are discussed below. The influencing factors considered are joint stiffness, pavement structure (thicknesses of slab and base layer), daily temperature gradients, and seasonal temperature change.

3.6.1 Effect of joint stiffness on joint performance

The effect of the joint stiffnesses K_z, K_x, and K_y ($K_x = K_y$) on the joint performance parameters, LTE, DD, and D_{max}, which are related to the transverse joint faulting, is discussed here. A 4-inch thick FRC pavement on a 4-inch aggregate base layer is considered for this analysis. The thicknesses of the pavement layers were kept minimal so that the influence of the joint stiffness coefficients on the joint performance parameters is apparent. Other variables for this analysis were kept constant and are as follows: temperatures at the top and bottom surfaces of the slabs = 82.1°F and 60.7 °F (temperature gradient= 5.35 °F/inch), respectively; wheel load pressure = 93.75 psi; frictional pressure on the pavement surface = 14.1 psi; base modulus = 9,000 psi; modulus of subgrade reaction = 138.3 lbf/inch^3 and season = early spring.

When the effect of K_z on the joint performance parameters was established, the K_x and K_y were kept constant at 50 lbf/inch^3. Similarly, when the effect of K_x or K_y was studied, K_z was kept constant at 50 lb/inch^3. Figure 3.4(a) presents the variation of the LTE, DD, and D_{max} with respect to the Kz. It can be seen that the LTE can be increased from 40% to 90% when the K_z is increased from 0 to 2,500 lb/inch^3. The LTE (~40%) at K_z = 0 is the LTE provided by the base and foundation layers with no contribution from the concrete slabs. Figure 3.4(a) also shows that the increased K_z can decrease the DD and D_{max}, which may help mitigate transverse joint faulting. It may be reminded that in the thin FRC pavement, vertical joint stiffness can be achieved from the aggregate interlock and fibers' lateral stiffness. However, as the aggregate interlock is limited in thin pavements, the enhancement of the joint stiffness will depend on the lateral stiffness of the fibers.

Figure 3.4 (b) shows that the increases in the K_x and K_y values do not affect the LTE, DD, or D_{max}, which indicates that the longitudinal stiffness of the structural fibers is less influential in terms of joint performance in the finite element analysis.

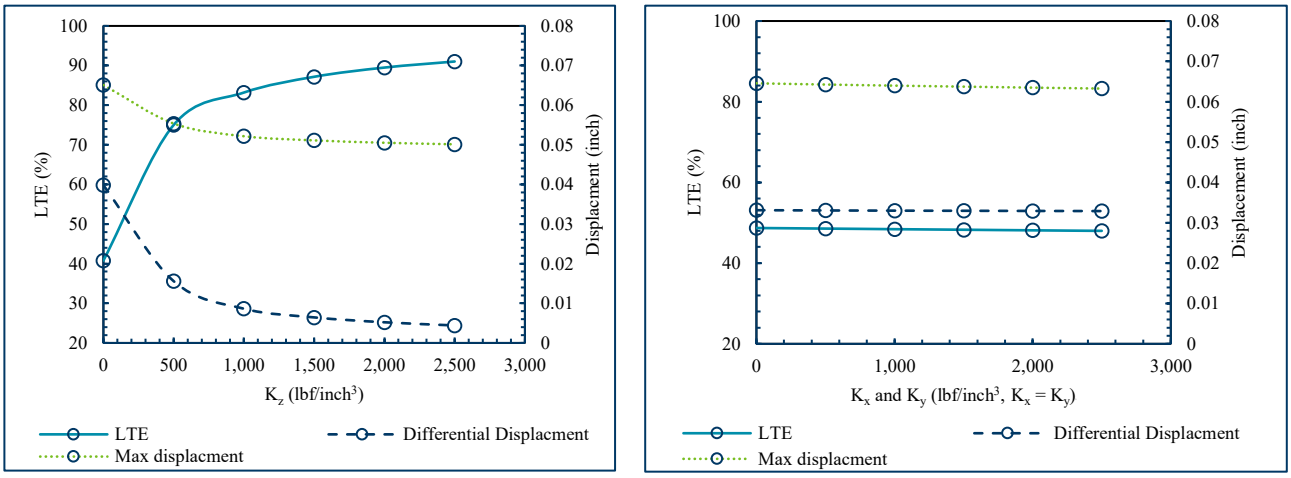

(a) (b)

Figure 3.4 Effect of joint stiffness on joint performance parameters (LTE, DD and D_{max}).

3.6.2 Effect of pavement structure on joint performance

The effect of FRC slab and base layer thicknesses on the joint performance parameters is discussed here. Joint performance parameters were computed for several pavement structures by varying the slab and base layer thicknesses. First, K_z, K_x, and K_y were kept minimal and constant at 50 lbf/inch^3, while the other variables were the same as in the previous analysis. Figure 3.5 shows the effect of the slab and base layer thicknesses on the joint performance. It can be observed that the increase in the slab thickness from 4 to 6 inches, on an eight inches thick base layer, did not improve the LTE, although the magnitudes DD and D_{max} slightly decreased with the increased slab thickness. The increase in the base layer thickness improved the LTE for the pavement with a 4-inch-thick slab. The LTE, which was 40% with a 4-inch base layer increased to 52% with an 11-inch-thick base layer. The D_{max} did not change much with the increase in base thickness, but the DD decreased with the increase in base layer thickness.

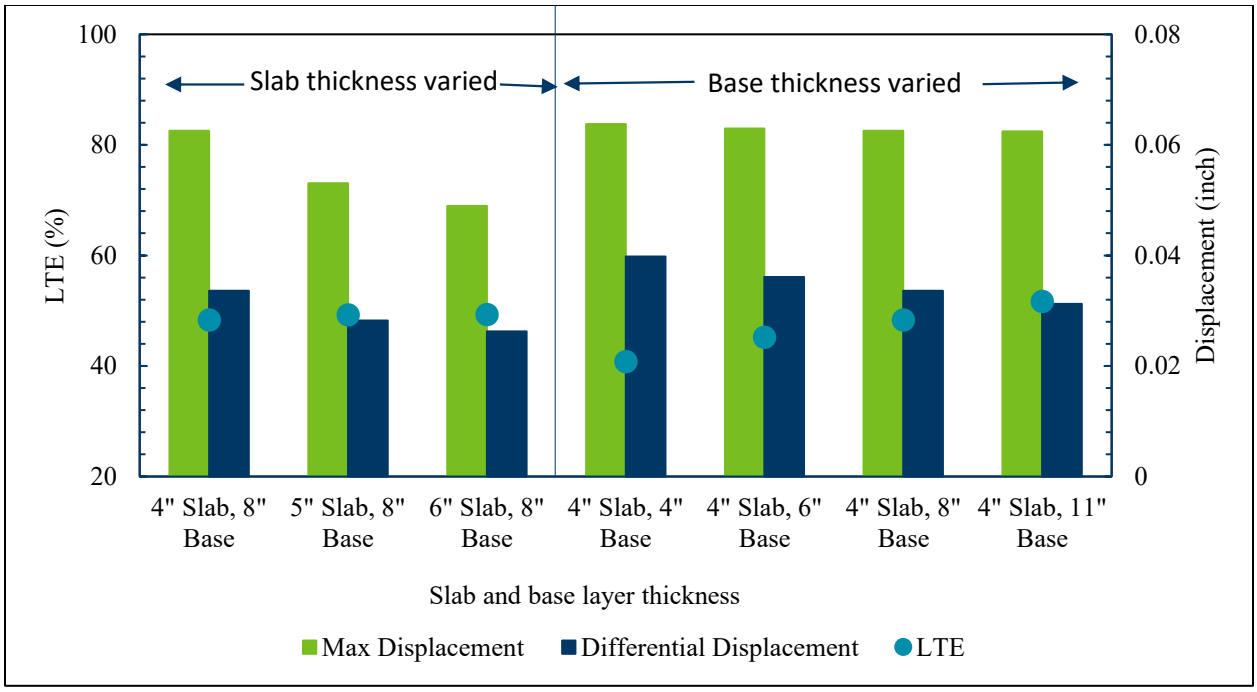

Figure 3.5 Effect of the thicknesses of the slab and base layer on the joint performance parameters.

Next, the effect of pavement structures on the LTE over a large range of vertical joint stiffness (K_z) is studied. Figure 3.6 presents the bar chart of LTE values with respect to K_z for various pavement structures. LTE values for the 4, 5, and 6-inch thick FRC slabs on 4-, 6-, 8-, and 11-inches base layers can be found in this figure. The LTEs of a total of seven different structures were compared with each other at a given value of K_z. Interestingly, the influence of the pavement slab and base layer thicknesses is less than the influence of the K_z on the joint performance. The weakest pavement structure, 4-inch slab on 4-inch base, resulted in the poorest joint performance at lower values of K_z. For this and all other designs, the LTE increased with the increase in K_z.

Another interesting observation is that the influence of the structures on the LTE minimizes at higher values of K_z. In other words, when the pavement structure is relatively weak (e.g., 4-inch slab on 4- to 6-inch base), a higher value of K_z is likely to be more beneficial than when the structure is strong or thicker (e.g., 6-inch slab on 8- to 11-inch base). For example, the LTE of the pavement with a 4-inch slab over a 4-inch base can be increased from 41 to 91% (50%) with aggregate interlock and structural fibers (K_z = 0 to 2,500 lbf/inch^3). When the structure is a 4-inch slab over an 11-inch base, then a 40% LTE increase is possible with the aggregate interlock and structural fibers.

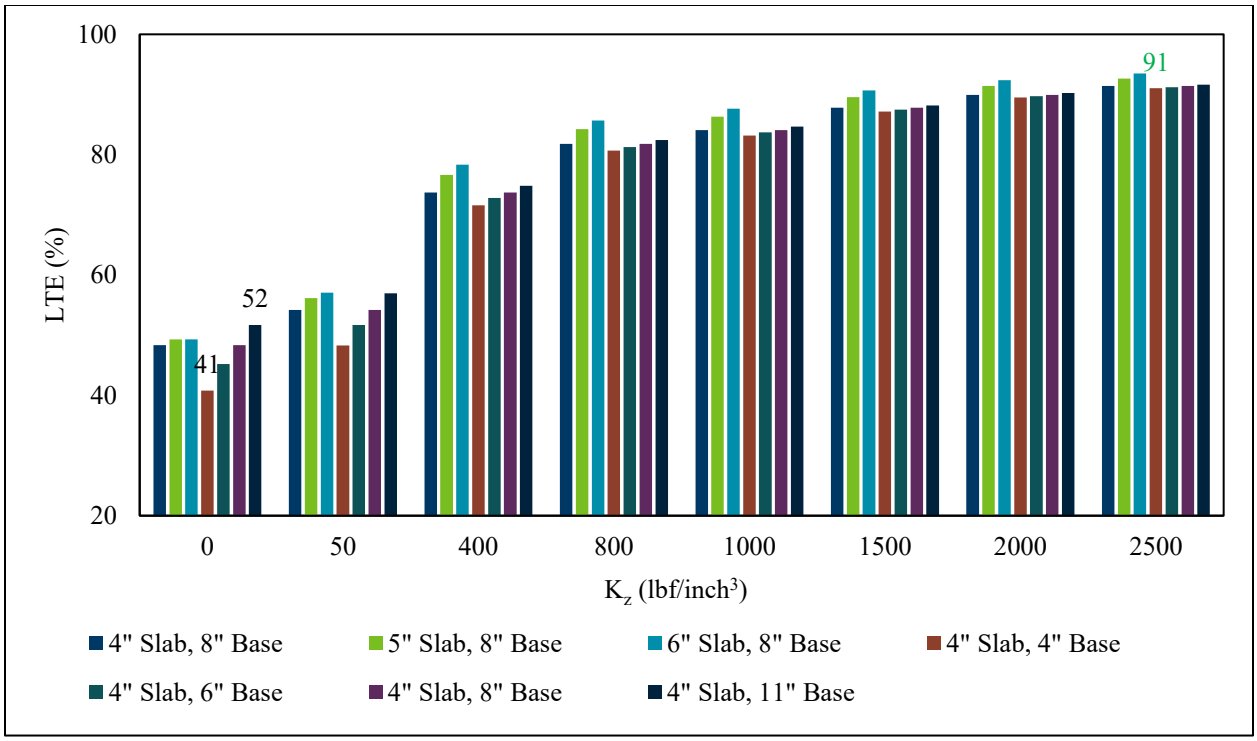

Figure 3.6 LTE vs. K_z for different pavement structures (for a given K_z value, the first three structures have 8-inch base layer and variable slab thickness; the next four structures have a 4-inch slab and variable base layer thicknesses).

3.6.3 Effect of daily temperature cycle on joint performance

The changes in the pavement slab temperature, temperature gradient, and moisture content of the base and subgrade layers can affect the joint performance, especially in a place like Minnesota, where the minimum and maximum pavement temperatures fluctuate between -15 °F and 120 °F, and the moisture from the rain and snowfall is significant. Figure 3.7 shows the influence of the temperature gradient on the LTE. For this analysis, the LTE values were computed for a 4-inch-thick pavement on a 6-inch base layer at three different temperature conditions as follows: (i) same temperature at the top and bottom of the slab (95 °F), (ii) upward curling at night (temperature gradient = - 2.15 °F/in), and (iii) downward curling at day (temperature gradient = 5.35 °F/in). The temperature gradients and the base and subgrade properties considered in the analysis are for the early spring season. K_z values were varied while the K_x and K_y were kept constant at 1,500 lbf/inch^3. No friction was considered between the vehicle tire and the slab surface for this analysis.

From Figure 3.7, it can be seen that the influence of the temperature gradient is only apparent at the lower joint stiffness values, which diminishes with the increase in the K_z value. In general, the downward curled slabs (positive temperature gradient) showed higher LTE than the upward curled slabs (negative temperature gradient) or the slabs with zero temperature gradient.

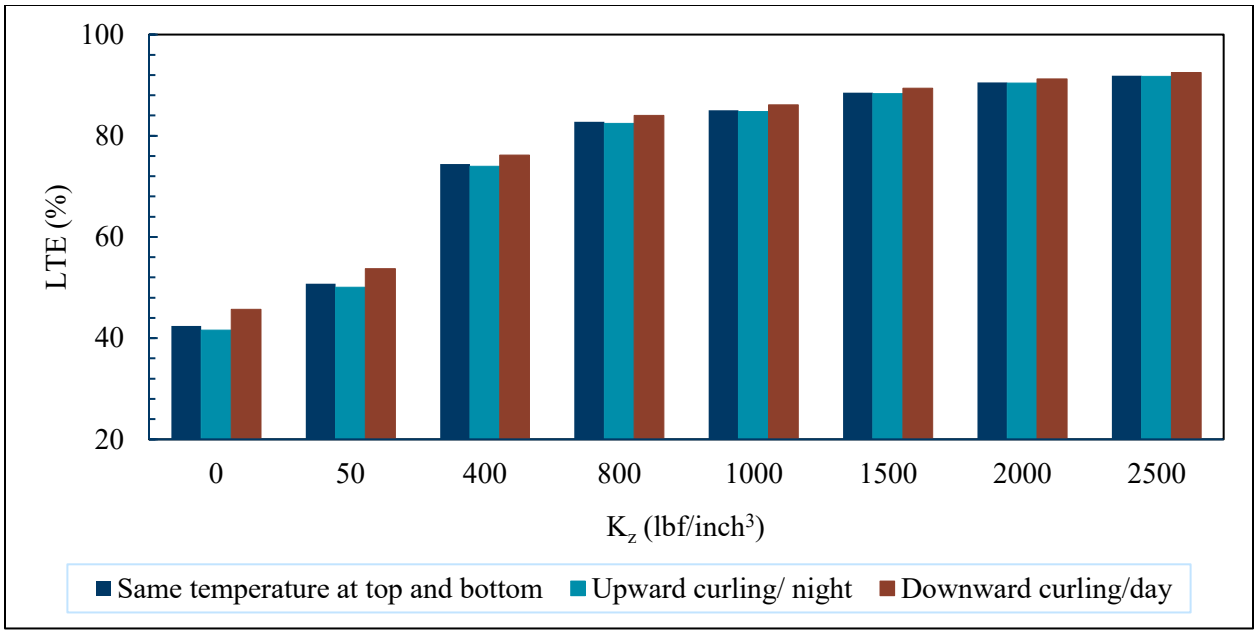

Figure 3.7 Effect of temperature gradient on LTE (early spring).

3.6.4 Effect of season on joint performance

Figure 3.8 through Figure 3.10 show the variations in joint performance parameters across three seasons, namely, early spring, summer, and winter. Three different structural designs are considered for this analysis: (i) 4-inch slab, 6-inch base; (ii) 4-inch slab, 11-inch base; and (iii) 6-inch slab, 6-inch base. The values of K_z, K_x, and K_y were assumed as 50 lbf/inch^3. Table 3-2 shows the other variables considered for this analysis.

From Figure 3.8 through Figure 3.10, it can be seen that the LTEs between seasons changed, with the LTE in the early-spring (weak foundation) higher than the two other seasons considered. As anticipated, the magnitude of the change is higher for the weaker structure (e.g., 4-inch slab, 6-inch base). Even though higher LTE in the early spring may sound counter-intuitive, the significantly higher deflection magnitudes on both the loaded and unloaded slabs are the reason for this result. Realistically, the moisture content within the slabs increases in the spring and leads to slightly longer slabs and tighter joints. However, the contribution of the base layer likely decreases, thus nullifying some of the benefits from swelled slabs. During the winter, the slabs are shorter, the joints are wider, again reducing the available LTE. The cold temps also curl up the slabs, negating the potential contribution of the frozen (stiff) base.

The higher LTE in the early spring does not, therefore, indicate that the joint performance is better in that season. The higher values of D_{max} and DD in the early spring indicate that the joint performance is inferior in this season compared to the summer and winter and possibly for the rest of the year. It shall be noted that the relatively low values of LTE (40 to 58%) in Figure 3.8 through Figure 3.10 are due to the consideration of the negligible value of K_z, which is considered as 50 lbf/inch^3.

Table 3-2 Selected material properties for three seasons.

	Early-spring	Summer	Winter
Base layer modulus (psi)	9,000	30,000	50,000
Modulus of subgrade reaction (psi/inch)	138	461	786
Temperature gradient (°F/inch)	5.35	4.71	4.48

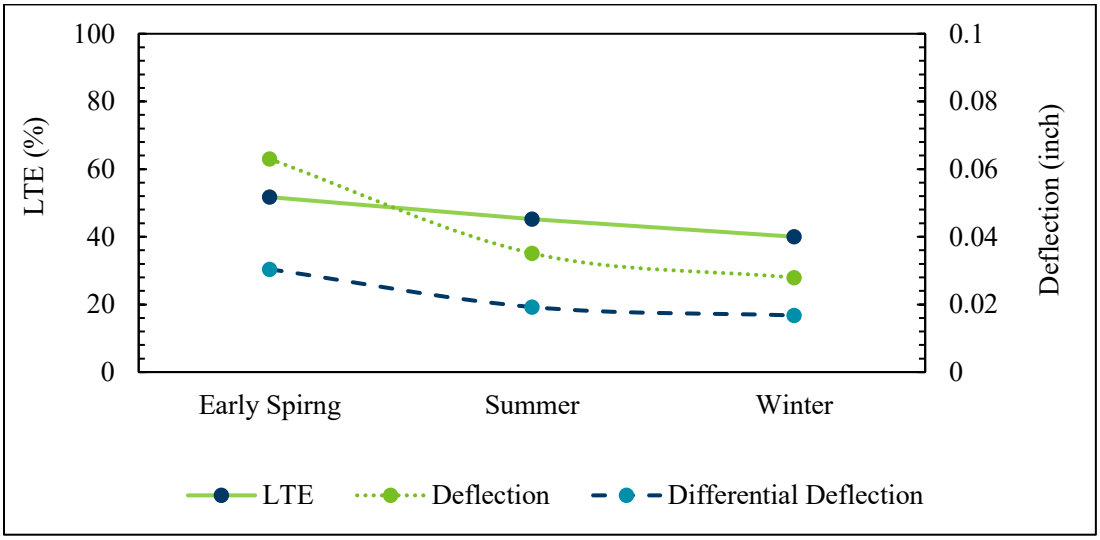

Figure 3.8 Effect of seasonal conditions on joint performance parameters (4" slab, 6" Base).

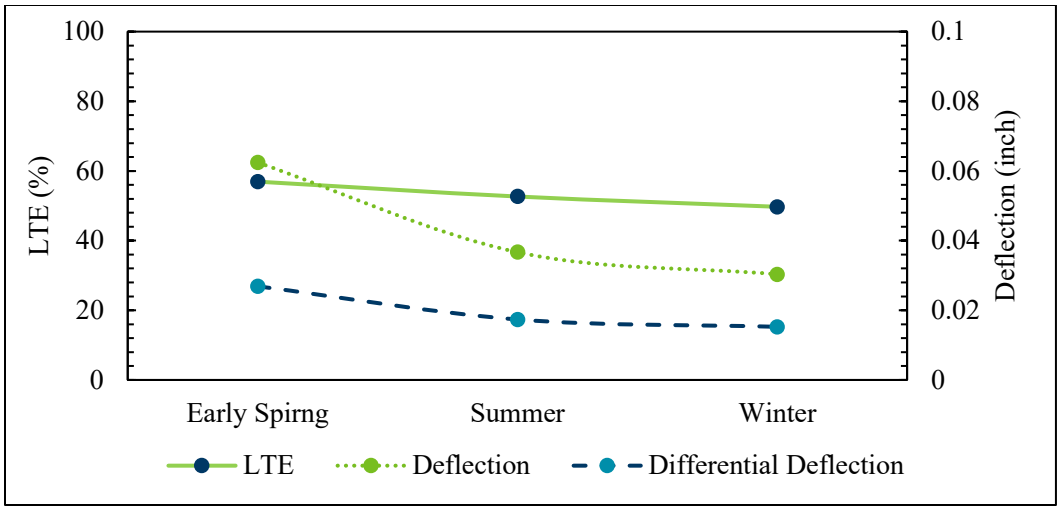

Figure 3.9 Effect of seasonal conditions on joint performance parameters (4" slab, 11" Base).

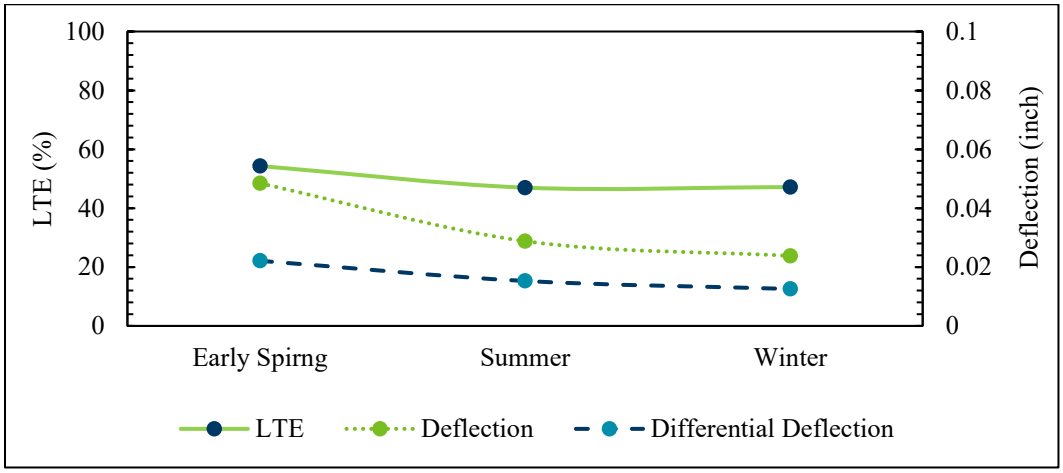

Figure 3.10 Effect of seasonal conditions on joint performance parameters (6" slab, 6" Base)

Chapter 4: DESIRED JOINT PERFORMANCE

This chapter focused on establishing the desired joint performance of the thin concrete pavements so that the pavement does not fail by transverse joint faulting within the design life. Transverse joint faulting, international roughness index and the load transfer efficiency (LTE) of two MnROAD cells are analyzed and discussed in this chapter. The possible LTE from the base layer and foundation, aggregate interlocking and the needed LTE from the fibers are established in established.

4.1 Critical distress, terminal IRI, and transverse joint faulting

The performance of the MnROAD's fiber reinforced concrete test sections (Barman et al., 2021) indicated that the critical distress of the thin concrete pavements was the transverse joint faulting, which increased the road roughness beyond the allowable limit. The international roughness index (IRI) is considered a standard measure of pavement roughness and ride quality (Izevbekhai and Akkari, 2011) and the terminal IRI is defined as 170 inches/mile (Elbheiry et al., 2011). In the case of thin concrete pavements and overlays, the limited aggregate interlock of the thin slabs below the saw cut is insufficient to provide the desirable joint load transfer. Fiber reinforced concrete was found to improve the joint load transfer and decrease the transverse joint faulting and IRI when sufficient fiber dosage was implemented (Barman et al., 2021). To understand the desirable joint performance of the thin concrete pavements and the required contribution from structural fibers, the IRI results of two MnROAD cells are compared in Figure 4.1. The two cells considered here are Cells 506 and 806, which were 5-inch-thick pavements constructed over an 11-inch thick granular/stabilized base layer. Cell 506 was constructed with plain concrete, and Cell 806 was a thin fiber reinforced concrete pavement. The typical design equivalent single axle load (ESAL) for such thin concrete is about 2 million and is usually recommended for low and moderate-traffic volume roads. The trend of the IRI data for Cell 806 in Figure 4.1 shows that the IRI reaches the terminal value of 170 inches/mile at around 2 million ESALs, which fortunately meets the anticipated design ESAL as mentioned above. The IRI of Cell 506 at 2 million ESALs was about 200 inches/mile and was above 170 inches/mile even at 1 million ESALs. It may be noted that short slabs at MnROAD test sections usually result in high initial IRI values because of more number of transverse joints.

The transverse joint faulting results of these two cells, shown in Figure 4.2, indicate the influence of the fibers as well. Joint faulting of Cell 506 was always higher than Cell 806. The faulting magnitude of Cell 506 was more than twice that of Cell 806. Interestingly, the average joint faulting of Cell 806 at 2 million ESALs reached 0.1 inch, which is the terminal faulting value for concrete pavement in California (Mack et al., 2012). It may be noted that the effect of the transverse joint faulting on the IRI is more in the thin concrete pavements and overlays because of the small slab size (e.g., 6 ft x 6 ft) or high number of transverse joints compared to thick and large-slab conventional pavements. The correlation between the IRI and transverse joint faulting established from the data of Cells 506 and 806 is shown in Figure 4.3. Based on the above-mentioned discussion on the IRI and transverse joint faulting trend of Cells 506 and 806, it can be assumed that the performance of Cell 806 met the performances (IRI and joint

faulting) anticipated from a successful thin concrete pavement. However, the relatively high dosage of fiber in Cell 806 compared to normal fiber dosages, would likely result in a much higher cost for the concrete. It may be noted that there were two more cells (Cells 606 and 706) constructed with the above mentioned two cells. Out of all the four cells, the joint performance of Cell 806 was only found to satisfactory throughout the anticipated design life (Barman et al., 2021).

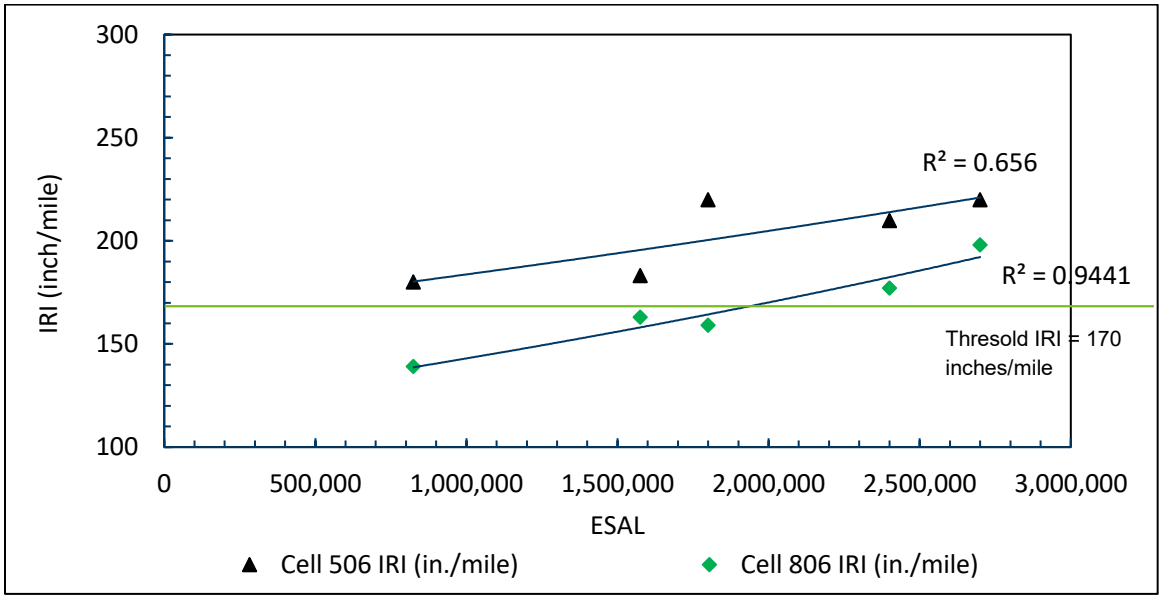

Figure 4.1: IRI of the MnROAD Cells 506 (plain concrete) and 806 (FRC with 11.7 lb/yd^3 fiber dosage).

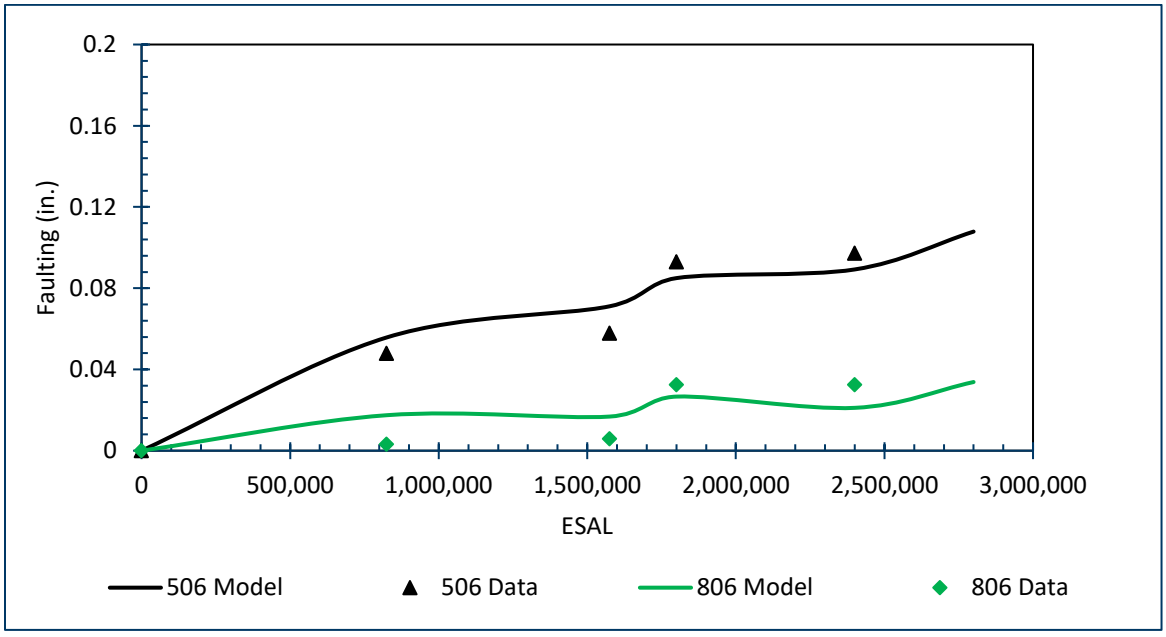

Figure 4.2: Faulting of the MnROAD Cells 506 (plain concrete) and 806 (FRC with 11.7 lb/yd^3 fiber dosage).

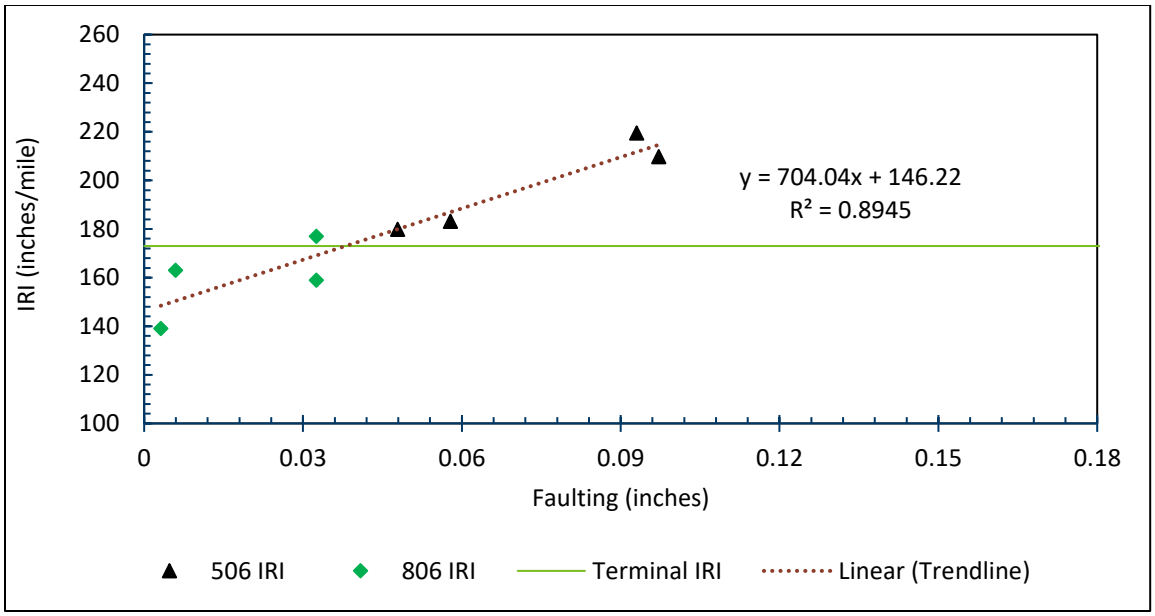

Figure 4.3: Relationship between faulting and IRI for thin concrete pavements.

4.2 Desired joint load transfer from the structural fibers

Figure 4.4 shows the LTE data of the driving lane of Cells 506 and 806 measured at different times between September 2017 (after construction) and January 2021 (when the joint performance became significantly low) (Barman et al., 2021). During this period, Cells 506 and 806 carried close to 3 million ESALs (beyond the typical design life). This figure shows that the LTE of Cell 806 varied between 85% to 90% for the first one million ESALs and then dropped to 60% at 2 million ESALs. For cell 506, the LTE was 60% or lower for most of the service life, except for a couple of measurements, including the very first one, which was taken at ~2 months after the construction. The comparison of the LTEs between Cells 806 and 506 indicates that the FRC cell exhibited about 30 to 40% higher LTE on average than the plain concrete cell. Fortunately, this additional LTE was enough for Cell 806 to yield the desired performance level by keeping the IRI below 170 inches/mile until 2 million ESALs. This finding assures that structural fibers can improve the performance of thin concrete pavements. Figure 4.5 shows the comparison of the maximum deflections of the slab under the FWD load plate for Cells 506 and 806; the average slab deflection of Cell 506 was 50% to 60% higher than that of Cell 806. In summary, it can be stated that for a successful thin concrete pavement, the structural fibers shall provide 30 to 40% joint load transfer and decrease the slab deflections by at least half.

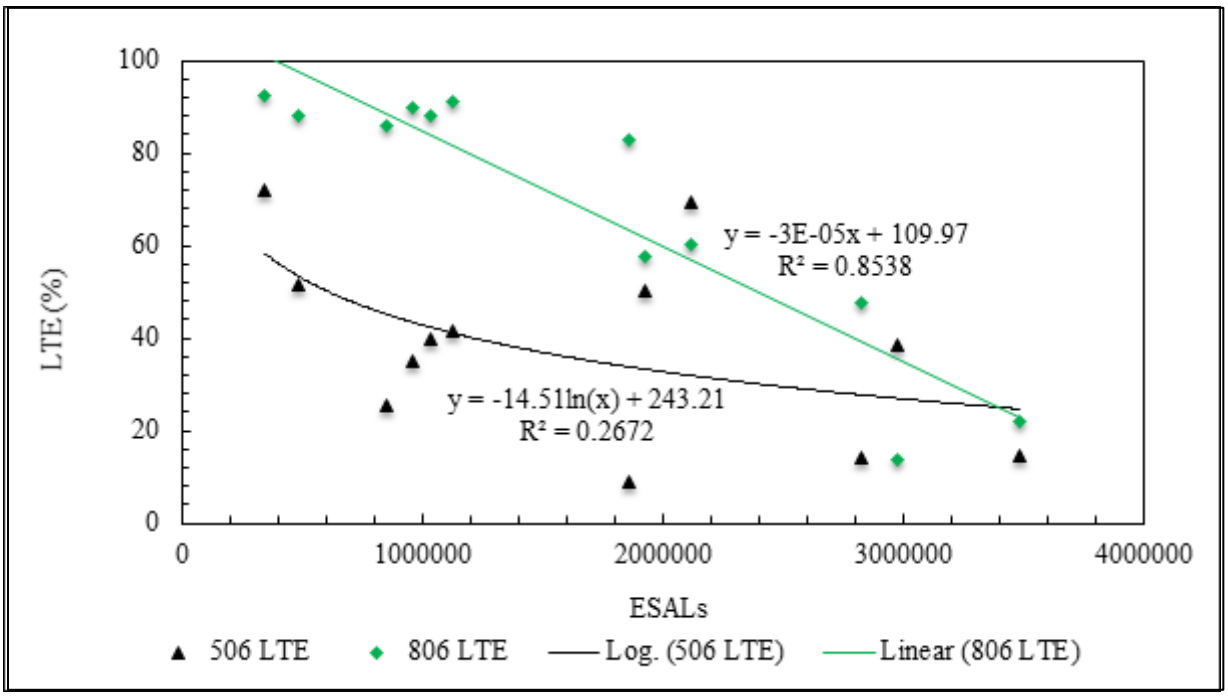

Figure 4.4: Joint load transfer of Cells 506 and 806.

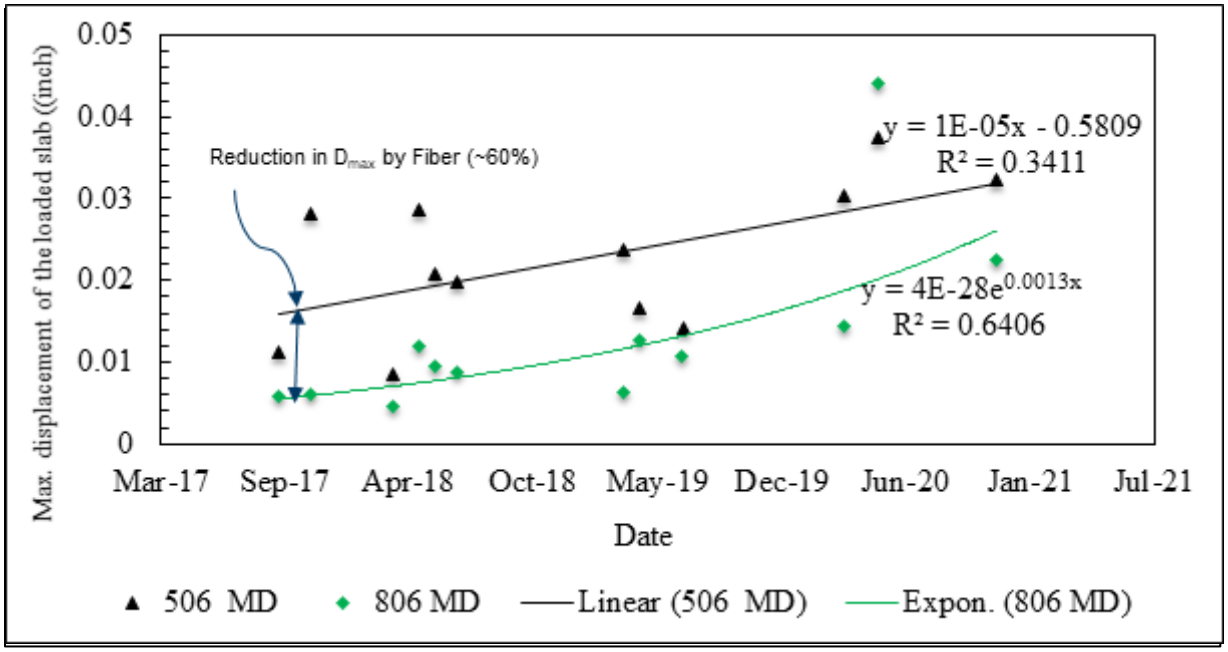

Figure 4.5: Maximum slab deflection under FWD load for Cells 506 and 806.

4.3 Joint load transfer from aggregate interlock and base layer

In thin FRC pavements, the transverse joint load transfer occurs through three different mediums, (i) base layer (and the foundation), (ii) aggregate interlock, and (iii) structural fibers. In the previous chapter, the load transfer by these three components was modeled using a finite element analysis, considering various designs, seasons, joint stiffnesses, and temperature-induced load combinations. The FEM results showed that around 30% to 50% LTE is contributed by the base layer (and the foundation), depending on structural design, including base layer thickness and season. See Figure 3.6, Figure 4.6 and Figure 4.7. In these figures, LTEs for various joint stiffnesses are presented for some possible thin concrete pavement designs for the early spring (the weakest condition of the base layer and foundation) and winter (the strongest condition) seasons. When the joint stiffness (K_z) is zero, the contribution from the concrete slab is nil, or in other words, the load transfer is only provided by the base layer (and the foundation).

The FEM results presented in the previous chapter and FWD test results presented in this chapter were used to establish ranges of the LTEs for the three joint load transfer mediums. From the FEM analysis, it was found that the base layer (and the foundation) can provide up to 30% to 40% (conservatively) LTE. The difference between the LTEs of Cells 806 and 506 indicates that the structural fibers can and should provide about 30% to 40% LTE. The difference between the Cell 506 LTE and the base layer's LTE (from FEM analysis) indicates that the aggregate interlock-based LTE is about 15-20%. Figure 4.8 shows the split of the LTEs by the above-mentioned three mediums.

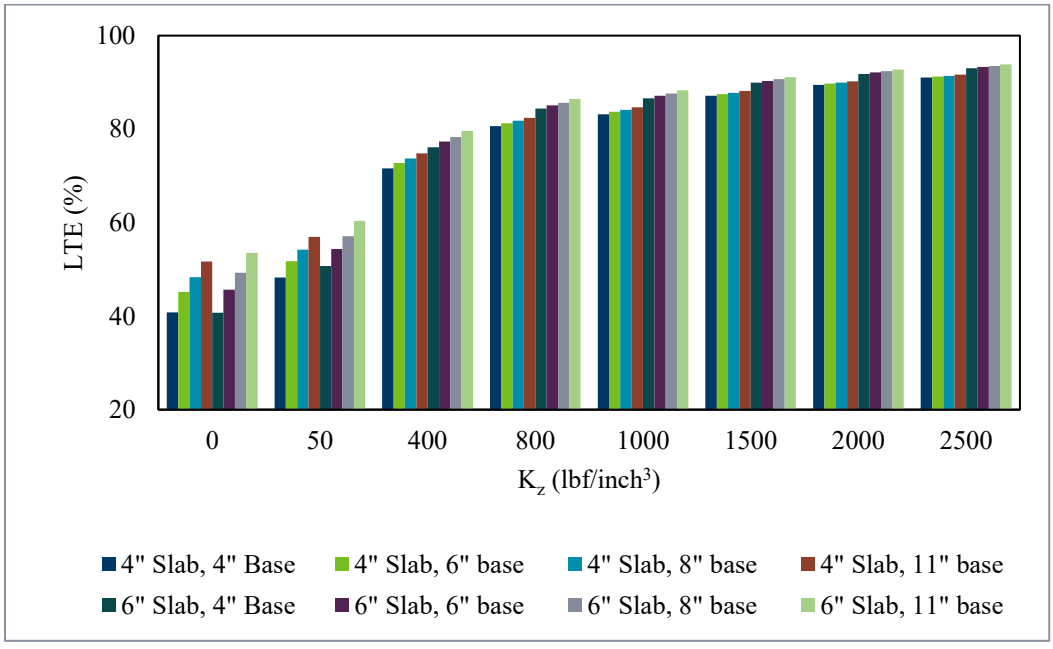

Figure 4.6: LTE vs. joint stiffness for various designs in the early spring season.

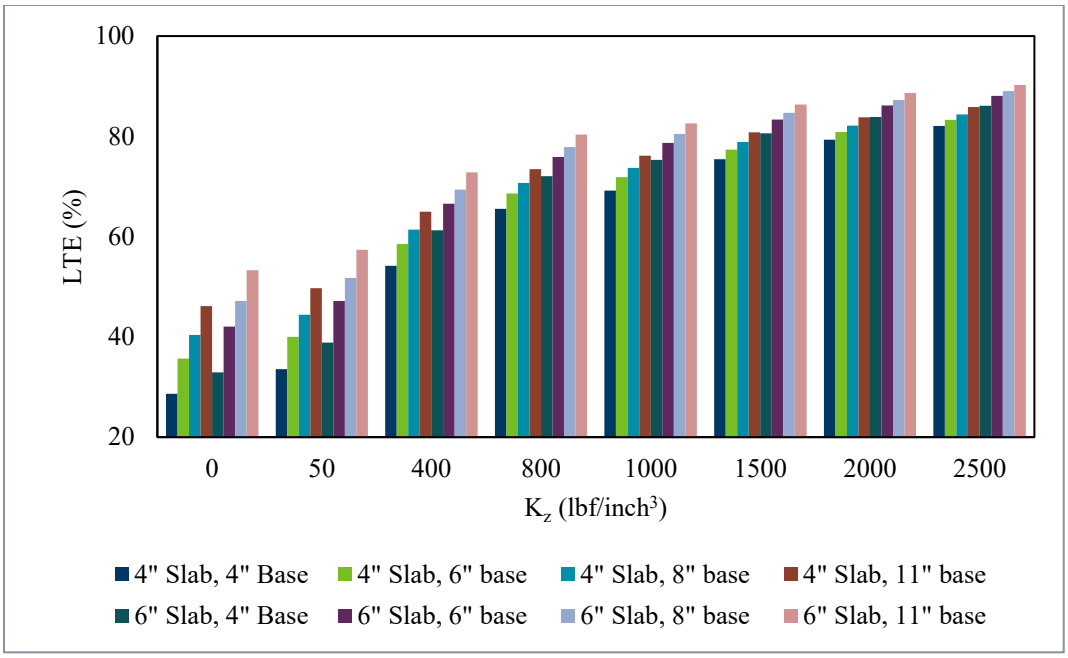

Figure 4.7: LTE vs. joint stiffness for various designs in the winter season.

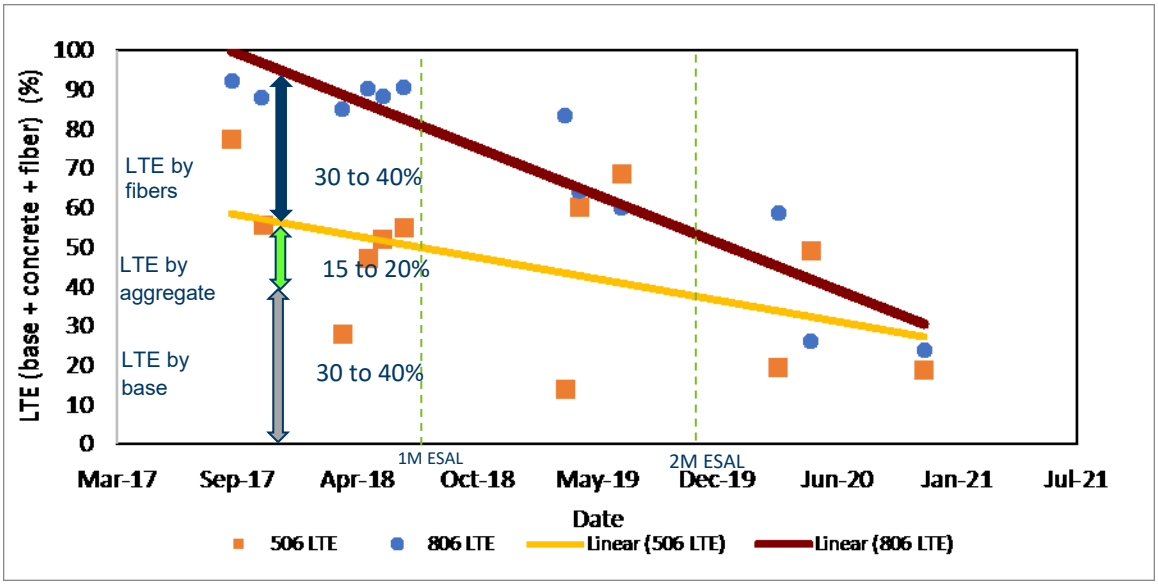

Figure 4.8: LTE contribution of base, aggregate interlocking and fibers.

Figure 4.9 shows the relationship between the LTE and vertical joint stiffness (K_z) established from the FEM results, for three different designs. While the thickness of the slab increases the LTE, the increment is much less. In this figure the LTE contribution by the base layer is not included; only the LTEs by the fibers and aggregate interlock are considered. It can be seen that for the initial ~30% LTE, the joint stiffness requirement is less. But post 30% LTE, the needed K_z for increasing the LTE is much more. From Figure 4.9, where LTE of only aggregate interlock and fibers are considered, the first 15 to 20% LTE can be achieved with relatively less joint stiffness (~250 lbf/inch^3), which can be achieved from the aggregate interlock. The remaining LTE will be contributed by the fibers.

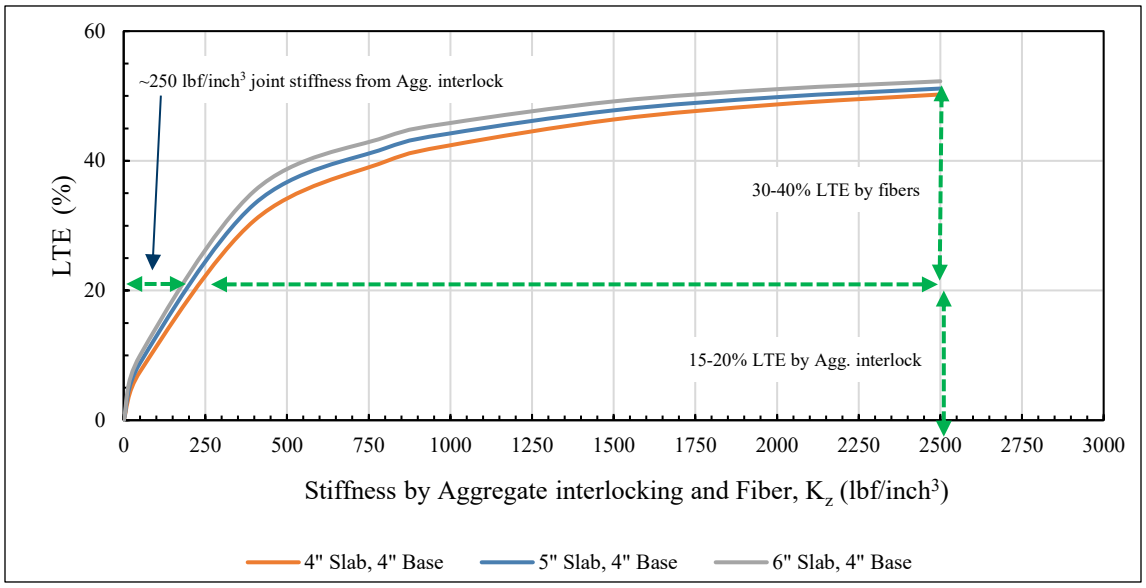

Figure 4.9: LTE vs vertical joint stiffness from aggregate interlock and fibers (Kz)

Chapter 5: ACCOUNTING FOR THE CONTRIBUTION OF FIBERS

This chapter focuses on establishing a method to account for the fibers' contribution and introduces a parameter to characterize the fibers through laboratory testing. Similar to the "modulus of dowel bar support, K_d" concept (Timoshenko, F., 1940; Huang, Y. H., 2004) for the conventional concrete pavement, this study established the "modulus of fiber support", K_f for thin FRC pavements. The needed value of K_f to help improve the joint load transfer of the thin concrete pavements and overlays is established to meet the desired performance (with respect to faulting and IRI) over the design life.

5.1 Modulus of fiber support K_f through FEM

Chapter 3 of this report included the results of the FEM analysis. Figure 5.1 shows the relationship between the LTE vs joint stiffness, K_z. The two graphs (Figure 5.1 a and b) are drawn using the data from the FEM modeling of the MnROAD Cell 806, which had 5 inches thick slab over 11 inches thick base layer. The base layer seems to be providing around 53% LTE (LTE at 0 joint stiffness (K_z = 0), Figure 5.1 (a)) for this Cell as per the FEM analysis. K_z is the joint stiffness provided by the aggregate interlock and fibers together. As discussed in Chapter 4, the aggregate interlock joint stiffness is around 250 lbs/ inches^3 which can offer up to 20% LTE for 5-inch slabs (based on FEM analysis). The joint stiffness offered by the fibers, referred to as "modulus of fiber support", K_f, and its relationship with LTE is included in Figure 5.1 (b). It can be seen that when the K_f is 2,250 lbs/inches^3, fibers can offer about 25% LTE. However, a significantly higher K_f is required to further increase LTE beyond 25%, and only 30% maximum LTE can be achieved from the fibers, according to the FEM analysis.

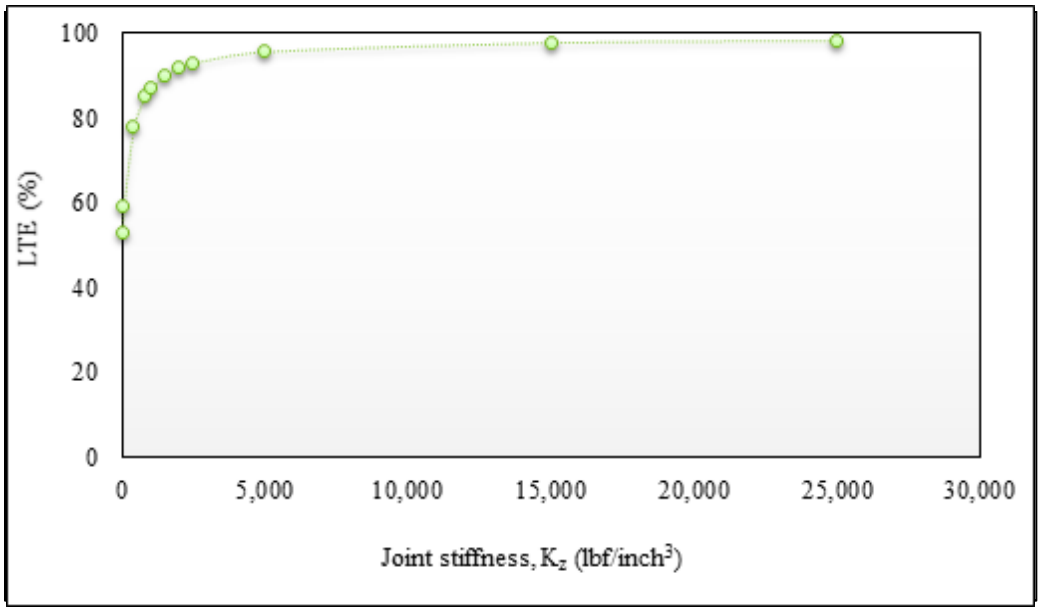

(a) Joint stiffness by fibers and aggregate interlock.

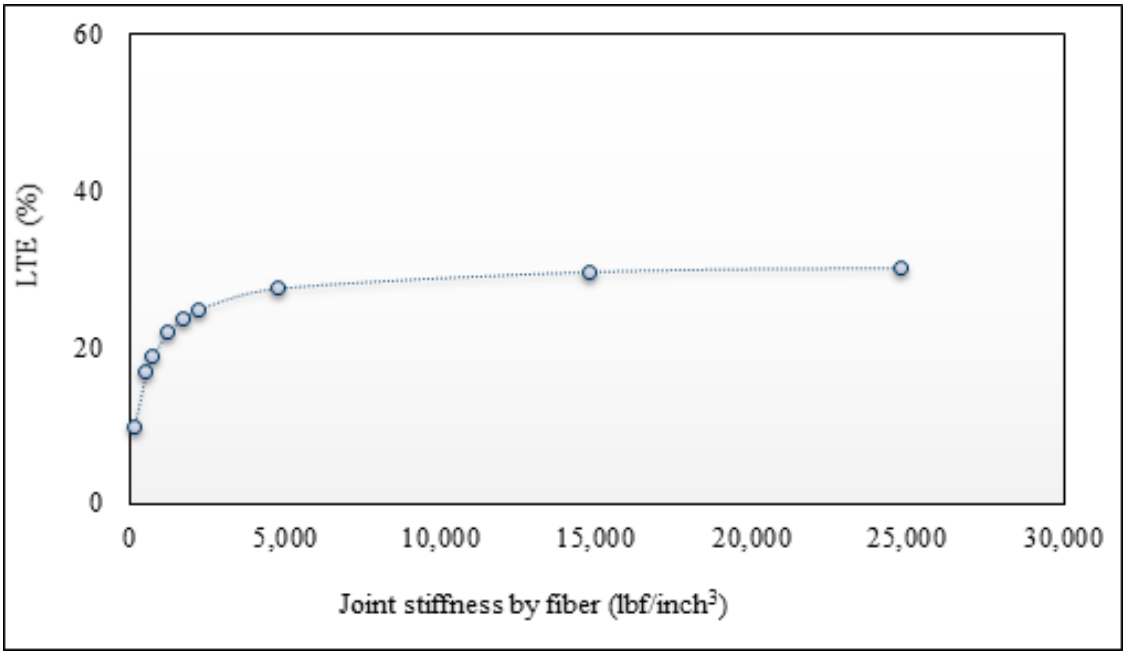

(b) Joint stiffness by only fibers.

Figure 5.1: LTE vs joint stiffness from FEM analysis.

5.2 Modulus of fiber support K_f from FWD data

As the FEM analysis included several assumptions and may not exactly represent the field conditions, the FWD data collected for Cells 506 and 806 were used to investigate the relationship between the joint stiffness and LTE in the next effort. FWD deflection data were used to determine the LTE, and joint stiffness, K_z. The joint stiffness is calculated using the following Equation.

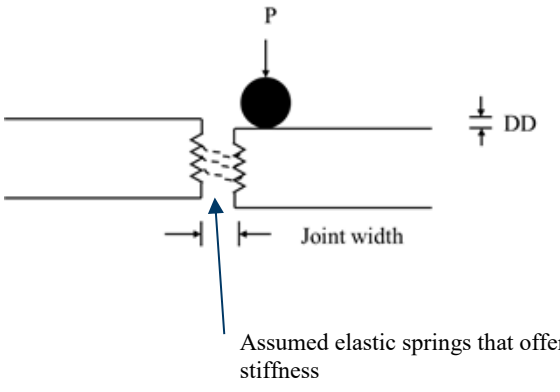

$$k_z = \frac{P}{l.h'.DD} \qquad (3)$$

Where,

k_z= Joint stiffness provided by aggregate interlock and fibers together

P= Wheel load

l= Radius of relative stiffness

h'= Thickness of the slab below saw cut

DD= Differential displacement between the loaded and unloaded slab

$$l = \left(\frac{E_c h^3}{12(1-\mu^2)k}\right)^{0.25} \quad (4)$$

Where,

h= Thickness of the slab

E_c= Modulus of elasticity of concrete

μ= Poisson ratio

k = Modulus of subgrade reaction

It is assumed that the differential displacement between the slabs at the joint is similar to the elastic deformation of the spring assumed in the FEM analysis. The joint stiffnesses (K_z) calculated for Cells 506 and 806 are provided in Figure 5.2. As anticipated, the K_z for Cell 806 was significantly higher than for Cell 506. The difference in the K_z values of these two cells is attributed to the contribution of the structural fibers in Cell 806. Therefore, the K_f for the FRC Cell 806 was computed as below.

K_f = K_z of Cell 806 – K_z of Cell 506 (5)

Figure 5.3 shows the K_f of Cell 806 against ESALs. It appears that the K_f of Cell 806 was around 4,500 lbf/inch^3 at the beginning of the service life, which then decreased with the ESAL and reached ~500 lbf/inch^3 at 2 million ESALs. Figure 5.4 shows the relationship between LTE and K_f computed from the FWD data; the general trends in the graphs are comparable to the trends observed in graphs plotted using FEM-generated data (Figure 5.1). The noticeable difference between the two figures is in the maximum LTE contribution by fibers; FWD results showed as much as 45% LTE can be achieved from the fibers as opposed to 30% for FEM analysis. Figure 5.4 is an important output of this study as it determines the required K_f for a desired level of joint load transfer; for example, if the required LTE from the fibers for a project is 40% (or the total LTE is about 95%), then enough fibers shall be used in the concrete which can provide a K_f of 3,000 lbf/inch^3.

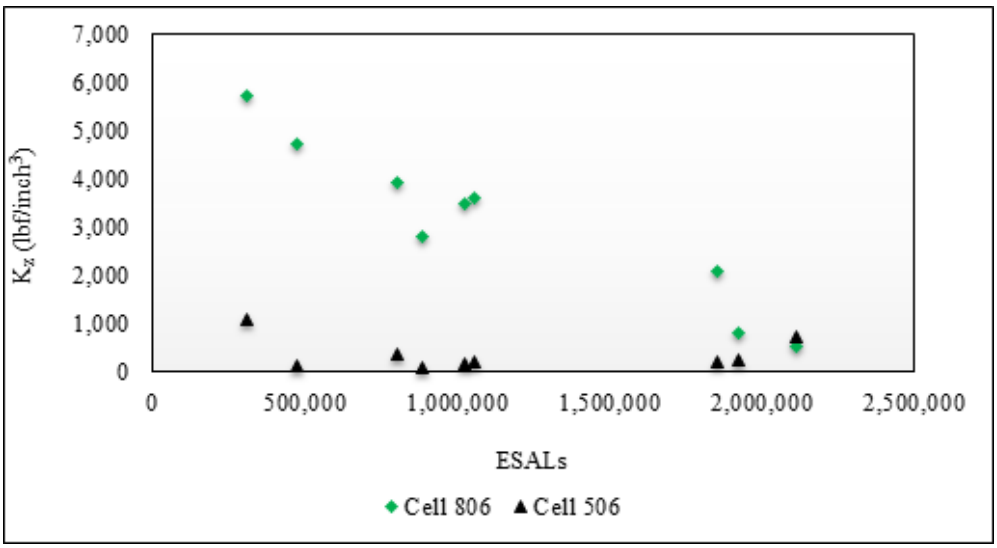

Figure 5.2: Joint stiffness, Kz of Cells 506 and 806 vs. ESALs

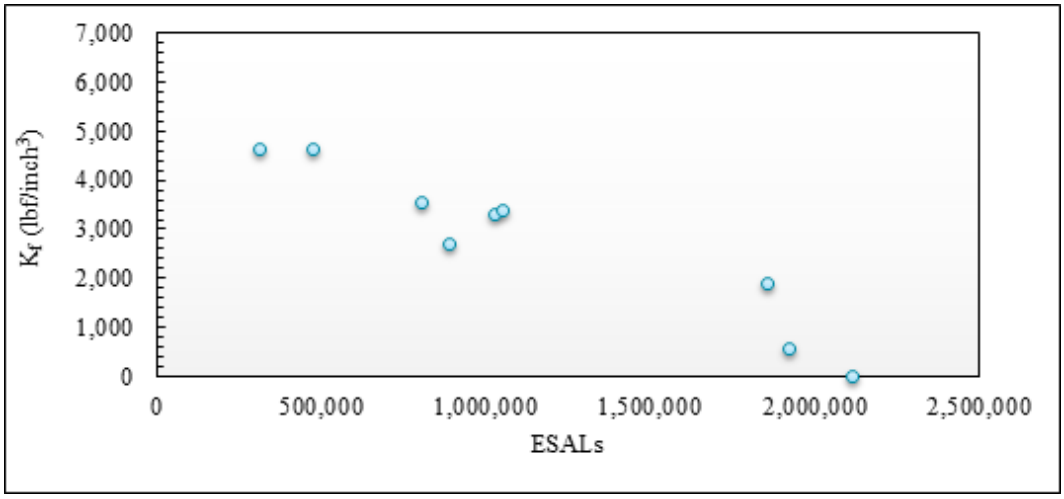

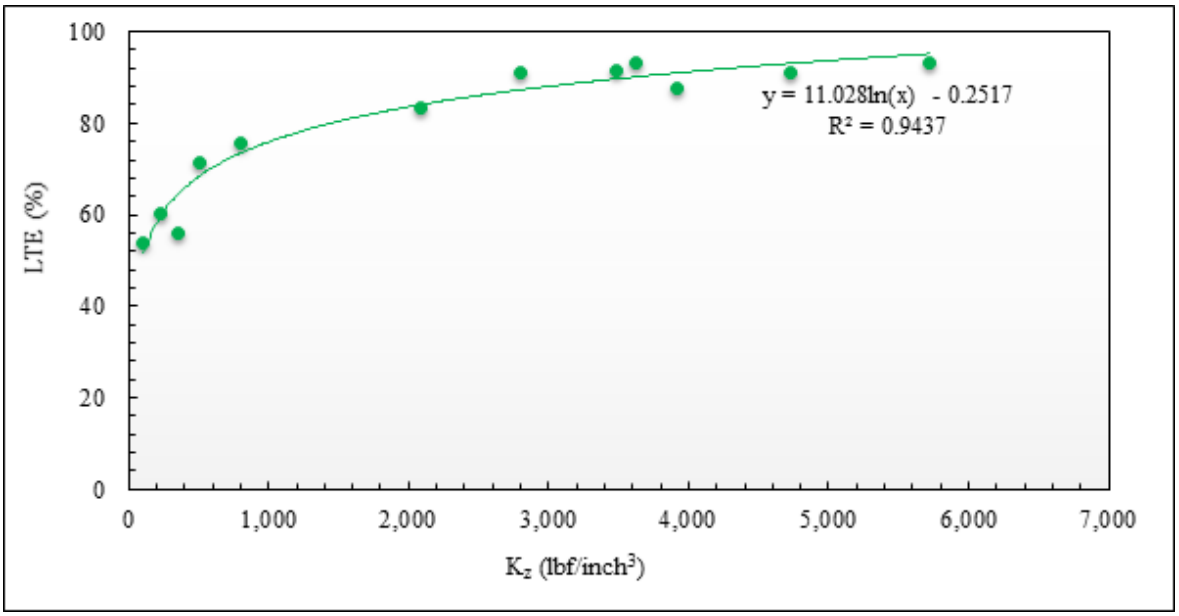

(a) LTE vs joint stiffness by fibers and aggregate interlock.

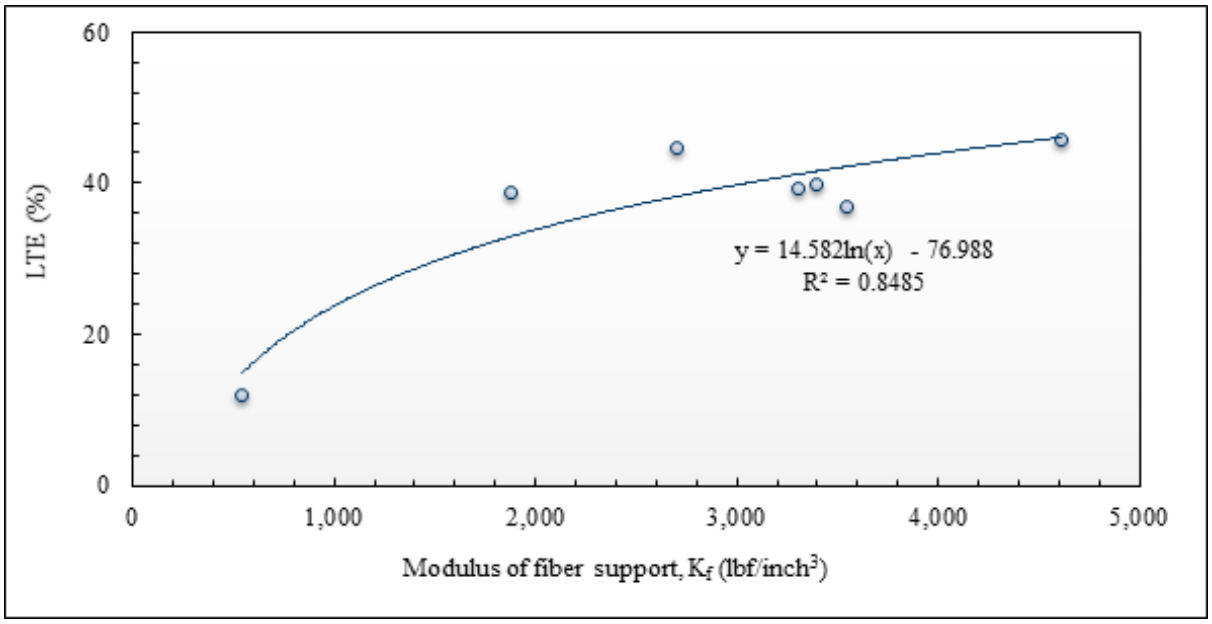

(b) LTE vs joint stiffness by only fibers.

Figure 5.4: LTE vs joint stiffness from FWD data analysis.

5.3 Laboratory test method to determine K_f

After developing the correlation between LTE and the modulus of fiber support, K_f, the next important task is to develop a procedure to determine the K_f using a laboratory test setup. This will facilitate testing FRC before the construction of the project to (i) optimize the fiber dosage and, (ii) also to develop the pavement-specific fibers in Phase 2 of this project.

As discussed in Chapter 2, the University of Pittsburgh developed a small-scale LTE test setup in 2014 under the supervision of Dr. Julie Vandenbossche, which is described in the PI's Ph.D. Dissertation (Barman, 2014). In this test setup, 24-inch x 6-inch x 6-inch size beams can be tested to determine the joint performance. A similar test setup was also fabricated at the UMD as shown in Figure 5.5.

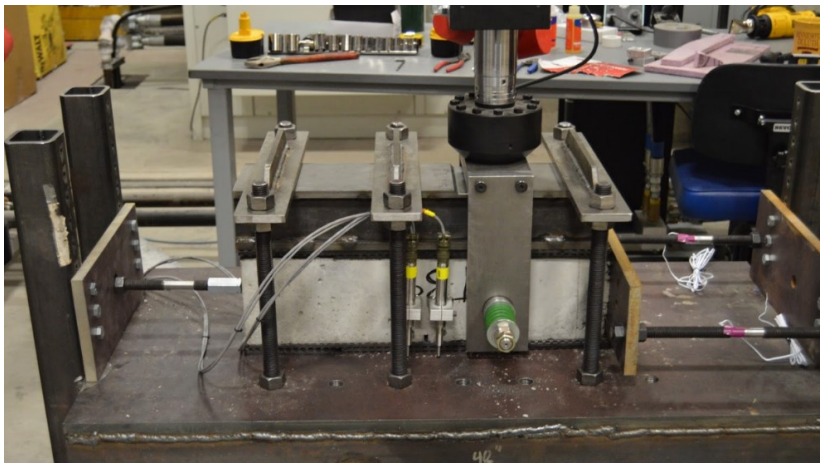

Figure 5.5 UMD's joint load transfer test setup (originally developed at the University of Pittsburgh).

The joint performance test was conducted for FRC beams with different volume fractions of fibers (0.25%,0.5%,0.75%) and PCC beams for comparison. Some beams were tested under the scope of a previous study. Table 5-1 shows the number of beams considered for the analysis.

The type of fiber for the lab study and MnROAD's Cell 806 was the same; Cell 806 was constructed with 0.75% V_f fiber dosage (11.70 lb/yd^3). It may be mentioned that the mixture designs of the MnROAD Cell 806 concrete and the laboratory concrete were not identical, and neither were designed based on the PEM procedure. As fibers contribution was determined by deducting the joint performance of the plain concrete from the corresponding FRC concrete, the effect in the concrete mixture design was neutralized. ASTM Type I cement was used for preparing concrete. Table 5-2 shows the base concrete design for the mixtures used in this study. Note that the mix used in the joint performance test was not PEM based mix. Both the volume fraction and mass of the ingredients are provided in this table. The air-entraining admixture (AEA) was increased for an increase in fiber dosage to maintain an entrained air content in the range of 5.5 percent to 9 percent by volume. AEA dosage ranged between 0.98 to 1.06 ounces per 100 lbs of cement. Mid-range water reducer was used as needed to achieve the required workability.

Table 5-1 Joint performance test details

Fiber volume fraction	Number of beams tested
0 (PCC)	3
0.25 %	3
0.50 %	5
0.75 %	3

Table 5-2 Base mixture design for joint performance beam samples

	Volume (%)	Approx. Mass (lb/yd^3)
Cement (Type I)	11.6	615.0
Coarse Aggregate	42.0	2024.0
Fine Aggregate	25.1	1188.8
Potable Water	13.9	233.7
Fibers	varied	varied
BASF MasterAir® 400 (fl. Oz)	-	6.08
MasterPolyheed® 1020 (fl. Oz)	-	36.5

Figure 5.6 shows the LTE vs. crack width relationship for various dosages of fibers. This figure shows that the test setup could capture the contribution of the fibers, with the highest LTE recorded for the concrete with 0.75% V_f fiber dosage. The plain concrete resulted in the lowest LTE. The differential deflection data measured in the lab test was used to determine the joint stiffness (K_z) using the same procedure that was used for the FWD data as discussed in the previous section.

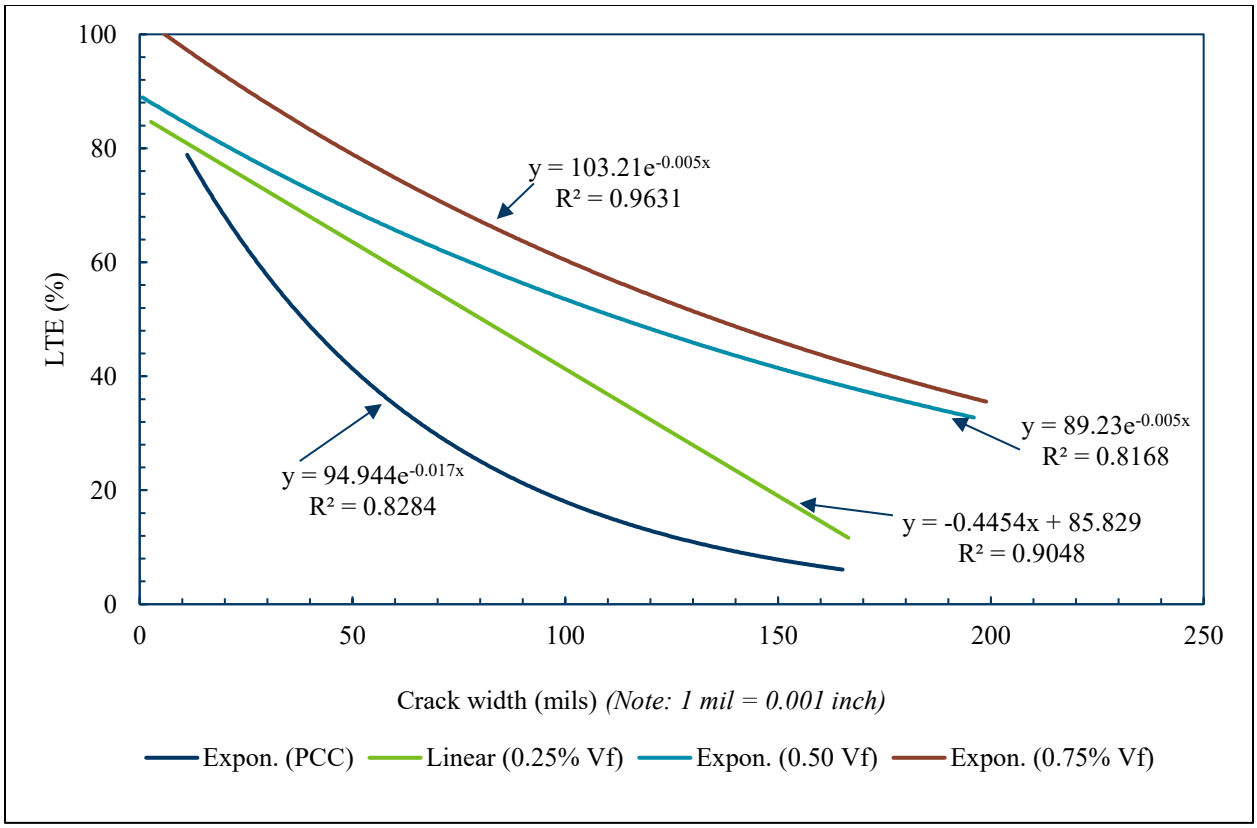

Figure 5.6: LTE vs. crack width for concrete with different fiber volume fractions (lab test result).

Figure 5.7 compares the joint stiffnesses of the plain concrete and FRC with 0.75% V_f (same as the Cell 806) at an increasing crack width. The difference in the K_z values between the FRC and plain concrete beams is the K_f from the laboratory data and is comparable to the K_f calculated from the FWD data. Figure 5.8 shows the relationship between the K_f and crack width. As the fibers' contribution varies with crack width, it is important to determine a representable crack width at which the K_f or modulus of fiber support shall be determined. To this point, the possible crack widths were investigated from multiple angles, such as (i) the measured joint width movement of Cell 806, (ii) the theoretical value of the crack width opening because of the temperature change and shrinkage, and (iii) the LTE vs K_f relationships for various cracks widths using the laboratory test results.

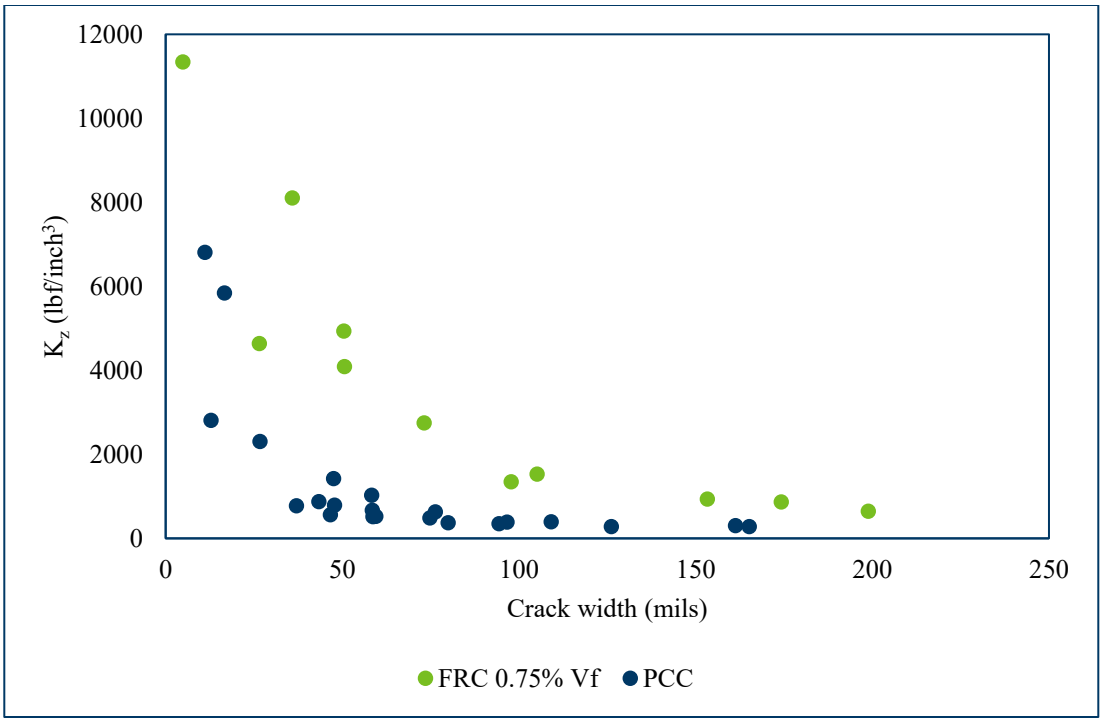

Figure 5.7: Comparison of the joint stiffness vs. crack width relationships between plain concrete (same as Cell 506) and FRC with 0.75% V_f fibers (same as Cell 806).

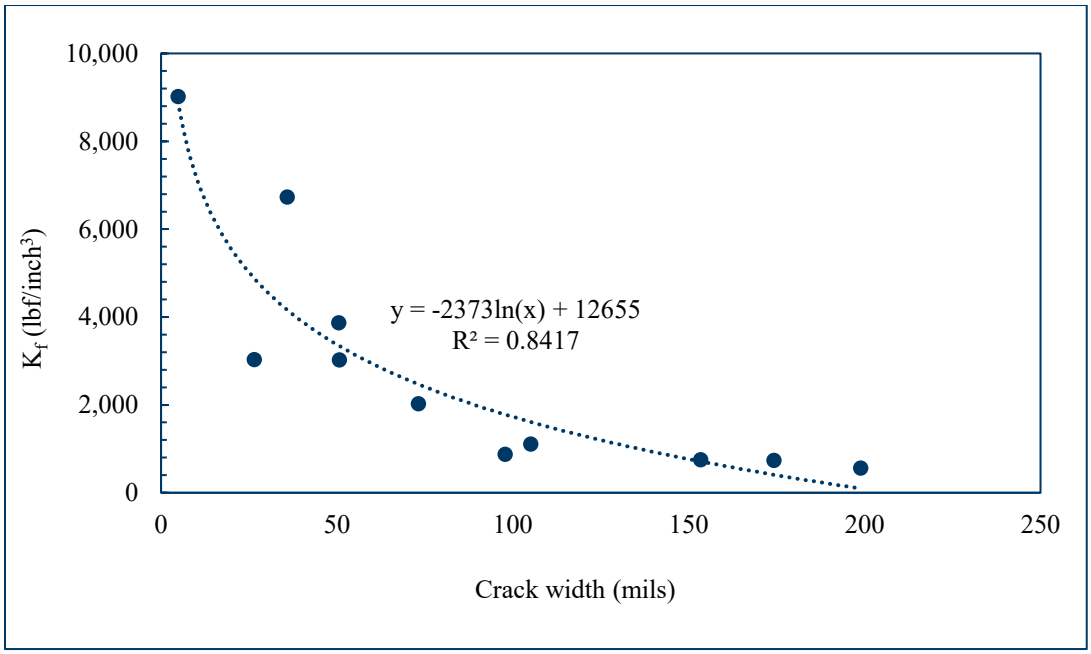

Figure 5.8: K_f vs. crack width relations for FRC with 0.75% V_f fibers (same as Cell 806).

Figure 5.9 shows the measured joint width movement of Cell 806 (Barman et al., 2021). Three joint width measuring sensors were installed in Cell 806. Except for some outliers of Sensor 2, three sensors showed that the joint movements were within 40 to 80 mils (1 to 2 mm) for the first 1.5 million ESALs (Dec 2019) and then opened significantly, indicating the decrease in the effectiveness of the fibers in holding the cracks tight. The joint width movement data collected after Feb 2019 indicates that slabs were experiencing large movement, maybe even sliding of the slabs over that base layer.

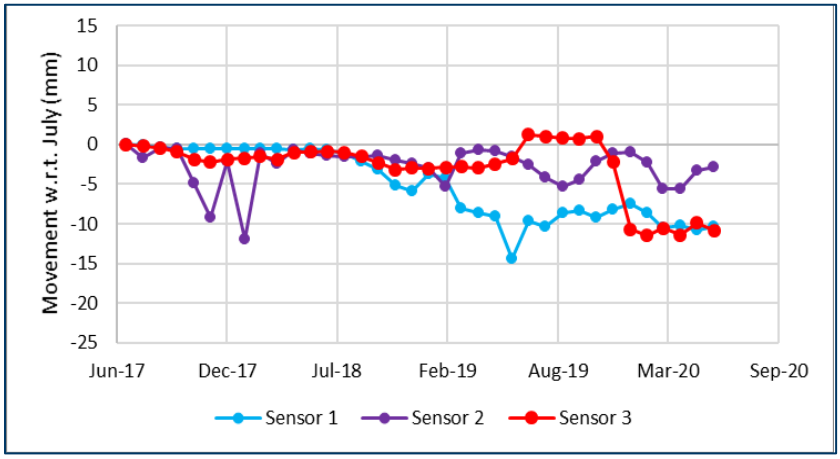

Note: 25.4 mm = 1 inch; 1 inch = 1000 mils.

Figure 5.9: Crack width movement of Cell 806 (Barman et al., 2021).

The theoretical crack width opening for 6-ft-long slabs due to maximum possible seasonal temperature change and shrinkage strain is calculated using the following equation.

$$\Delta L = C\,L\,(\alpha\,\Delta T + \varepsilon) \qquad (6)$$

Where,

ΔL = the expected change in slab length, in (mm)

C= the subbase/ slab frictional restraint factor (0.65 for stabilized material, 0.80 for granular material

L= the slab length, in (mm)

α = the PCC coefficient of thermal expansion

ΔT = the maximum temperature range (generally the concrete temperature at placement minus the minimum ambient temperature in January, °F (°C)

ε = the shrinkage coefficient of concrete

For 6-ft-long slabs and with the following assumed variables as α = 5.3 x 10-6/°F, ΔT = 100°F, ε = 0.0003, and C = 1.5, the crack width is approximately 90 mils or 0.09 inches.

Figure 5.10 shows the relationships between LTE and K_f for various crack widths (40 to 100 mils). It may be noted that the fibers' contribution remains the largest only at a certain crack width range. At a lower crack width, the contribution of fibers is less because of the high aggregate interlocking. When the crack width is excessively wide, the fibers are stretched beyond their elastic limit and the contribution from the fibers becomes less. Figure 5.10 shows the LTE contribution from the fibers maximized at 60 mils crack width, below which the LTE is less for a given K_f. The K_f decreases above 60 mils crack width for a given LTE because of the increase in the differential deflection.

From the above discussion, it may be concluded that consideration of a 60-mil crack width for determining the K_f may be the best approach. Figure 5.11 compares the LTE vs K_f correlations between the FEM, FWD, and lab test results. As mentioned previously, FEM-generated correlation limits the maximum LTE by fibers to 30%. The FWD-based K_f and the lab-based K_f calculated at 60 mils crack width agree with each other. For example, if the required LTE from the fibers for a project is 40% (or total LTE is about 95%), then enough fibers shall be added to the mixture so that a minimum of K_f of 3,000 lbf/inch^3 is achieved. The influence of fiber distribution is not considered. A large number of beam samples shall be tested to obtain a reliable standard deviation of the results that can be used for determining a required K_f value with higher reliability, e.g., 95%.

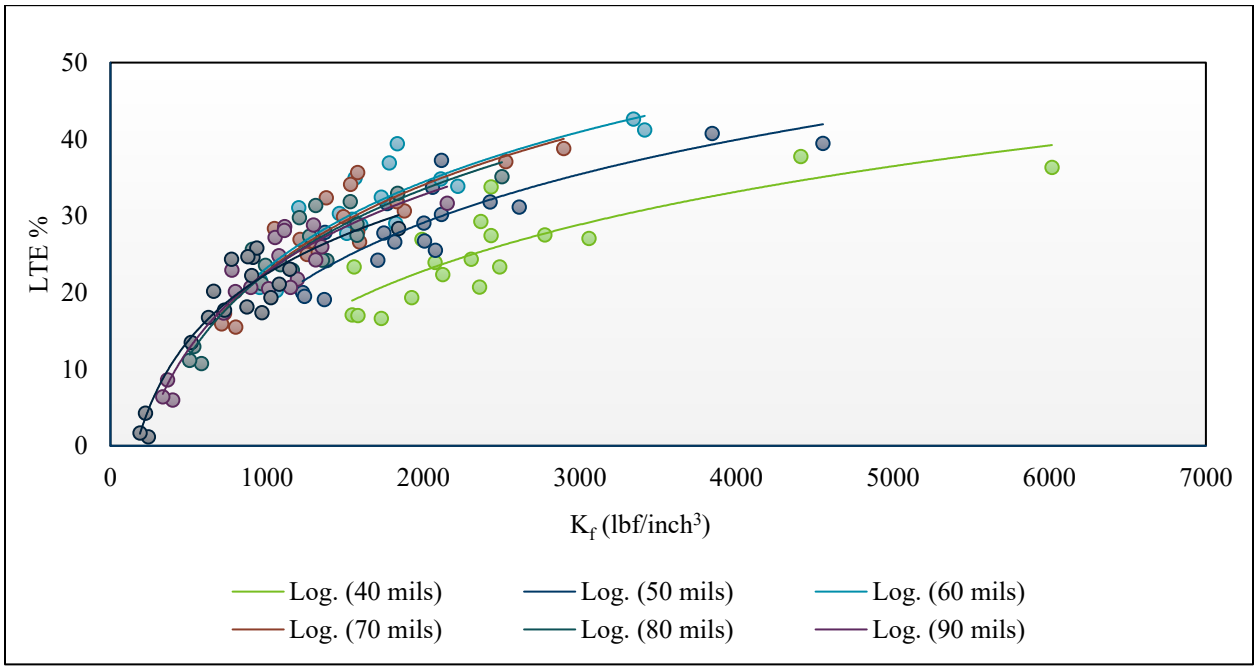

Figure 5.10: LTE vs K_f for various crack widths (laboratory data).

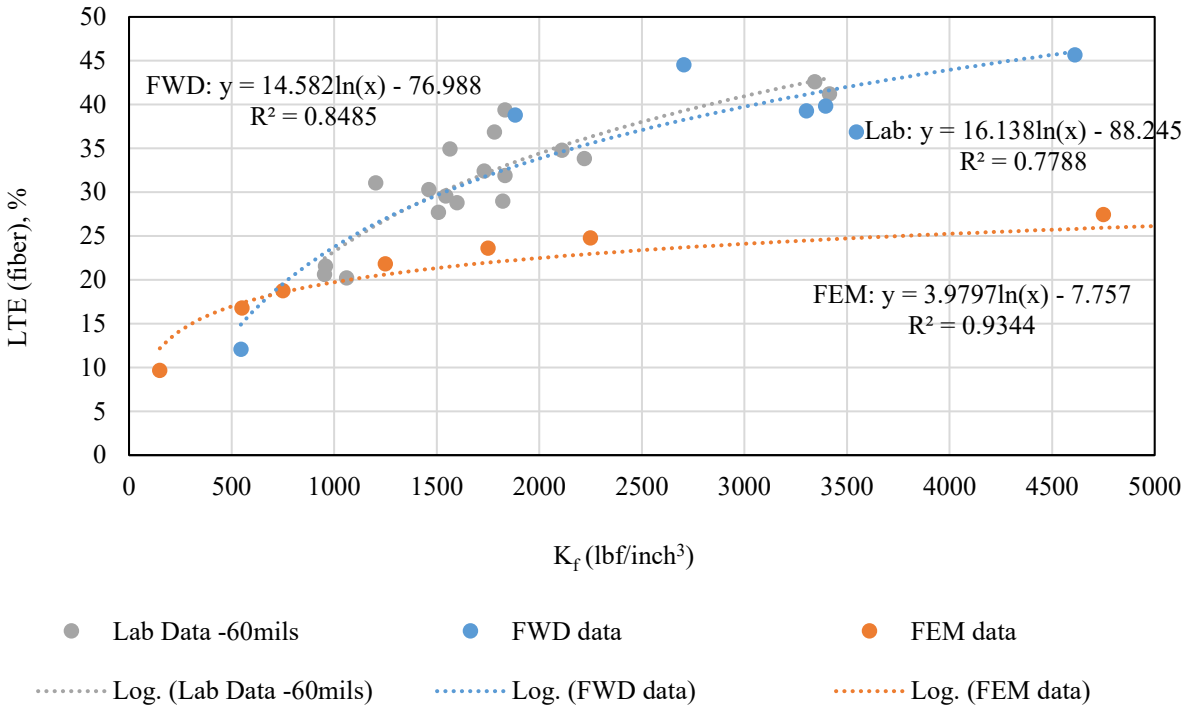

Figure 5.11: Comparison of LTE vs K_f correlations between the FEM, FWD, and laboratory test results.

Chapter 6: SINGLE FIBER PULLOUT TEST

The joint width of thin concrete pavement varies with the season. Crack width expands in winter and contracts in summer. The expansion and contraction of the crack width combined with the wheel load affect the joint load transfer of the fibers. If the expansion of the crack width leads to the pullout and/ or plastic elongation of synthetic fibers, their effectiveness decreases. This study investigated the load-displacement behavior of a few commercially available structural fibers. The purpose of this test to investigate the effect of fiber properties on the load-displacement behavior of fibers embedded in concrete, not necessarily evaluating any fibers in particular. One of the key properties that was investigated is the range of elastic elongation of the fibers embedded in concrete as a function of fiber geometry.

6.1 Single fiber pullout test method

A test setup was developed to conduct the test in which one single fiber embedded in concrete is pulled out using a uniaxial load. The fiber is embedded in the concrete prepared inside a 4-inch x 8-inch plastic mold. Plastic molds were drilled through the bottom using a 7/16-inch drill bit to install a bolt (Figure 6.1), which facilitates the application of the uniaxial load during the testing. A 6-inch-long bolt with a 3/8-inch diameter was attached to the bottom of the mold keeping 1.25 inches of length sticking out of the bottom of the mold. The length of the bold inside the concrete specimen was approximately 4.70 inches.

Figure 6.1: Plastic mold arranged for the single fiber pullout test sample preparation.

An 8-ft long 2-inch x 4-inch wood plank was used as the casting platform. Holes were drilled on the wood plank by using the same 3/8-inch drill bit, 6 inches apart from each other so that plastic molds could be positioned vertically to place and compact the concrete. This allowed the cylinders to sit straight up during and after the casting (Figure 6.2). Once the concrete was compacted in the mold, one single fiber was pushed into the concrete (by hand); the length of the fiber inside the concrete was 0.85 inches, which is equal to half of the length of the shortest fiber used in the study (Figure 6.3). The

embedded length was kept constant for all the fiber samples. It may be noted that the fibers were not included with other ingredients during concrete mixing. Concrete samples were cured in an environmental chamber at 95% relative humidity and 23°C.

Samples were tested using a tensile testing machine with a 1,000 lb capacity load cell, sensitive enough to measure 0.1 lb of load. Each test was run at a constant speed of 0.25 inches per minute. A part of the fibers was coated with super glue and fine sand particles to improve grip and reduce slippage during the testing (Figure 6.4). Fiber pullout tests were conducted in two phases (Phases 1 and 2). In Phase 1, a uniaxial tensile load was applied on the fiber until the failure, i.e. breakage or pullout of fiber from the concrete cylinder. The results from Phase 1 were used to (i) evaluate the effect of concrete ingredients on the peak load and toughness of the fiber embedded in concrete and (ii) elongation of the fiber at the elastic limit. In Phase 2, fiber was loaded multiple times with increasing load to (i) emulate the effect of slab contraction and expansion on the fiber embedded in concrete because of the change of seasons, and (ii) to investigate the effect of the above on the elongation of fiber (embedded in concrete).

Figure 6.2: Casting platform with cylinders installed.

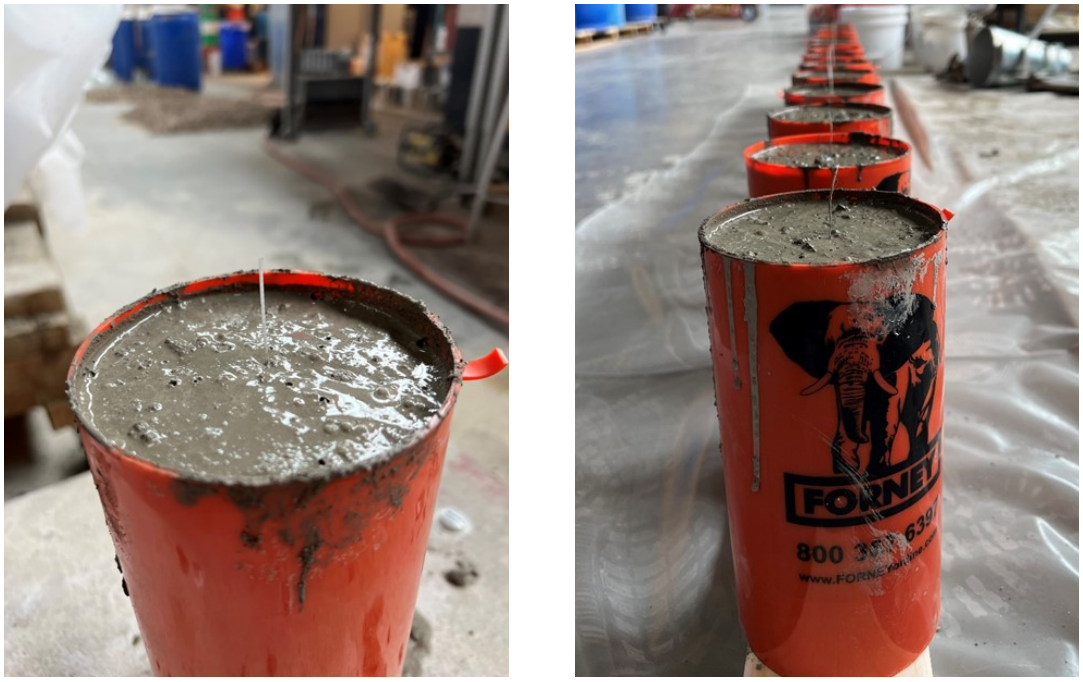

Figure 6.3: Embedded fibers in fresh concrete cylinders.

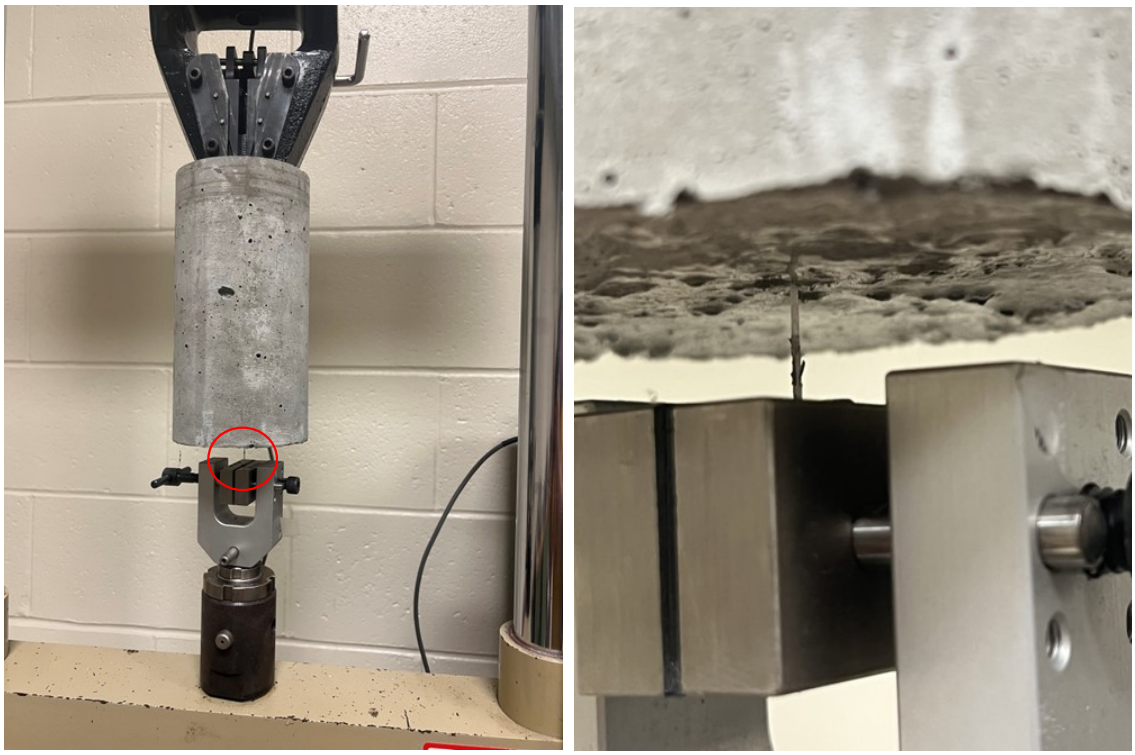

Figure 6.4: Single fiber pullout test in progress.

6.2 Single fiber pullout test, Phase 1

In Phase 1, three aggregate classes (MnDOT Class A, B, and C) and three different cement contents, and four types of fibers (Fiber 1 through 4) were considered. The description of the materials and the test plan matrix can be found in the Appendix. The mixes were designed as per PEM procedure. A tabular summary of the single fiber pullout test results can be found in the Appendix as well. It should be noted that the initial plan was to test fibers at an age of seven days. Due to an unforeseen circumstance, the fibers were tested at 24 to 40 days. Five to eight fibers were tested for each fiber type. However, a separate side investigation was performed to verify the influence of curing age (day) on the peak load and toughness and to implement any correction needed because of the difference in the curing age of the test samples.

6.2.1 Influence of curing age

Fiber 1 was used for this side investigation and two samples were tested at various curing ages, 1, 2, 6, 31, and 36 days. The average toughness (computed from the area of the load-displacement curve) for the fibers tested at different curing ages is shown in Figure 6.5. The fibers tested at 1 day had an average toughness of just under 10 lb-in. This is just over 50% of the average toughness of the fibers tested at 6 days of curing or later. The fibers tested at 2 days had an average toughness of 12.5 lb-in. This is around 67% of the average toughness of the fibers tested between 6 and 36 days of curing. After six days of curing, the average toughness did not increase much with the curing age.

The peak load did not increase between 2 and 6 days of curing (Figure 6.6). This agrees with findings from Singh (2004) that showed curing age has a negligible effect on pullout characteristics of fibers after 2-3 days. As all the single fiber pullout tests for the rest of the test program were conducted between 24 and 40 days of age, it can be assumed that the variability in the curing age of the cylindrical specimens had little to no effect on the peak load and toughness results found in this research, and thus no correction factor was required to be implemented.

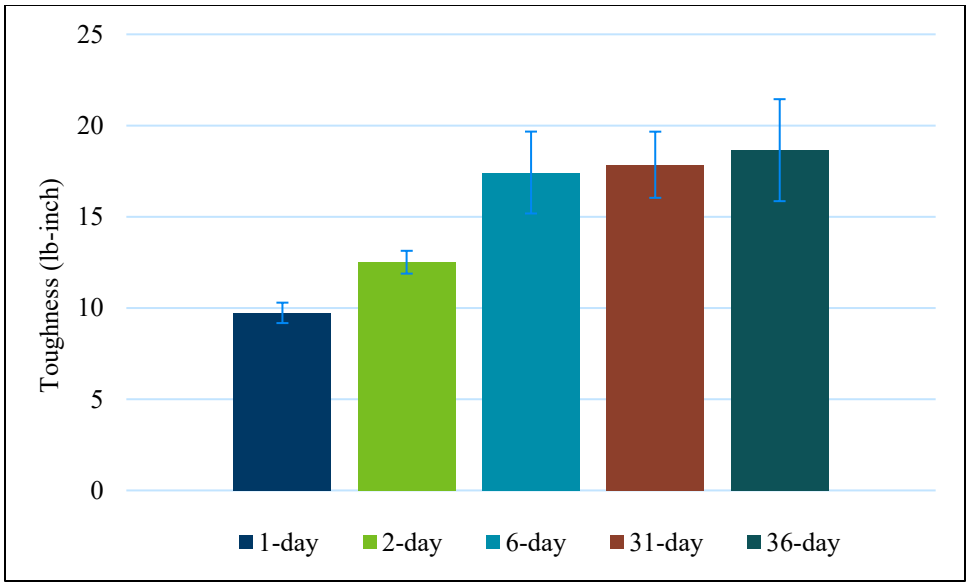

Figure 6.5: Effects of curing age on toughness.

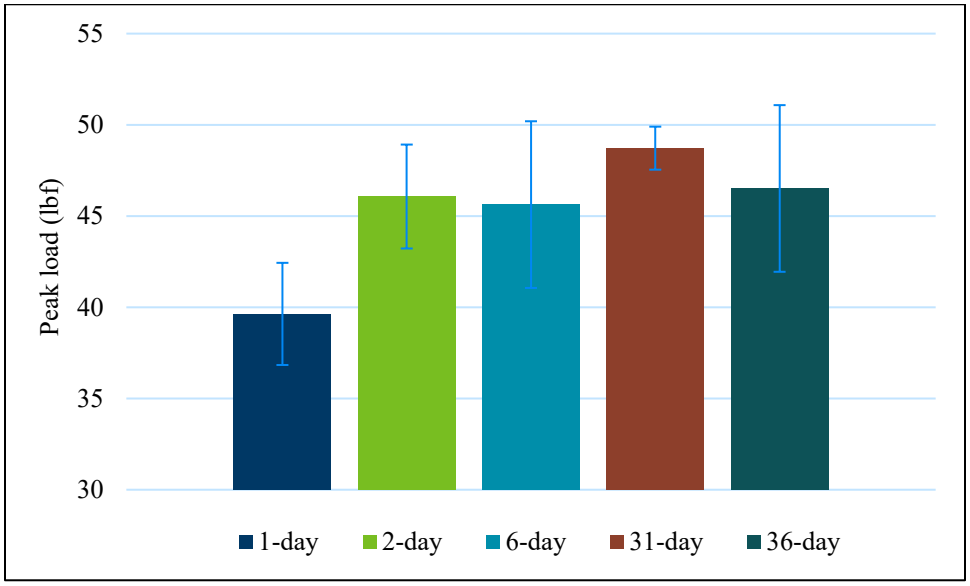

Figure 6.6: Effects of curing age on peak load

6.2.2 Influence of fiber type, aggregate type, and cement content

The average peak load for each fiber type is shown in Figure 6.7. Fiber 2 (alkali-resistant glass) performed the best, with an average peak load of 66.9 pounds. This is likely due to the fiber having a lower aspect ratio and higher stiffness than the other fibers, along with a helical geometry. The other

specimens are all made from polypropylene. Fiber 3 had the lowest peak load with an average of 7.7 pounds. It should be noted that Fiber 3 is smaller and thinner compared to other fibers. Fiber 4 performed significantly better than Fiber 3. This is likely due to its continuously crimped geometry, while also having a lower aspect ratio than Fiber 3. Of all the polypropylene specimens, Fiber 1 performed the best with an average peak load of 57.3 pounds. This is likely due to the embossed geometry and lower aspect ratio compared to the other polypropylene fibers. These results agree with Singh (2004), who showed that indentation increases pullout loads when compared to the same fiber that is smooth, and not indented.

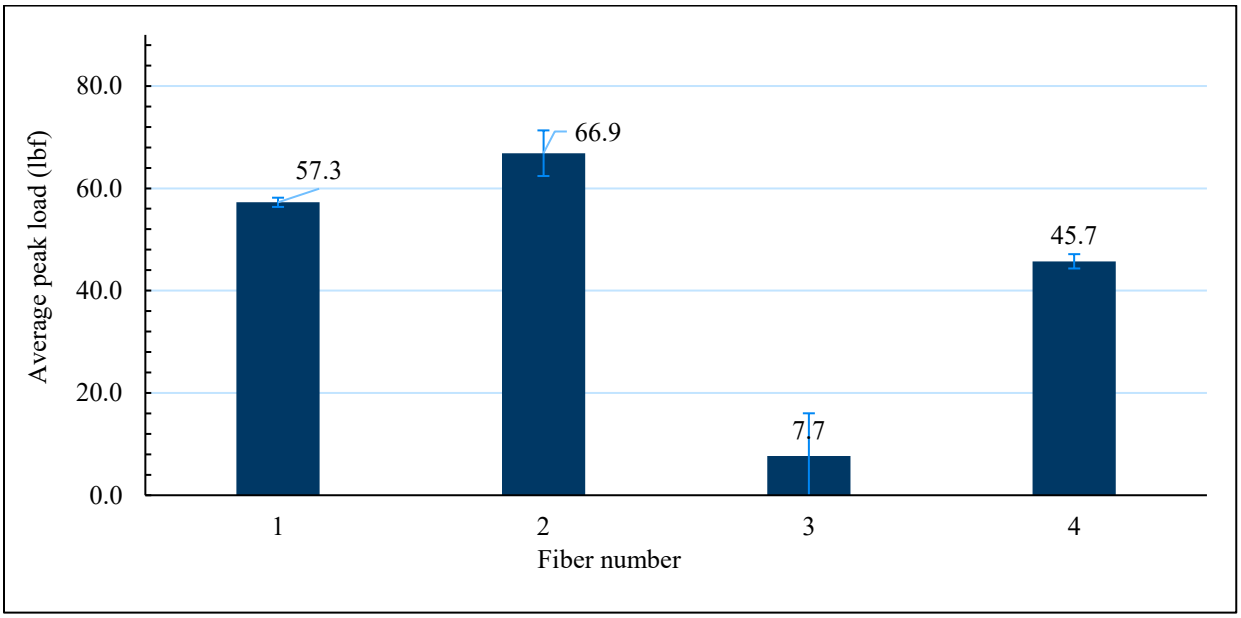

Figure 6.7: Average peak load by fiber type.

The average peak load for each fiber type and concrete batch is shown in Figure 6.8. The peak load for each fiber type, sorted by aggregate class, is shown in Figure 6.9. The peak load for each fiber type, sorted by cement content, is shown in Figure 6.10. There is no apparent trend based on aggregate type or cement content used in the mix design. In summary, the single fiber pullout test results showed that the cement content and aggregate type had negligible effects on the peak load, toughness, or load-displacement behavior of the fibers embedded in concrete in comparison to the effect of the fiber type.

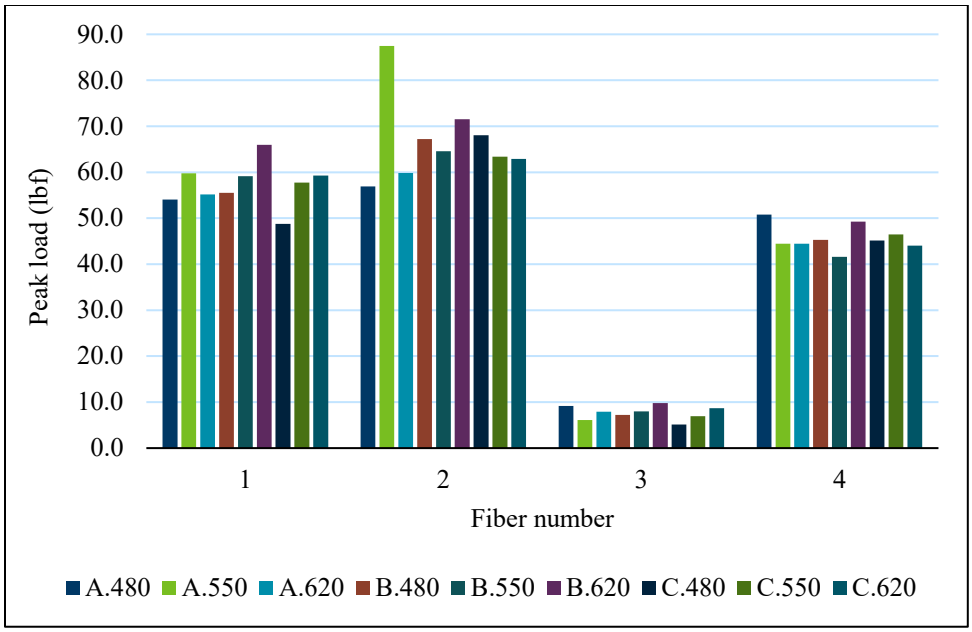

Figure 6.8: Peak load vs. fiber type (all mixes) ***(Note: A, B, and C are the aggregate class; 480, 550, and 620 are cement contents in lb/yd³).***

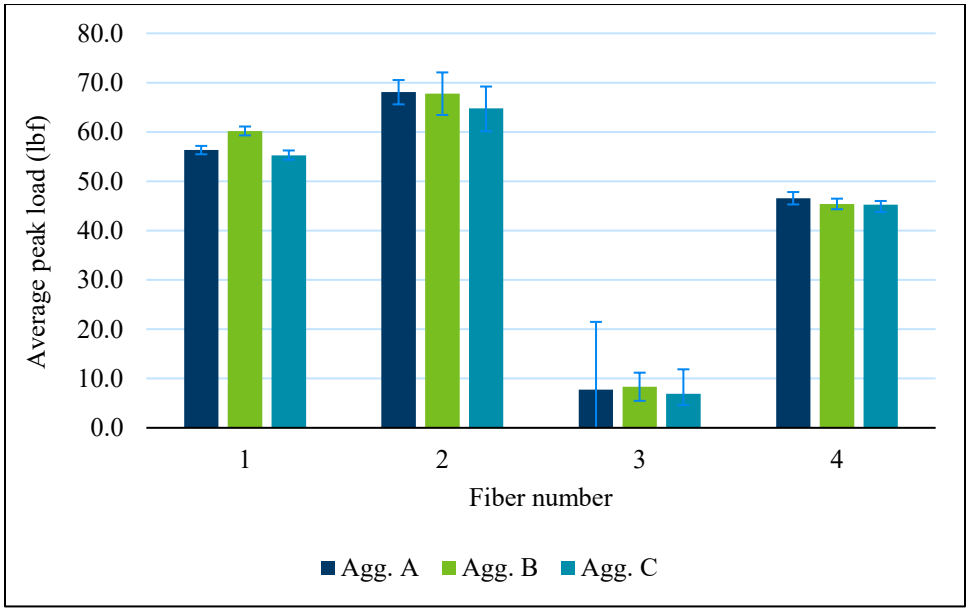

Figure 6.9: Average peak load vs. aggregate class.

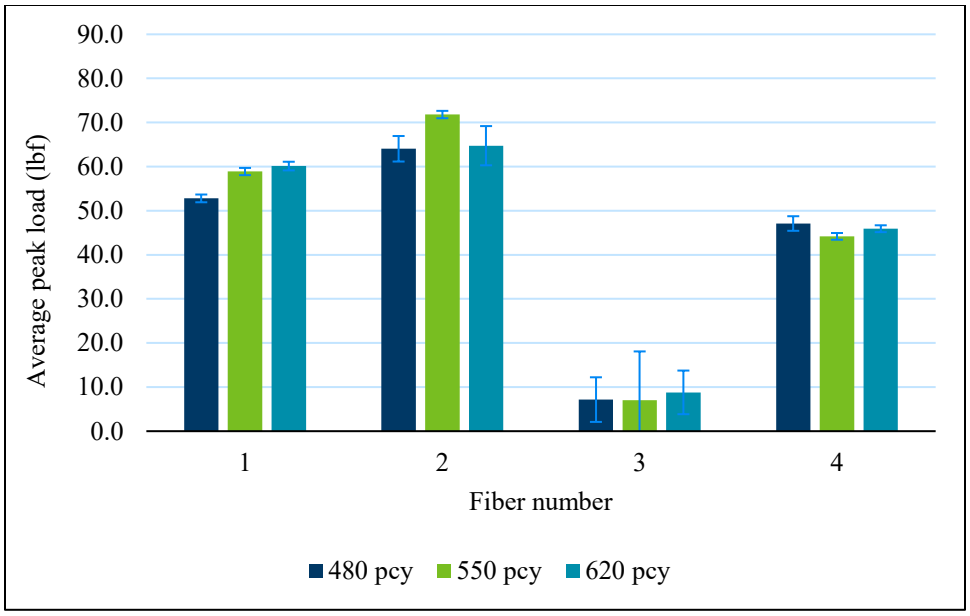

Figure 6.10: Average peak load vs. cement content (pcy = lb/yd^3).

Figure 6.11 shows the load-displacement curves for Fibers 1, 2, and 4 specimens belonging to the A.480 concrete mix (Aggregate class A, cement content 480 lb/yd^3), for example. The average toughness for all four fiber types is shown in Figure 6.12. While Fiber 2 (alkali-resistant glass) had the highest peak load, the average toughness was just 13.6 in-lb. This is likely due to the brittle behavior of the fiber, which limits the elongation of fibers at failure, rupture, or pullout. For this fiber type, after the initial bond broke, the load rapidly declined as the fiber pulled out. Fiber 3 exhibited the lowest toughness, 4.2 in-lb. Fibers 1 and 4 performed significantly better than Fibers 2 and 3.

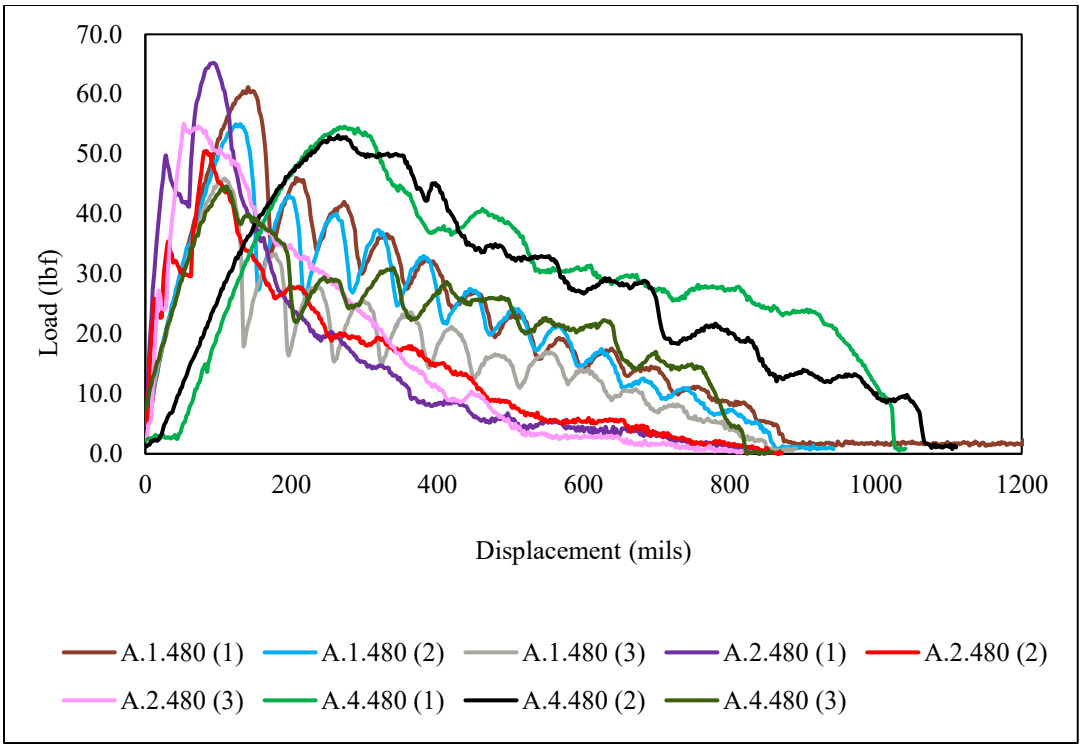

Figure 6.11: Load-displacement curves for concrete batch (Class A aggregate, cement content 480 lb/yd^3, fibers 1, 2, 4).

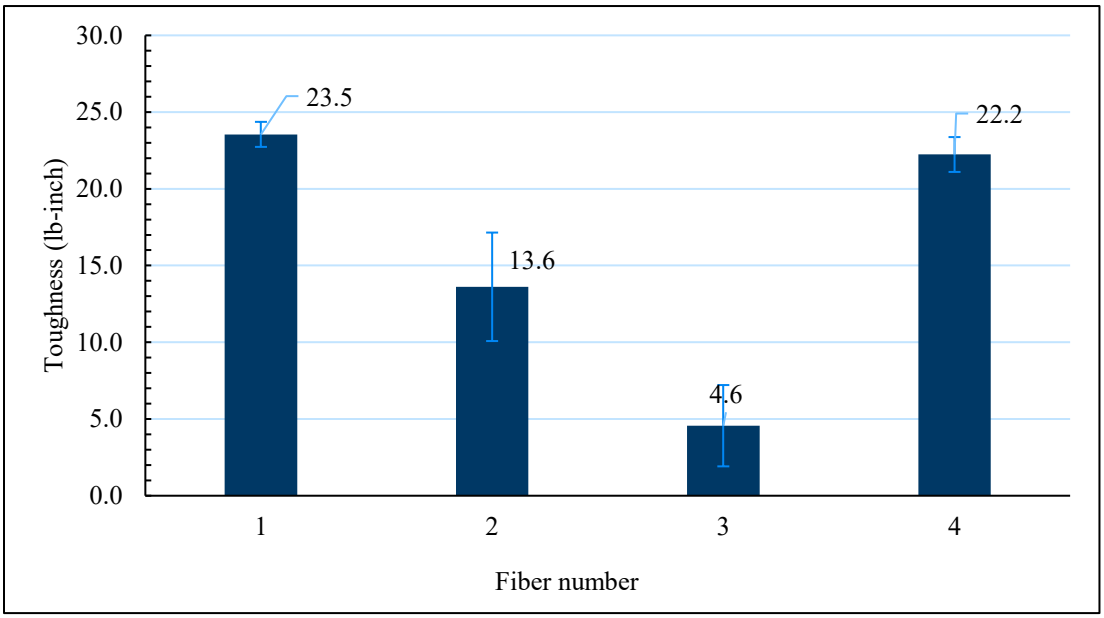

Figure 6.12: Average toughness by fiber type.

6.2.3 Failure modes of fibers

This section discusses how each fiber type failed in the pullout tests conducted in Phase 1. Table 6-1 gives information about the failure mode of each fiber. Fibers 1 and 3 failed by pullout. For Fiber 4, 75% of the fibers were pulled out of the concrete and the rest ruptured under the tension load. Fiber 4's behavior is related to its strong interfacial bond with the concrete matrix and thinner cross-section. About one-quarter of the Fiber 2 specimens failed by pullout and the rest by rupture. This is likely because of its brittle behavior, as it was made from glass fiber. The load-displacement plots provided in this section were scaled to best show each failure curve and hence have different scales for better clarity.

Table 6-1: Failure type of each fiber

Fiber Number	Failure Type	
	Pullout	Fiber Rupture
1	100.0%	0.0%
2	22.2%	77.8%
3	100.0%	0.0%
4	74.1%	25.9%

6.2.3.1 Fiber 1

A photograph of two failed (tested) fibers and an untested fiber is shown in Figure 6.13. The untested fiber is at the bottom of the photograph, and the failed fibers are the two fibers at the top of the photograph. The left ends of the failed fibers are the ends that were embedded in the concrete. The embedded end of both the failed specimens had smoothened, stretched out, and frayed. The visible stretching of this fiber indicates that these kinds of fibers offer high interfacial bonding but result in plastic elongation. Load vs. displacement curves for seven different samples of Fiber 1 are shown in Figure 6.14. Each specimen peaked at about 150 mils of displacement when the bond between the specimen and concrete failed. The plot shows a decreasing waveform as displacement increased until the specimen was fully pulled out of the concrete. This may be an indication that the specimens failed as each indentation failed independently.

Figure 6.13: Fiber 1 (failed fibers vs new fiber).

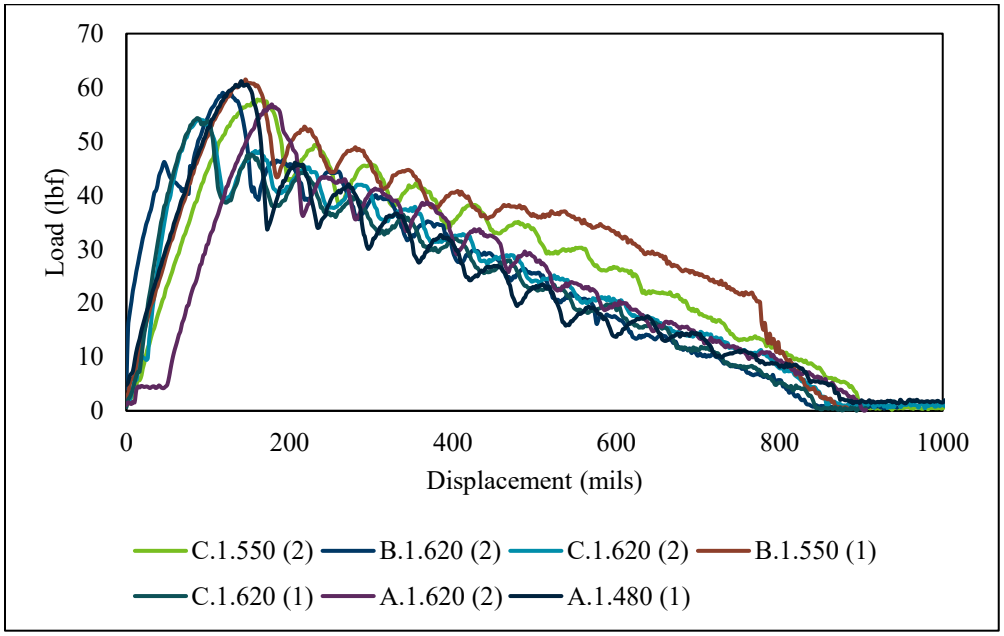

Figure 6.14: Load vs. Displacement Curves (Fiber 1) ***(Note: A, B, and C are the aggregate class; 480, 550, and 620 are cement contents in lb/yd^3, and numbers in the parenthesis are sample numbers)*****.**

6.2.3.2 Fiber 2

A photograph of failed fibers and an untested fiber is shown in Figure 6.15. There were two ways in which Fiber 2 failed. Because Fiber 2 is brittle glass, the specimens were either pulled out of the concrete or broke off and remained embedded in the concrete. When the specimen is pulled out of the concrete, there is little to no distress evident in the specimen as shown in the second fiber from the bottom in Figure 6.15. When the specimen broke off, it failed at either the grip interface or the concrete interface. Figure 6.16 and Figure 6.17 show concrete cylinders with broken fibers still embedded in them after testing.

Load vs. displacement curves for five different specimens of Fiber 2 are shown in Figure 6.18. Each fiber peaked at about 100 mils displacement when the bond between fiber and concrete failed or the specimen itself failed by breaking off. In Figure 6.18, samples C.2.480 (1), B.2.550 (2), and A.2.620 (2) (A, B, and C are the aggregate class; 480, 550, and 620 are cement contents in lb/yd^3, and numbers in the parenthesis are sample numbers) all show sharp drop-offs to zero load after peaking near 100 mils of displacement. This is evidence of specimen rupture. The other two specimens have load-displacement curves that peak around 100 mils and trail off rapidly as the specimen pulls out. This is evidence that after the initial bond is broken, there is little residual strength provided by these fibers.

Figure 6.15: Fiber 2 (failed fibers vs new fiber)

Figure 6.16: Fiber 2 (failure at grip interface)

Figure 6.17: Fiber 2 (failure at concrete interface)

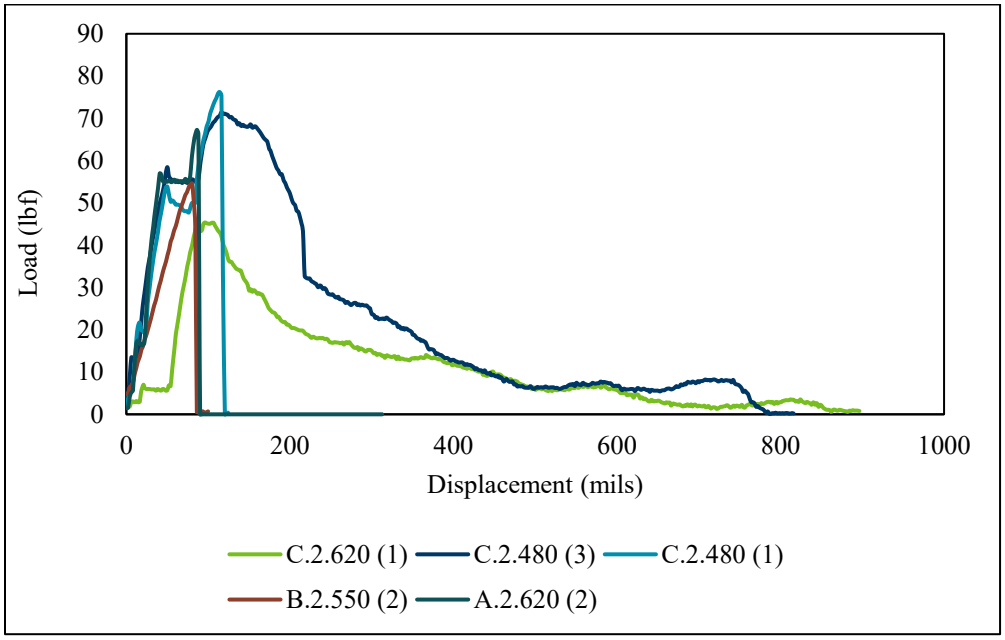

Figure 6.18: Load vs. displacement curves (Fiber 2)

6.2.3.3 Fiber 3

A photograph of three failed fibers and an untested fiber is shown in Figure 6.19. The left end of the failed fibers were the ends embedded in the concrete. There is significant fraying on the left end of the failed fibers.

Load vs. displacement curves for seven different samples of Fiber 3 are shown in Figure 6.20. Each fiber sample had an initial peak at about 50 mils displacement when the bond between fiber and concrete began to fail as the specimen started pulling out. However, the load did not fall off after this peak, and this was not the ultimate peak load in many cases. The load remained steady as displacement increased, even increasing in some cases. The true peak did not occur until about five hundred mils of displacement in many cases but the magnitude of the load at which fibers pulled out the concrete was significantly lower than the other three fibers tested. It may be noted that while the load one single fiber is not as large as the loads the other three fibers can sustain, the numbers of fibers for a given fiber dosage will likely be higher for the fiber 3 as it is thinner and lighter.

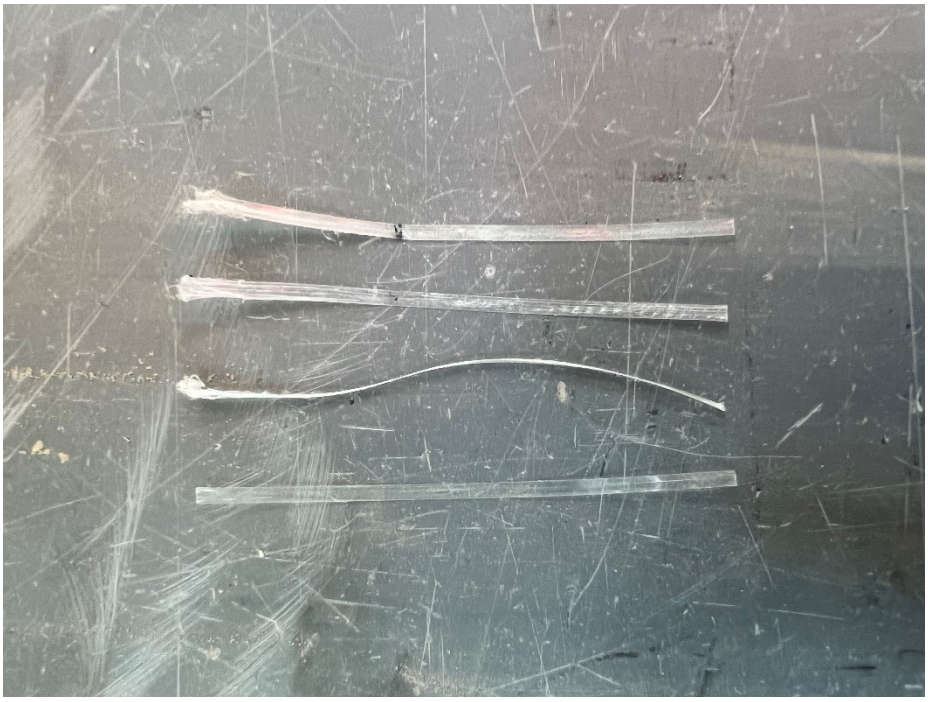

Figure 6.19: Fiber 3 (failed fibers vs new fiber)

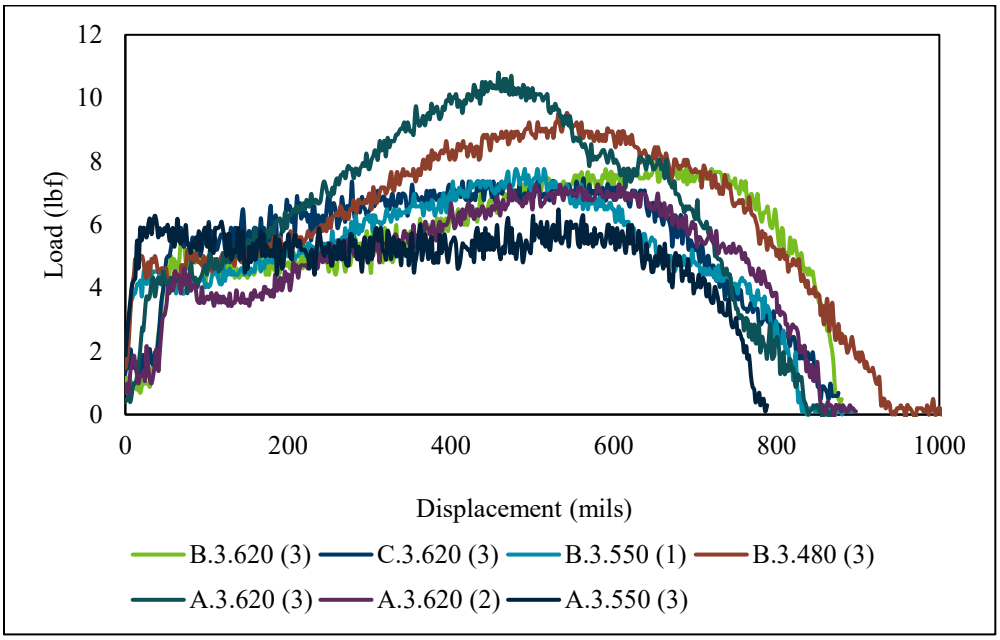

Figure 6.20: Load vs. displacement curves (Fiber 3) ***(Note: A, B, and C are the aggregate class; 480, 550, and 620 are cement contents in lb/yd^3, and numbers in the parenthesis are sample numbers)*****.**

6.2.3.4 Fiber 4

A photograph of two failed fibers and a new fiber is shown in Figure 6.21. The left end of the failed fibers are the ends that were embedded in the concrete. The ends of the specimens are smoothed, stretched out, and frayed. In some cases, the specimen failed and was pulled apart (Figure 6.22). An additional photograph of a concrete cylinder with a frayed specimen is shown in Figure 6.23. Fiber rupture may have happened for a couple of reasons. Fiber 4 has a good bond with the concrete due to its continuously crimped geometry. While this fiber is laterally stiffer than Fiber 3, it is thinner and less stiff than Fiber 1.

Load vs displacement curves for eight different samples of Fiber 4 are shown in Figure 6.24. Each specimen peaked at about 100 mils displacement when the bond between specimen and concrete failed or the fiber itself failed by breaking off. In Figure 6.24, sample B.4.480 (1) shows a sharp drop off to zero load after peaking near 100 mils of displacement. This is evidence of fiber rupture. Fibers A.4.550 (2), A.4.480 (3), B.4.480 (2), C.4.480 (1), and C.4.550 (3) all have load-displacement curves that peak around 100 mils and then trailed off, like Fiber 1. Although not a smoothly decreasing sinusoidal waveform, there is evidence of several lower peaks as displacement increases. This is likely due to the continuously crimped geometry of the fibers.

Specimens A.4.480 (2) and C.4.480 (2) show a unique phenomenon. The peak load occurs far past 100 mils, and after a slow, but steadily increasing load. This is an indication of partial grip failure. The fiber was slowly slipping out of the grips while the load was still increasing. After the initial bond broke between the specimen and concrete, the specimen stopped slipping in the grips and entered a failure pattern like the other specimens.

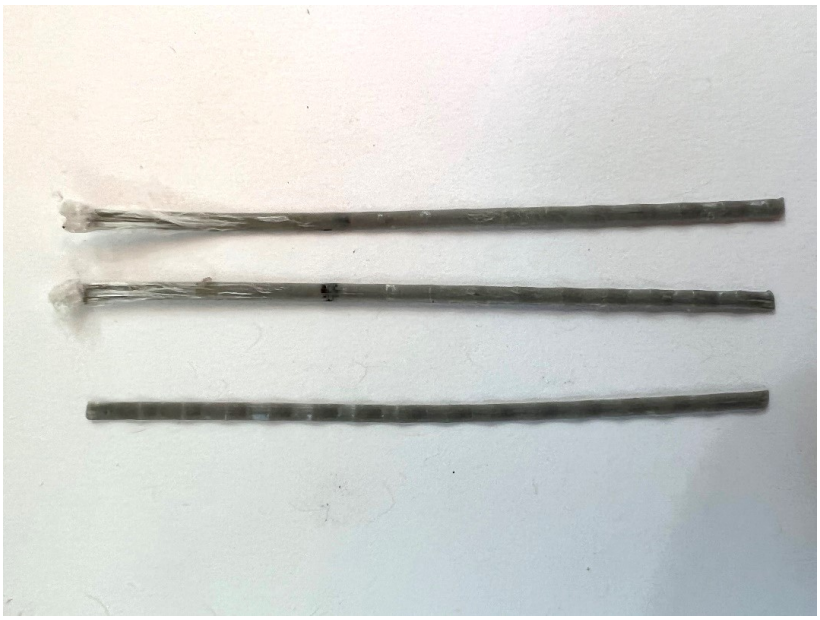

Figure 6.21: Fiber 4 (failed fibers vs new fiber).

Figure 6.22: Fiber 4 (failed fibers compared to original fiber).

Figure 6.23: Fiber 4 (failure at the concrete interface).

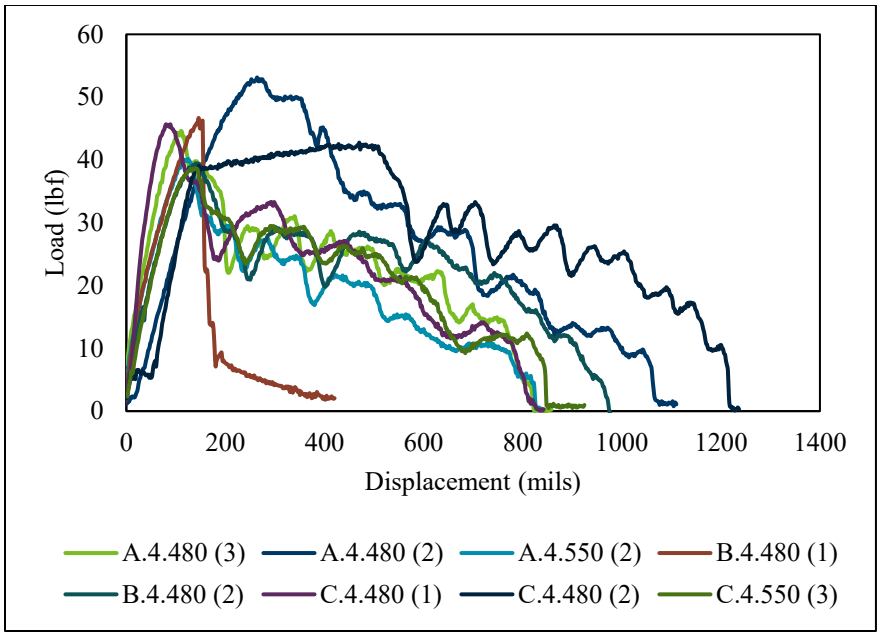

Figure 6.24: Load vs. displacement curves (Fiber 4) ***(Note: A, B, and C are the aggregate class; 480, 550, and 620 are cement contents in lb/yd^3, and numbers in the parenthesis are sample numbers)*****.**

6.3 Single fiber pullout test, Phase 2

As mentioned before, the Phase 2 test included multiple loading and unloading of individual fibers. The sample preparation procedure was the same as the Phase 1 testing. The only difference was in the test load application. Loading was done in small increments of 5 lbs followed by unloading and reloading with a higher load. After each loading, the grip was loosened so the stress in fibers became zero. While this may not be the simulation of the exact field condition, the consecutive application and removal of the load reflect the effect of slab length change on the fiber pull-out behavior. After unloading, the lower grip was raised back to its previous position such that the fiber could be gripped in the same location when loading again. The consecutive loading and unloading were done until the fiber eventually failed. Four fiber samples were tested for each fiber type and their load-displacement relationship was studied.

For Fiber 1, three out of the four samples could be loaded up to 20 lbs before the fiber's failure (Figure 6.25 through Figure 6.28). The load-displacement behaviors of Samples 1,3 and 4 show the fiber's elongation remains elastic until 40 to 50 mils. Effort was made to identify the elastic limit (EL) based on the load-displacement curves at varying loads. For example, the load-displacement curves of all four loads of Sample 1 overlap until 20 lbs of load, indicating the fiber could gone back to its original shape. The displacement up to about 20 lbs was therefore an elastic elongation of the fiber. It may be noted that the fiber-concrete interface debonding is not within the elastic zone because such displacement is permanent. Sample 2 of Fiber 1 seemed to experience a slight slippage in the grip, therefore, the EL was not identified.

All 4 samples of Fiber 2 behaved similarly as can be seen in Figure 6.29 through Figure 6.32. The EL of the samples between 30 and 40 mils. All the samples show a linear load-displacement curve up to 40 mils.

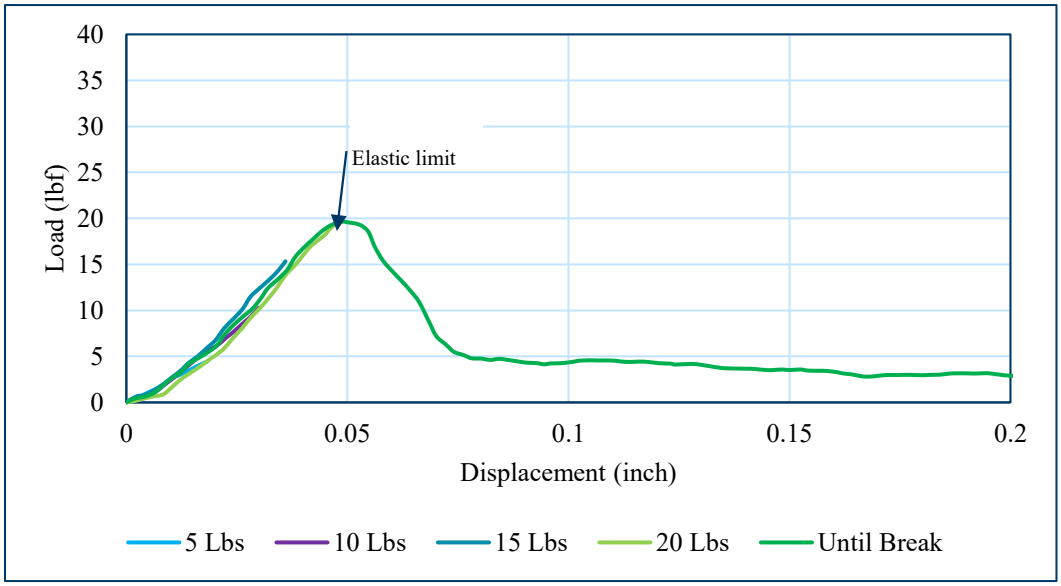

Figure 6.25: Loading behavior of Fiber 1 (Sample 1).

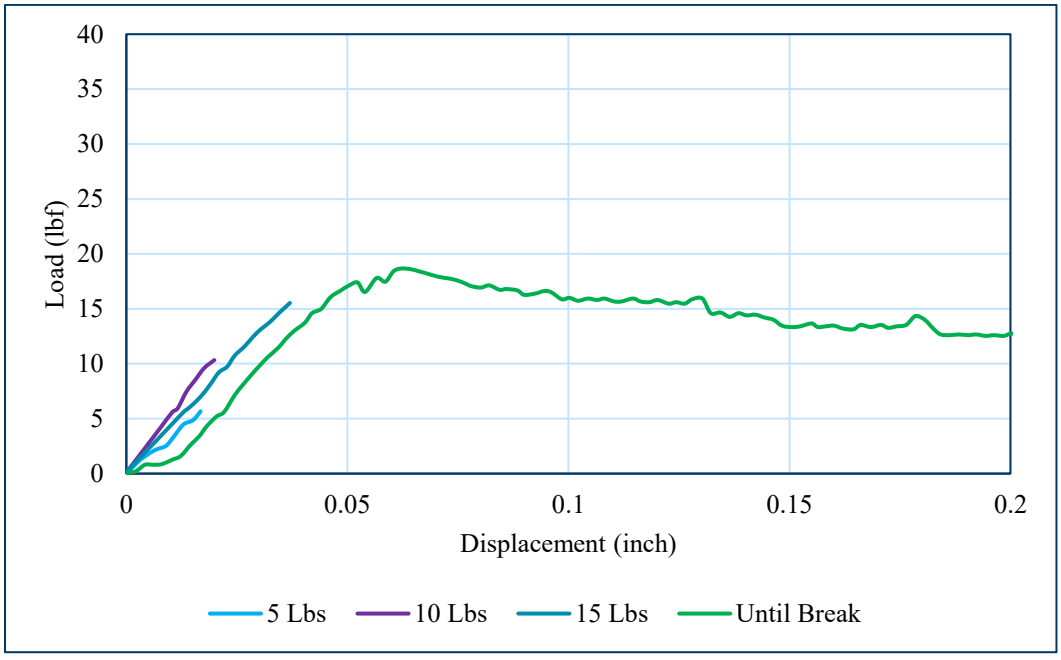

Figure 6.26: Loading behavior of Fiber 1 (Sample 2).

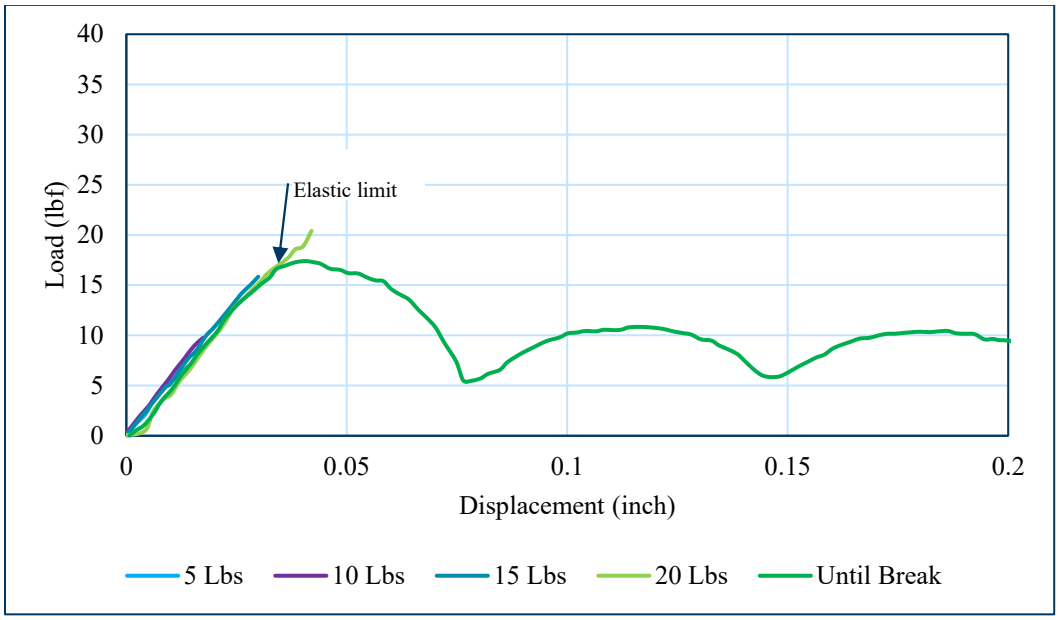

Figure 6.27: Loading behavior of Fiber 1 (Sample 3).

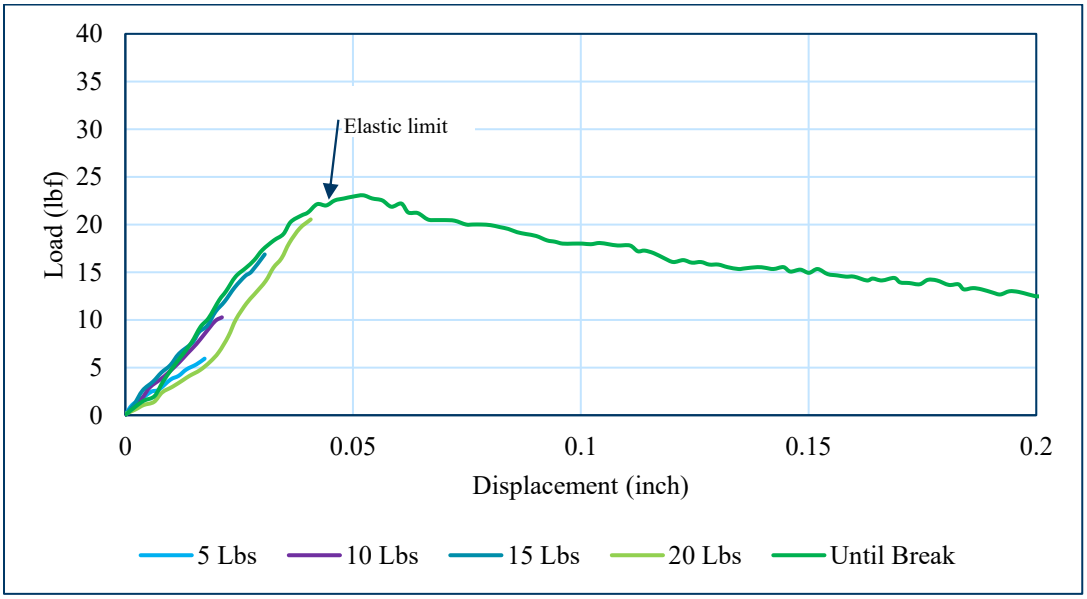

Figure 6.28: Loading behavior of Fiber 1 (Sample 4).

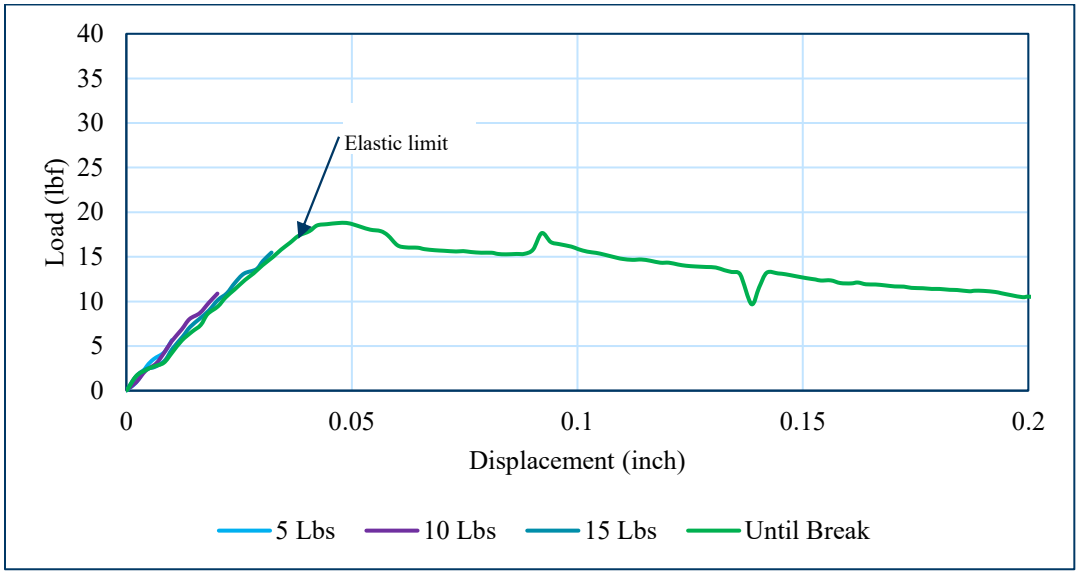

Figure 6.29: Loading behavior of Fiber 2 (Sample 1).

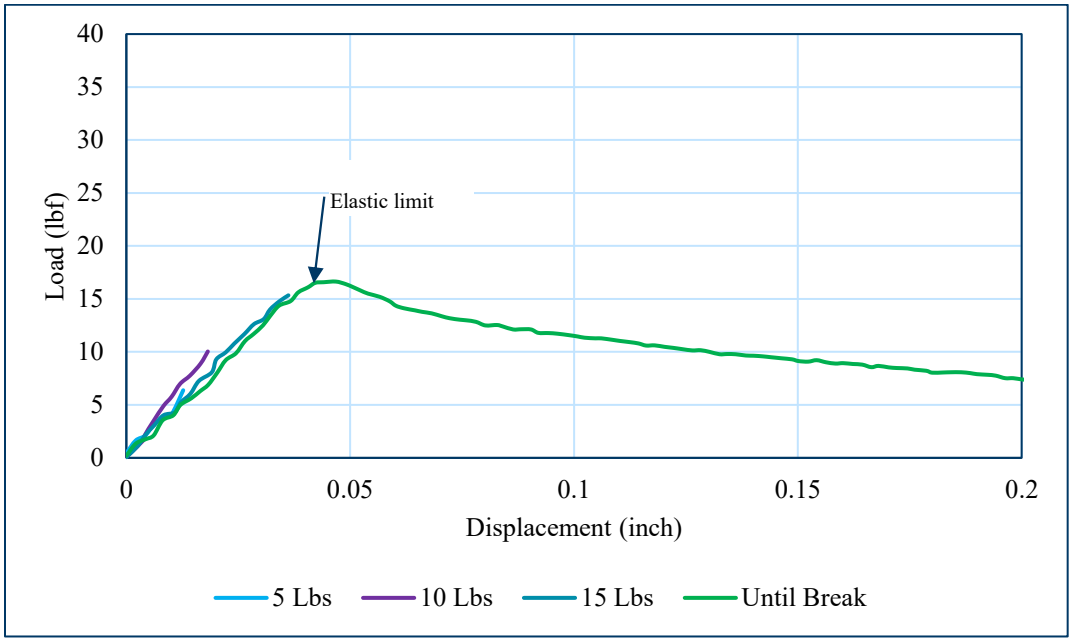

Figure 6.30: Loading behavior of Fiber 2 (Sample 2).

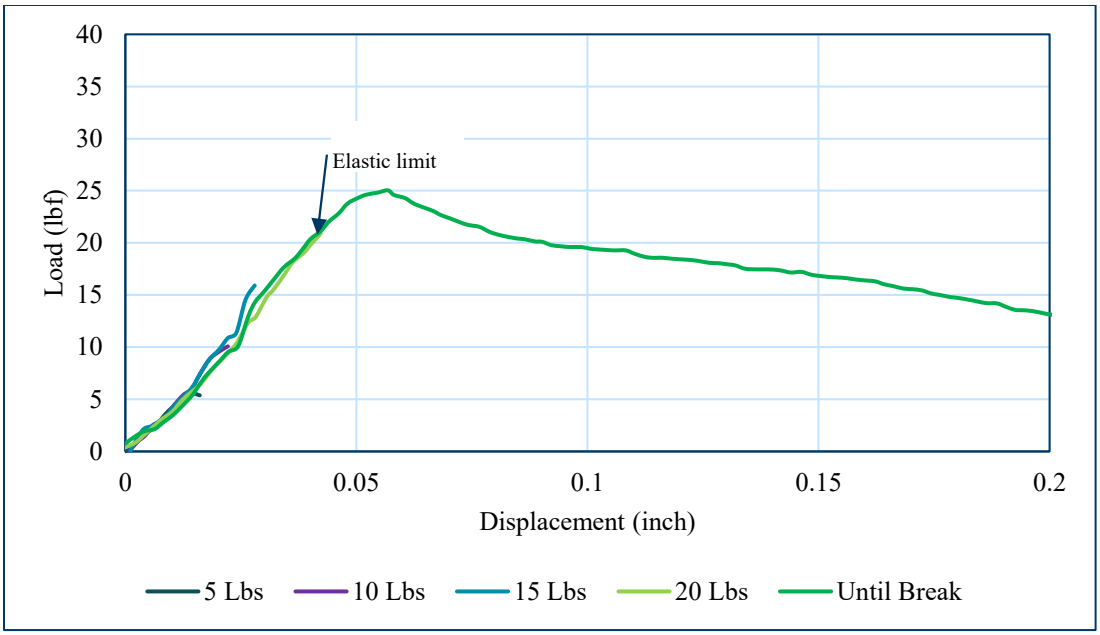

Figure 6.31: Loading behavior of Fiber 2 (Sample 3).

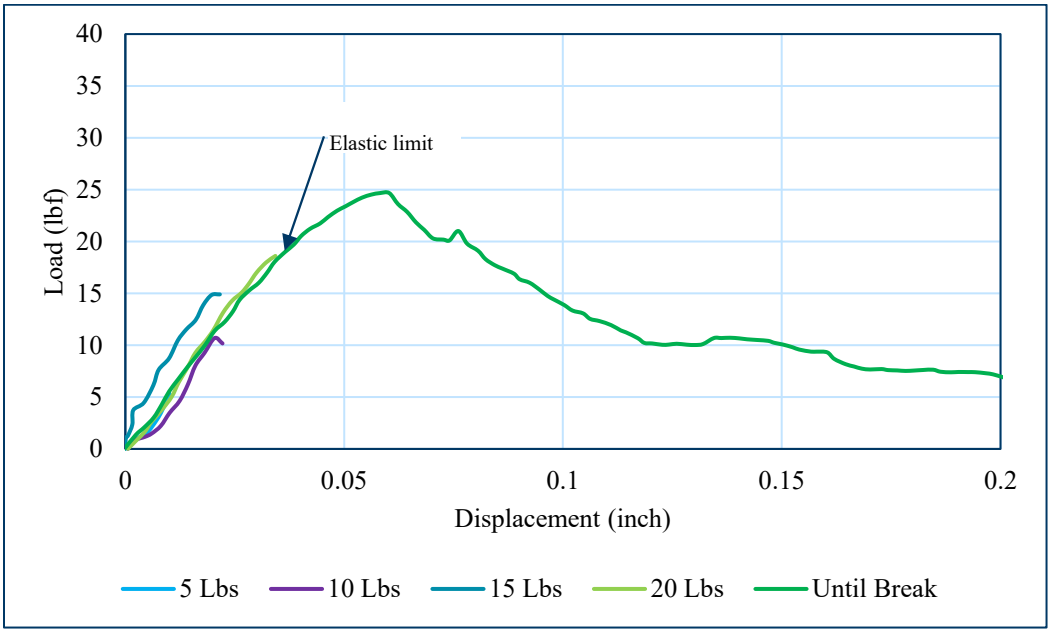

Figure 6.32: Loading behavior of Fiber 2 (Sample 4).

The results of Fiber 3 varied among the samples due to its smooth surface as can be seen in Figure 6.33 through Figure 6.36. Sample 1 could be loaded only up to 10 lbs and the other three peaked at about 15 lbs. The load-displacement curve of sample 1 shows a relatively easy pullout of the fiber. Because of the variability in the results, EL is not identified for this fiber.

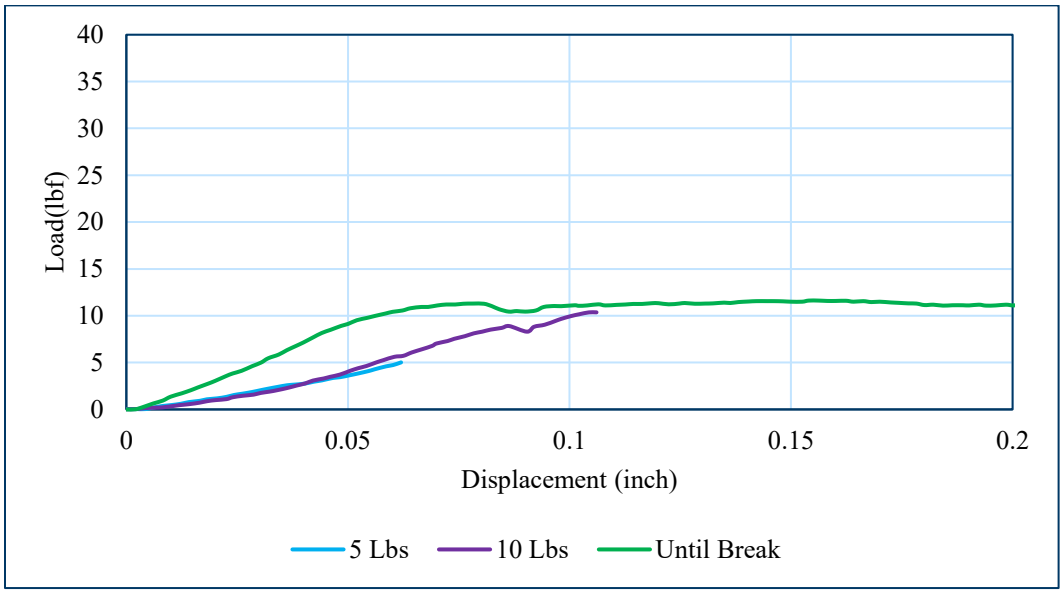

Figure 6.33: Loading behavior of Fiber 3 (Sample 1).

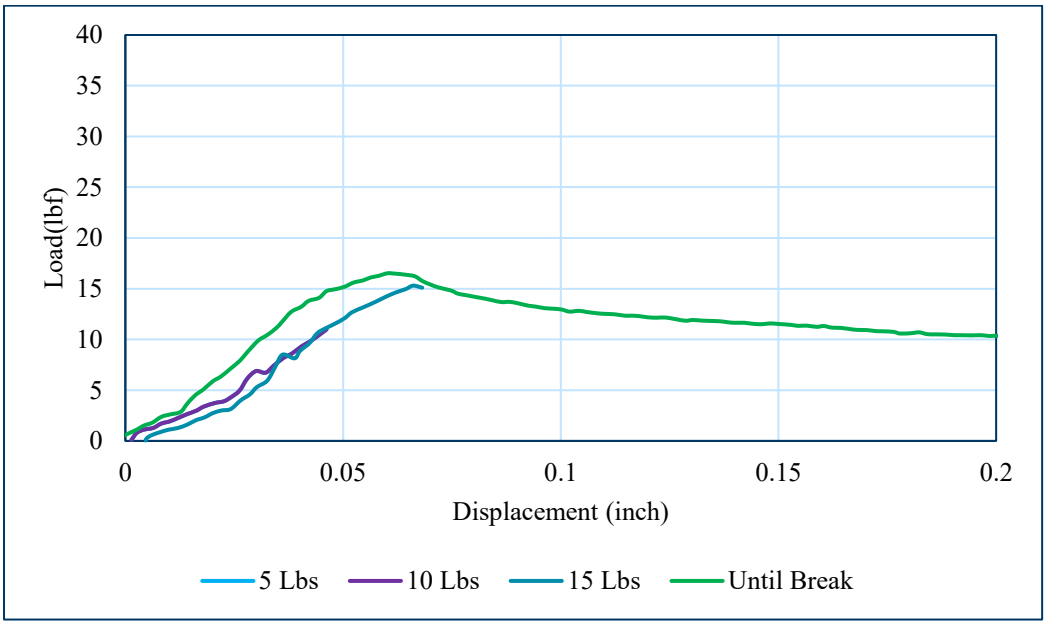

Figure 6.34: Loading behavior of Fiber 3 (Sample 2).

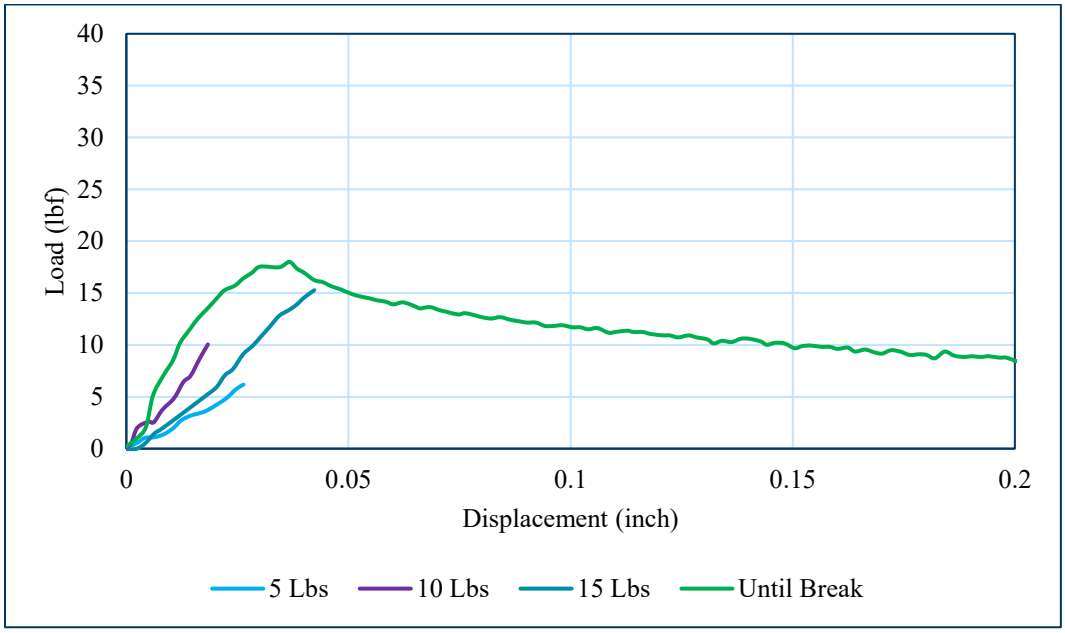

Figure 6.35: Loading behavior of Fiber 3 (Sample 3).

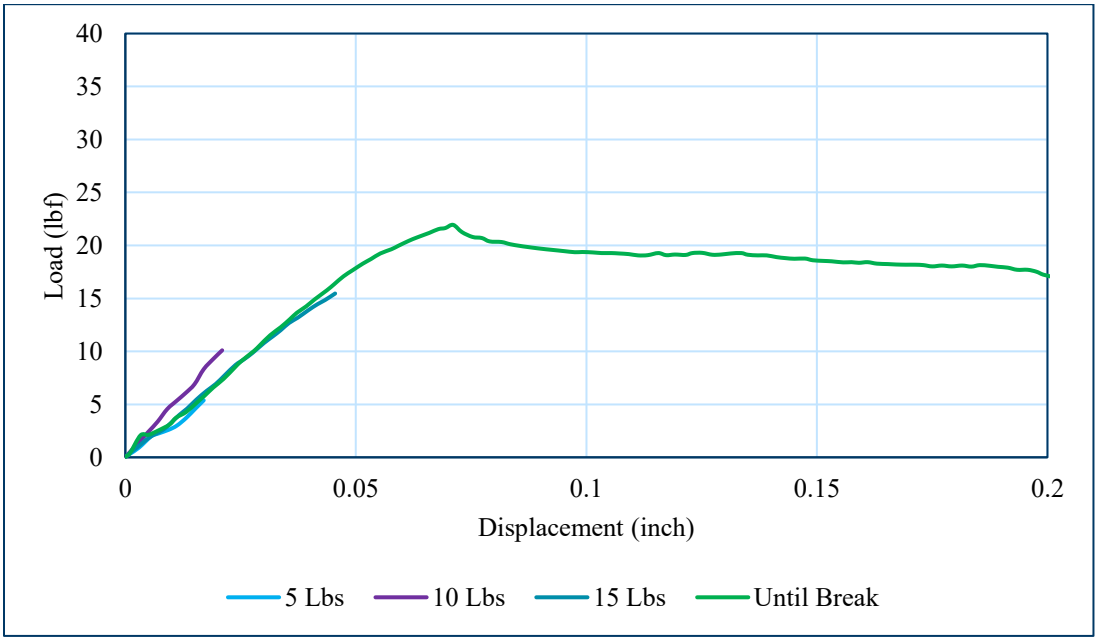

Figure 6.36: Loading behaviour of Fiber 3 (Sample 4).

Fiber 4 is crimped and stiff, thus having a strong mechanical bonding with the embedding concrete (Figure 6.37 through Figure 6.40). Three of the four samples peaked at 35 lbs (except for the sample 2, Figure 6.38). The effect of reloading the fiber is apparent for this fiber. Even though the fiber could be loaded up to 35 lbs, it appears that fibers remained elastic only at about 20 lbs load and up to 50 mils of displacement (conservatively).

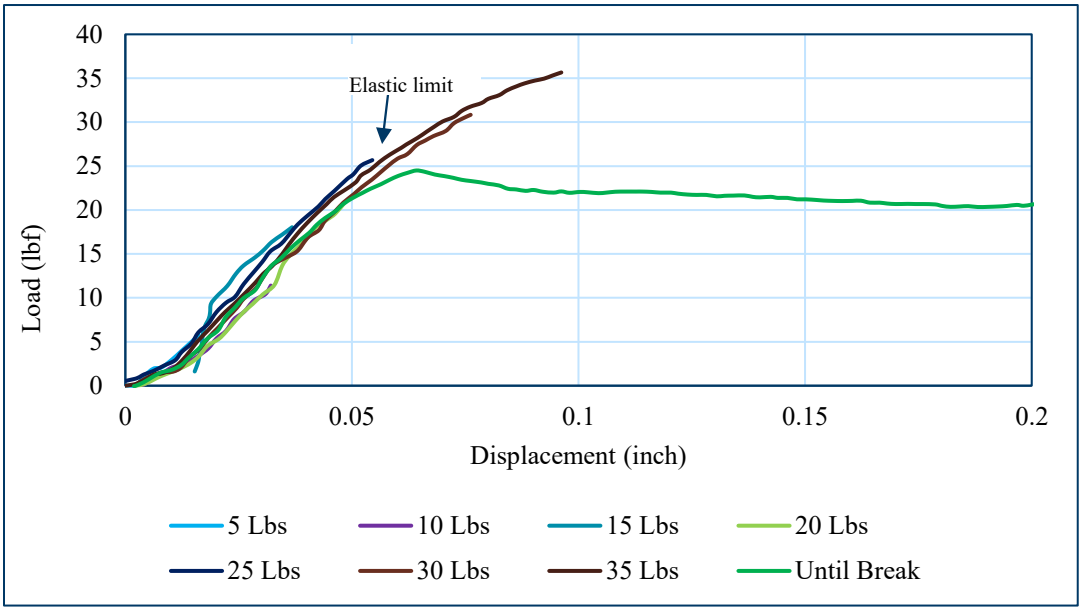

Figure 6.37: Loading behaviour of Fiber 4 (Sample 1).

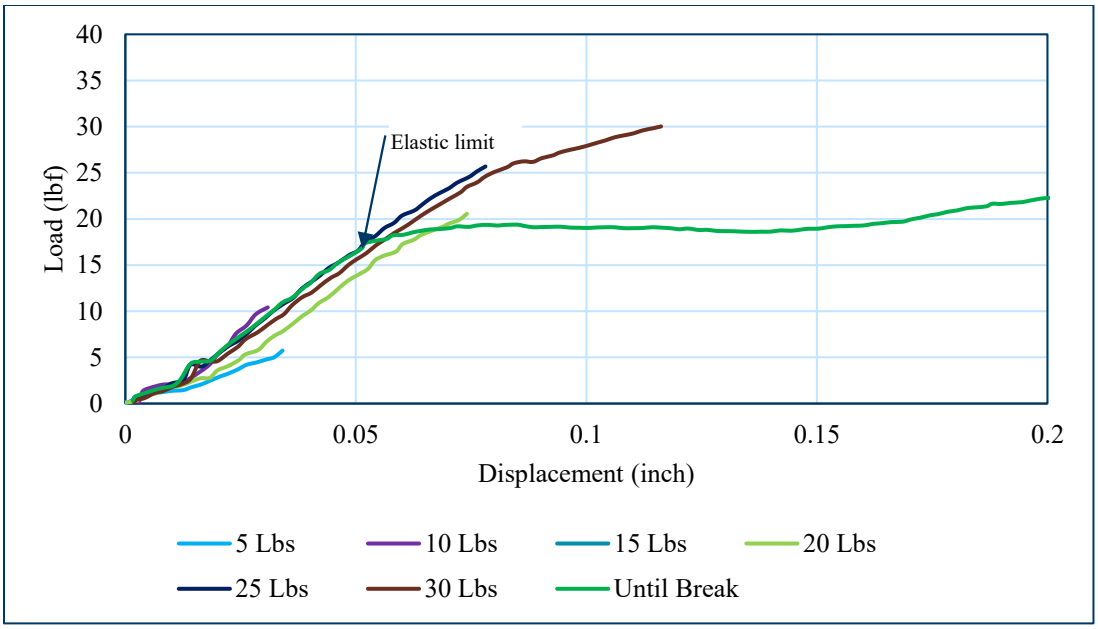

Figure 6.38: Loading behaviour of Fiber 4 (Sample 2).

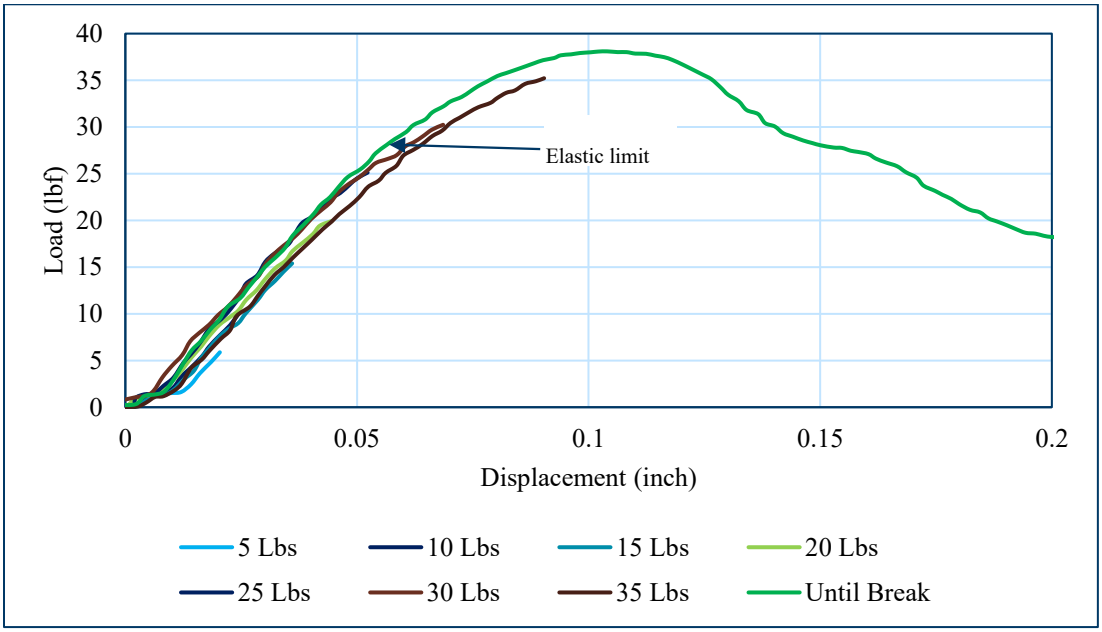

Figure 6.39: Loading behaviour of Fiber 4 (Sample 3).

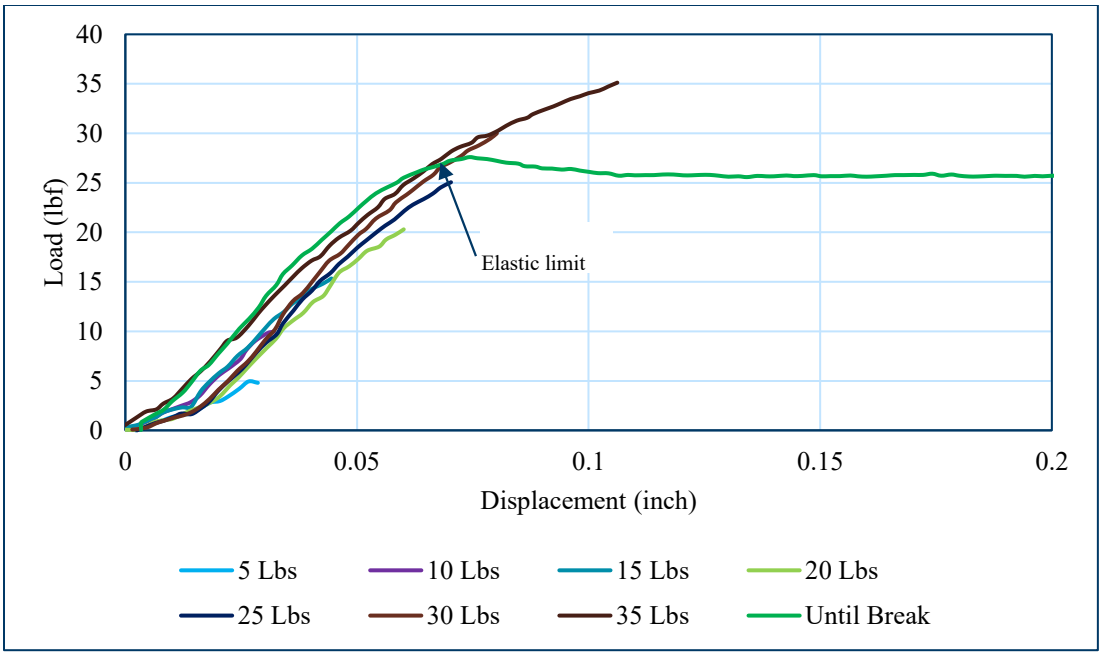

Figure 6.40: Loading behaviour of Fiber 4 (Sample 4).

Chapter 7: Conclusions

Thin fiber reinforced concrete pavements and overlays can be economical for low and moderate-traffic volume roads. These can be constructed over a new granular aggregate base layer or old pavements, depending on the existing distresses and structural strength. The distress data of various thin concrete pavements and overlay projects revealed that transverse joint faulting is one of the critical distresses that can shorten their service lives and structural fibers potentially can mitigate that distress for thin concrete pavements and overlays.

Under the scope of the study, an effort was made to determine the needed fiber properties with an overall goal to develop pavement-specific fibers. The study included a literature review, finite element modelling of thin concrete pavements, analysis of falling weight deflectometer data of MnROAD FRC pavements, and laboratory testing. The main conclusions from the study are listed below.

Literature Review

- The major distresses that occur in thin concrete pavements and overlays are fatigue crack and joint faulting.
- Because of the lack of cover availability, dowel bars are not recommended in thin concrete pavement. Thin concrete pavements, however, can have their longevity increased with the inclusion of structural fibers, which have proven to increase the ductility of concrete by providing residual strength in post-crack pavements. In pavements where dowel bars cannot be used, the addition of structural fibers has been shown to increase joint load transfer compared to plain concrete.
- Finite element method (FEM) is a very reliable tool for determining the response of linear and non-linear structures under various loading conditions. For concrete pavement, traffic loading, curling and shrinkage of concrete slabs, and various pavement parameters can be considered in FEM modeling. The use of a spring element for modeling was found to be reliable in obtaining the required stiffness.
- Overall, the review of the previous studies shows a strong trend toward using fiber in thin concrete pavement. Yet, it is unclear what level of stiffness the fiber needs to have to function at its best in a joint.
- Studies have shown that the embedment depth and geometry of the fiber influence the pullout load due to the improved interfacial bond between the fiber and concrete.
- Cost is a key factor in the decision of whether to use concrete pavement. The addition of fibers allows the concrete pavement to be made thinner. However, the currently available fibers must be used at high dosages to achieve the required joint performance that can mitigate the transverse joint faulting. The development of pavement-specific fibers, which may allow for lower fiber dosages in concrete pavement, may bring down material costs.

FEM, FWD Analysis and Laboratory Study

- Joint performance (LTE, differential displacement (DD) and maximum displacement (D_{max})) of thin FRC pavements, which is the indicator for joint faulting, largely depend on the vertical stiffness of the joints.

- The aggregate interlock in the thin FRC pavement is not significant because of the limitation in the thickness of the slabs and the small aggregate size. A vertical joint stiffness of 250 lb/inch^3 can be achieved from aggregates, which can provide 15 to 20% LTE. The base layer can provide 30 to 40% LTE and the remaining 30 to 40% LTE can be achieved from structural fibers. As the thickness of the slabs in the thin concrete pavements is limited, achieving load transfer from fibers is a feasible approach to improve the overall performance of the pavement.

  This study introduced a procedure to characterize the fibers' contribution toward the joint load transfer. A new parameter, namely, the modulus of fiber support (K_f), was introduced. The minimum value of K_f as 3,000 lb/inch^3 is suggested for a 30 to 40% LTE required from the fiber. The laboratory joint performance testing is recommended to be conducted at 0.06 inches crack width while determining the K_f. This value will slightly change based on the pavement structure and service life of the pavement. Additional testing and analysis will be required to estimate a more accurate value of K_f as a function of pavement structure, traffic, and service life and at a higher reliability.

- Fiber pullout tests were conducted on four different types of fibers. Based on the test results, it was found that fibers with indentation on the fiber geometry help increase the peak load and toughness. The laboratory investigation helped determine the elastic limit of fibers with various geometries. The less indented fibers and smooth and brittle fibers performed on average less than the fibers with higher lateral stiffness and more indentation on the geometry. The finding from the single fiber pullout test will help develop the pavement-specific fiber.

- It may be noted that the joint load transfer test used in the laboratory takes a considerable amount of time. This test helps determine the joint load transfer, but the testing is quite complicated and may not be a good candidate for a simple screening test. Also, because of the limited size of the project, a large data setup could not be developed to perform any reliability analysis. The field study included only one type of fiber; therefore, the conclusions drawn in this study should be verified for other types of fibers as well.

- In the next phase of the study, the following may be pursued (i) designing and developing fibers that have 3,000 lb/inch^3 joint stiffness with irregular geometry, (ii) developing a simple test to determine the joint stiffness, which can be used as a screening test, (iii) expanding testing with more samples to derive statistically verified results, (iv) mixing two types of fibers to achieve joint stiffness and well as residual strength to mitigate joint faulting and fatigue cracking.

References

AASHTO (1993). *AASHTO Guide for Design of Pavement Structures*. Washington, DC: American Association of State Highway and Transportation Officials. https://trid.trb.org/view/375520.

Abbas, M., & Khan, M., (2016). *Fiber-Matrix Interfacial Behavior of Hooked-End Steel Fiber Reinforced Concrete*. Journal of Materials in Civil Engineering. American Society of Civil Engineers, 28(11), 04016115-1 - 04016115-10. https://doi.org/10.1061/(asce)mt.1943-5533.0001626.

Ahmed, I., Rahman, M. H., Seraj, S. M., & Hoque, A. M. (1998). *Performance of Plain Concrete Runway Pavement.* Journal of Performance of Constructed Facilities 12 (3): 145–52. https://doi.org/10.1061/(asce)0887-3828(1998)12:3(145).

Barborak, R. (2011). *Construction and Materials Tips*. Austin, TX: Texas Department of Transportation. https://www.txdot.gov/business/resources/highway/construction-materials-tips.html.

Barman, M. (2014). *Joint Performance Characterization of Bonded Whitetopping Overlays* (Doctoral dissertation), University of Pittsburgh, PA. Scholarship.pitt.edu. June 16, 2014. https://d-scholarship.pitt.edu/20454/.

Barman, M., & Hansen, B. (2018). *Comparison of Performances of Structural Fibers and Development of a Specification for Using Them in Thin Concrete Overlays*. St. Paul, MN: Minnesota Department of Transportation. https://rosap.ntl.bts.gov/view/dot/64621/dot_64621_DS1.pdf.

Barman, M., & Hansen, B. (2021). P*ost-Crack Flexural and Joint Performance Behaviors of Fiber Reinforced Concrete for Thin Pavement Overlays*. Transportation Research Record: Journal of the Transportation Research Board 2676 (2): 290–301. https://doi.org/10.1177/03611981211039839.

Barman, M., Roy, S, Tiwari, A., & Burnham, T. (2021). *Performance Benefits of Fiber-reinforced Thin Concrete Pavement and Overlays* (Final Report). St. Paul, MN: Minnesota Department of Transportation. https://rosap.ntl.bts.gov/view/dot/58442/dot_58442_DS1.pdf.

Barman, M., Vandenbossche, J. M., & Li, Z. (2015). *Characterization of Load Transfer Behavior for Bonded Concrete Overlays on Asphalt.* Transportation Research Record Journal of the Transportation Research Board, Vol. 2524 (December). https://doi.org/10.3141/252414.

Barman, M., Vandenbossche, J. M., & Li, Z. (2017). *Influence of Interface Bond on the Performance of Thin and Ultra-thin Concrete Overlays on Asphalt Pavement.* Journal of Journal of Transportation Engineering, Part B: Pavements 143 (January): 1–8. https://doi.org/10.1061/JPEODX.0000010..

Beckett, D. (1990). *Comparative Tests on Plain, Fabric Reinforced and Steel Fiber Reinforced Concrete Ground Slabs*. Concrete, 24(3), 43-45. https://api.semanticscholar.org/CorpusID:138813385

Beglarigale, A., & Yazici, H. (2015). *Pull Out Behavior of Steel Fiber Embedded in Flowable RPC and Ordinary Mortar*. Construction and Building Materials, 75, 255–265. https://doi.org/10.1016/j.conbuildmat.2014.11.037.

Bordelon, A. (2005). *Fracture Behavior of Concrete Materials for Rigid Pavement Systems* (Master's Thesis), University of Illinois at Urbana Champaign, IL. https://www.ideals.illinois.edu/items/13703

Brink, A. C., Horak, E., & Visser, A. (2005). *Improvement of aggregate interlock equation used in mechanistic design software*. Int. J. Concrete Pavements, 1(1), 1–22.

Burnham, T. R., Huerta, S. B., & Barman, M. (2016). *Characterizing the Movement of Thin Concrete Overlay Panels Subject to Truck Loads*. Paper presented at the 11th International Conference on Concrete Pavements, ISCP, August 28-31, San Antonio, TX.

Chanvillard, G., Aitcin, P. C., & Lupien, C. (1989). *Field Evaluation of Steel-Fiber Reinforced Concrete Overlay with Various Bonding Mechanisms*. *Transportation Research Record 1226,* 48-56. https://trid.trb.org/view/308741

Daniel, J. I., Tatnall, P. C., & Zollo, R. F. (2009). *Report on Fiber Reinforced Concrete (ACI 544.1R-96*). Farmington Hills, MI: American Concrete Institute.

Davenport, G.V. (2014). *A Concrete Legacy, The Past, Present, and Future of the American Concrete Pavement Association*. ACPA . https://www.acpa.org/wp-content/uploads/2019/02/ACPA-Concrete-Legacy-X2-LORES-1.pdf

Davids, W. G., Wang, Z., Turkiyyah, G., Mahoney, J. P., & Bush, D. (2003). *Three-dimensional finite-element analysis of jointed plain concrete pavement with EverFE2.2.* Transportation Research Record 1853 (January): 92–99. https://doi.org/10.3141/185311.

Dinh, H. (2009). *Shear Behavior of Steel Fiber Reinforced Concrete Beams Without Stirrup Reinforcement* (Ph.D Dissertation), University of Michigan, Ann Arbor, MI. https://deepblue.lib.umich.edu/handle/2027.42/64590.

Elbheiry, M. R., Kandil, K. A., & Kotb, A. S. (2011). *Investigation of Factors Affecting Pavement Roughness* (Doctoral dissertation), Arab Academy for Science and Technology and Maritime Transport, Cairo, Egypt

Falkner, H., Huang, Z., & Teutsch, M. (1995). *Comparative Study of Plain and Steel Fiber Reinforced Concrete Ground Slabs*. Concrete International, 17(1), 45-51.

Hansen, P. I., & Mohamed, A. R. (1998). *Three-Dimensional Finite Element Study on Effects of Nonlinear Temperature Gradients in Concrete Pavements.* Transportation Research Record, 1692, 58–66.

Harrington, D., Ayers, M., Cackler, T., Fick, G., Schwartz, D., Smith, K., & Dam, T. V. (2018). *Guide for Concrete Pavement Distress Assessments and Solutions: Identification, Causes, Prevention and Repair*. (Technical report). Ames, IA: National Concrete Pavement Technology Center, Iowa State University.

Huang, Y. (2004). *Pavement Analysis and Design*. Pearson.

Issa, M., A. (2017). *Effect of Early-Age Concrete Elastic Properties on Fatigue Damage in PCC Pavements Containing Fibers* (Publication FHWA-ICT-17-019). Chicago, IL.

Izevbekhai B. I., & Akkari A. (2011). *Pervious Concrete Cells on MnROAD Low-Volume Road* (Report MN/RC 2011-23). Saint Paul, MN: Minnesota Department of Transportation.

Jang, J. G., Kim, H. K., Kim, T.S., Min, B. J., Lee, and H. K. (2014*). Improved Flexural Fatigue Resistance of PVA Fiber-Reinforced Concrete Subjected to Freezing and Thawing Cycles*. Construction and Building Materials 59: 129–35. https://doi.org/10.1016/j.conbuildmat.2014.02.040.

Khazanovich L., Yu H. T., & Darter M. I. (2004). *Mechanistic–Empirical Model to Predict Transverse Joint Faulting*. Transportation Research Record, 1896, 34–45. https://doi.org/10.3141/1896-04

Ludirdja, D., & Young, J. (1992). *Synthetic Fiber Reinforcement for Concrete*. Champaign, IL: U.S. Army Construction Engineering Research Laboratories. https://fisher.bibliocommons.com/v2/record/S75C2870777.

Mack, J., Akbarian, M., Ulm, F.-J., Gregory, J., Kirchain, R. & Wildnauer, M. (2012). *Designing Sustainable Concrete Pavements Using the Mechanistic-Empirical Pavement Design Guide and Life Cycle Analysis.* Proceedings of the 2013 NRMCA International Concrete Sustainability Conference at San Francisco, CA.

Mahboub, K. C., Liu, Y., & Allen, D. L. (2004). *Evaluation of Temperature Reponses in Concrete Pavement.* Journal of Transportation Engineering 130 (3): 395–401.https://doi.org/10.1061/(asce)0733-947x(2004)130:3(395)

Maitra, S. R., Reddy, K. S., & Ramachandra, L. S. (2010). Load Transfer Characteristics of Aggregate Interlocking in Concrete Pavement. *Journal of Transportation Engineering, 136*, 190-195. https://doi.org/10.1061/(ASCE)TE.19435436.0000065

Maitra, S. R., Reddy, K. S., & Ramachandra, L. S. (2009). Load Transfer Characteristics of Dowel Bar System in Jointed Concrete Pavement. *Journal of Transportation Engineering, 135*(11), 813-821. https://doi.org/10.1061/(ASCE)TE.19435436.114

Masad, E., & Taha, R. (1996). *Finite-Element Analysis of Temperature Effects on Plain-Jointed Concrete Pavements.* Journal of Transportation Engineering 122 (5): 388–98. https://doi.org/10.1061/(asce)0733-947x(1996)122:5(388).

MnDOT. (2018). *MnDOT Pavement Design Manual*. St. Paul, MN: Minnesota Department of Transportation.

MnDOT. (2018). *Report on 2017 MnROAD Construction Activities* (MN/RC 2018-16). St. Paul, MN: Minnesota Department of Transportation.

MnDOT. (2019). *MnDOT Pavement Design Manual*. St. Paul, MN: Minnesota Department of Transportation.

Roesler, J., & Bordelon, A. (2008). *Design and Concrete Material Requirements for Ultra-Thin Whitetopping*. Urbana, IL: Illinois Center for Transportation.

Roesler, J. R., Lange, D., & Ulreich, G. (2003). *Fracture Behavior of Full-Scale, Fiber- 62 Reinforced Concrete Slabs* (Final Report). Urbana, IL: W.R. Grace, Inc., University of Illinois.

Sachs, S., Vandenbossche, J. M., Alland, K., DeSantis, J., & Khazanovich, L. (2016). *Effects of Interlayer Systems on Reflective Cracking in Unbonded Overlays of Existing Concrete Pavements*. Transportation Research Record: Journal of the Transportation Research Board 2591 (June). https://doi.org/10.3141/259106, 33-41.

Sadeghi, V., & Hesami, S. (2018). *Investigation of load transfer efficiency in jointed plain concrete pavements (JPCP) using FEM.* International Journal of Pavement Research and Technology 11 (3): 245–52. https://doi.org/10.1016/j.ijprt.2017.10.001

Singh, S., Shukla, A, & brown, R. (2004). Pullout Behavior of Polypropylene Fibers from Cementitious Matrix. *Cement and Concrete Research 34*(10), 1919-1925. https://doi.org/10.1016/j.cemconres.2004.02.014

Sobolev K., Tabatabai H. Moini M., & Titi H. (2017). *Class F Fly Ash Assessment for Use in Concrete Pavements*. Milwaukee, WI: University of Wisconsin. https://doi.org/10.13140/RG.2.2.31345.17769

Spyrakos, C. C. (1994). *Finite Element Modeling*. Morgantown. WV: West Virginia Univ. Press.

Tabatabaie, A. M., & Barenberg, E. J. (1978). Finite-Element Analysis of Jointed or Cracked Concrete Pavements. *Transportation Research Record, 671,* 11-19. https://onlinepubs.trb.org/Onlinepubs/trr/1978/671/671-003.pdf

Taylor, P. (2017). *Performance Engineered Mixtures Program*. Ames, IA: Iowa State University.

Taylor, P., Yurdakul, E., & Ceylan, H. (2014). *Performance Engineered Mixtures for Concrete Pavements in the US*. Ames, IA: National Concrete Paving Technology Center.

Uddin, W., Hachkett, R., & Joseph, A. (1995). Three-Dimensional Finite-Element Analysis of Jointed Concrete Pavement with Discontinuities. *Transportation Research Record, 1482,* 26-32. https://onlinepubs.trb.org/Onlinepubs/trr/1995/1482/1482-004.pdf

Vandenbossche, J. M. (2003). Performance Analysis of Ultrathin Whitetopping Intersections on US-169. *Transportation Research Record, 1823,* 18-27. https://doi.org/10.3141/182303

Vandenbossche, J., & Barman, M. (2010). Bonded Whitetopping Overlay Design Considerations for Prevention of Reflection Cracking, Joint Sealing, and the Use of Dowel Bars. *Transportation Research Record, 2155*, 3-11.

Van Deusen, D. A., Burnham, T. R., Dai, S., Geib, J., Hanson, C., Izevbekhai, B. I., & Worel, B., (2018). *Report on 2017 MnROAD Construction Activities* (No. MN/RC 2018-16). St. Paul, MN: Minnesota Department of Transportation.

Yoo, D., Park, J., & Kim, S. (2017). Fiber Pullout Behavior of HPFRCC: Effects of Matrix Strength and Fiber Type. *Composite Structures, 174,* 263-276. https://doi.org/10.1016/j.compstruct.2017.04.064.

Zollo, R. F. (1984). *Collated Fibrillated Polypropylene Fibers in FRC*. Farmington Hills, MI: American Concrete Institute.

Appendix A

Joint performance parameters for various structures at three different seasons

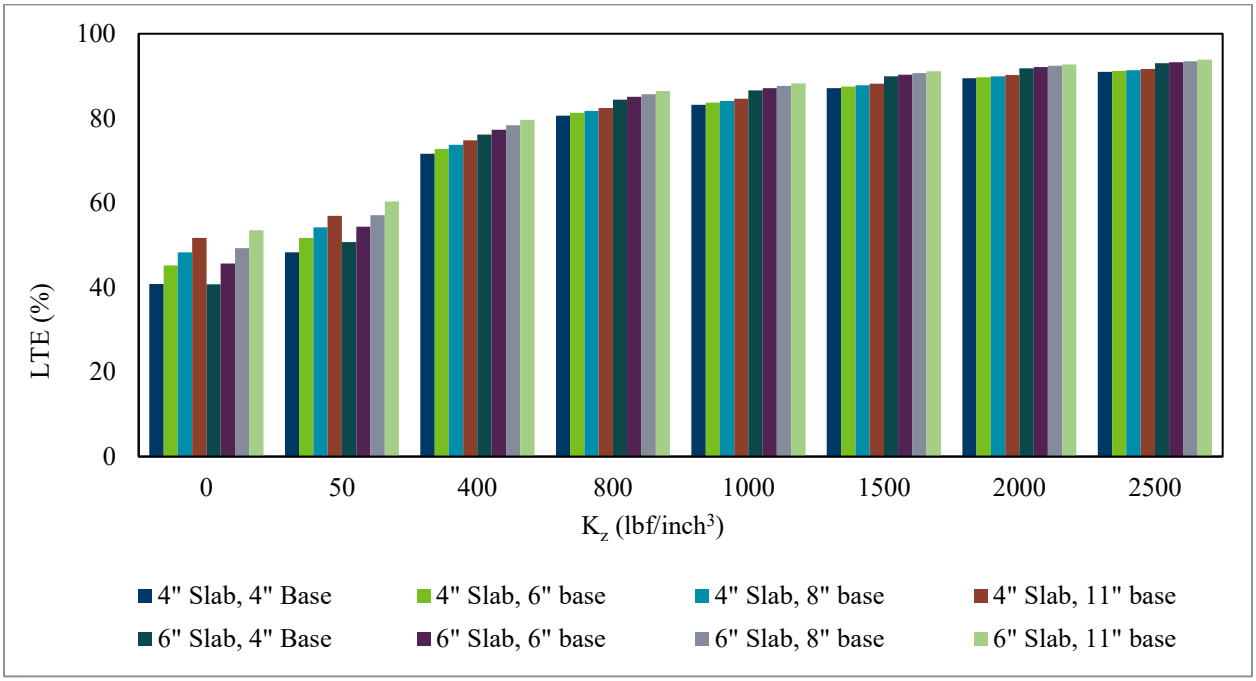

Figure A-1: LTE vs pavement structure over various values of K_z (early spring).

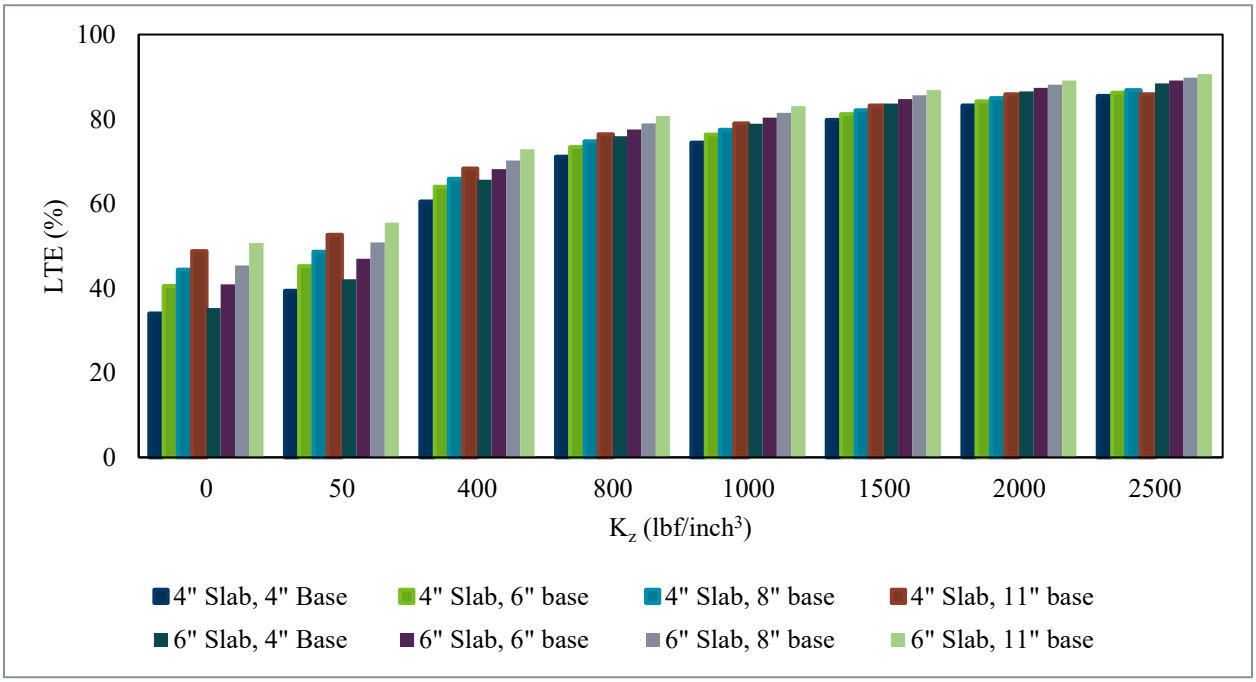

Figure A-2: LTE vs pavement structure over various values of K_z (summer).

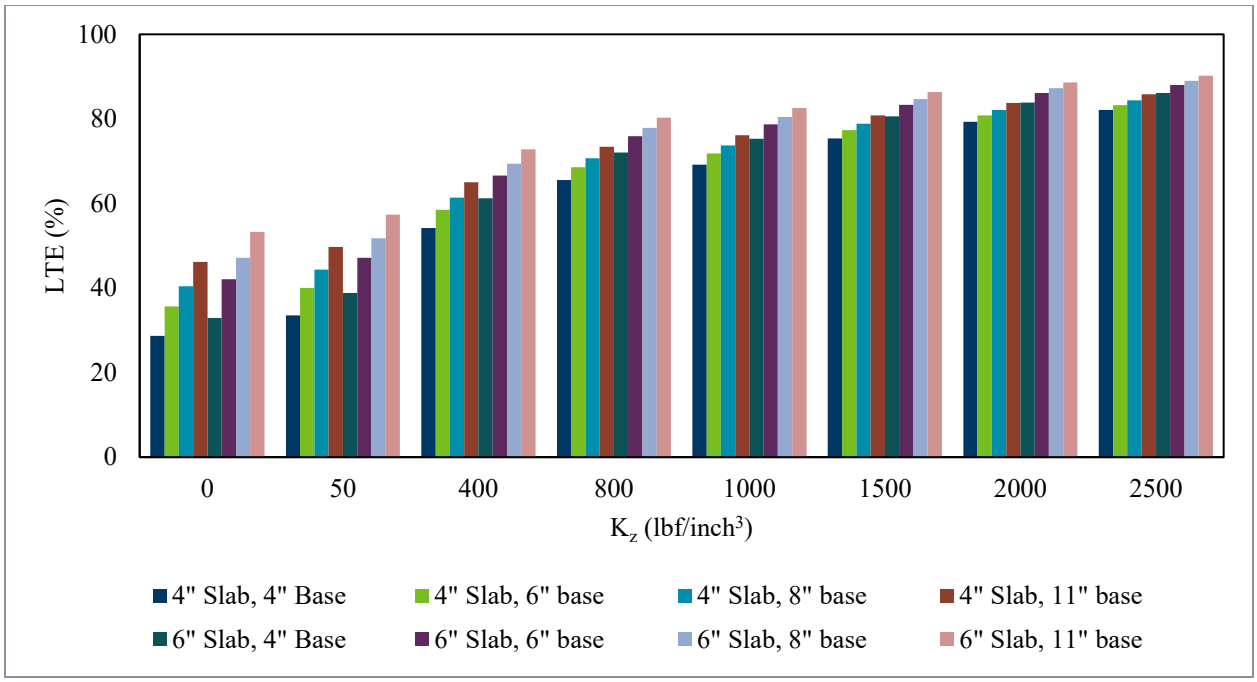

Figure A-3: LTE vs pavement structure over various values of K_z (winter).

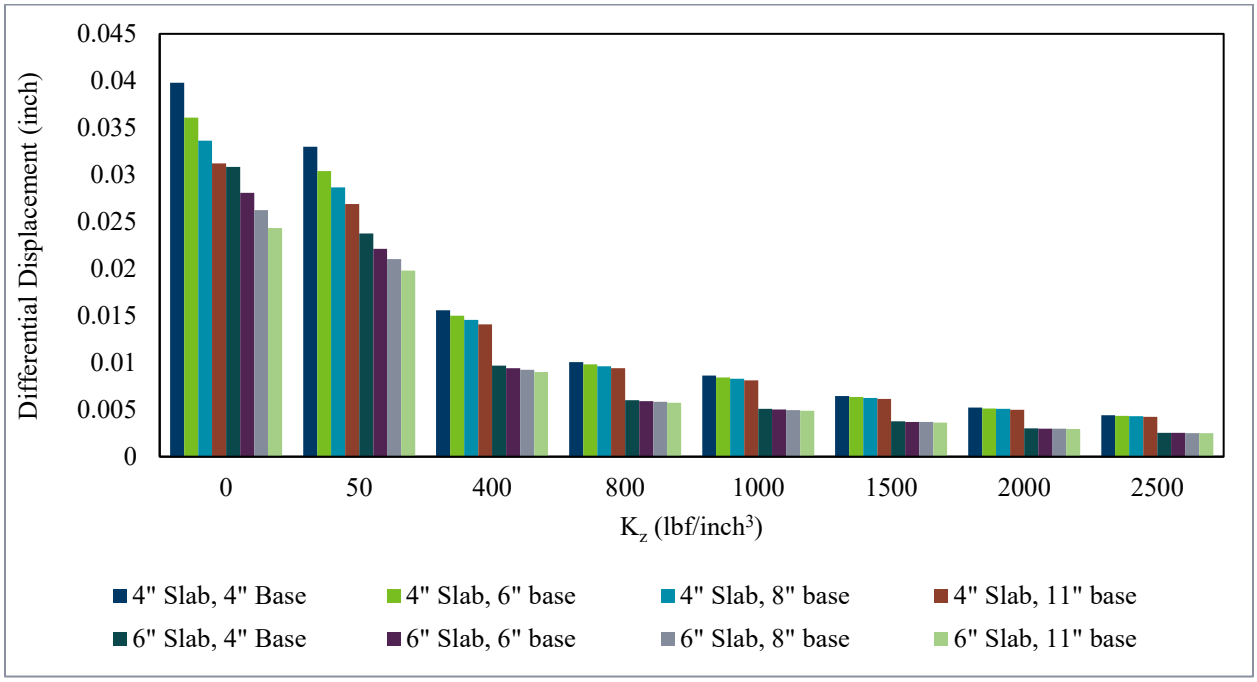

Figure A-4: Differential displacement vs pavement structure over various values of K_z (early spring).

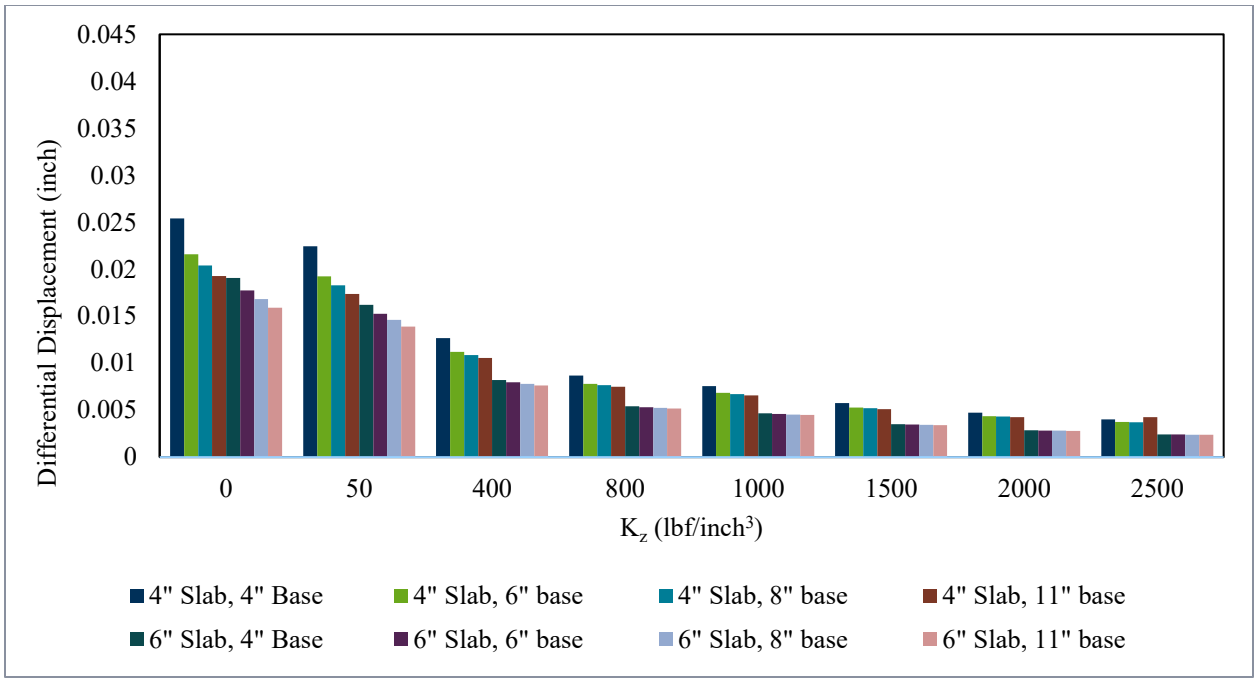

Figure A-5: Differential displacement vs pavement structure over various values of K_z (summer).

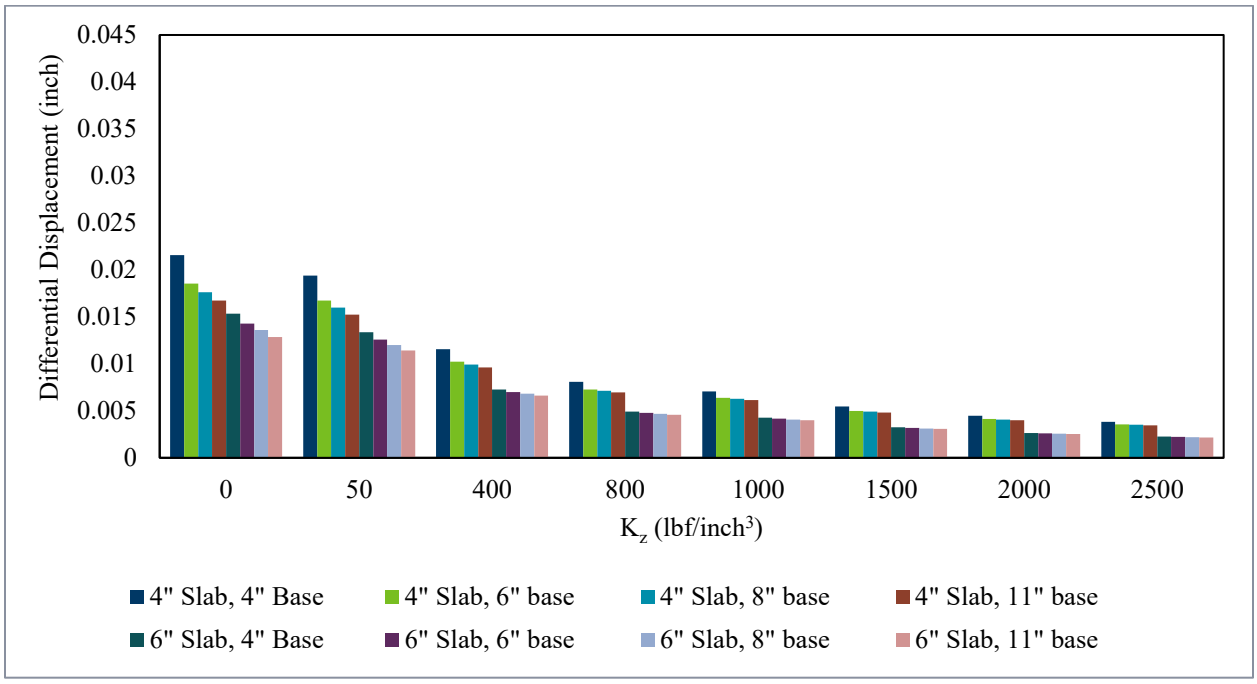

Figure A-6: Differential displacement vs pavement structure over various values of K_z (winter).

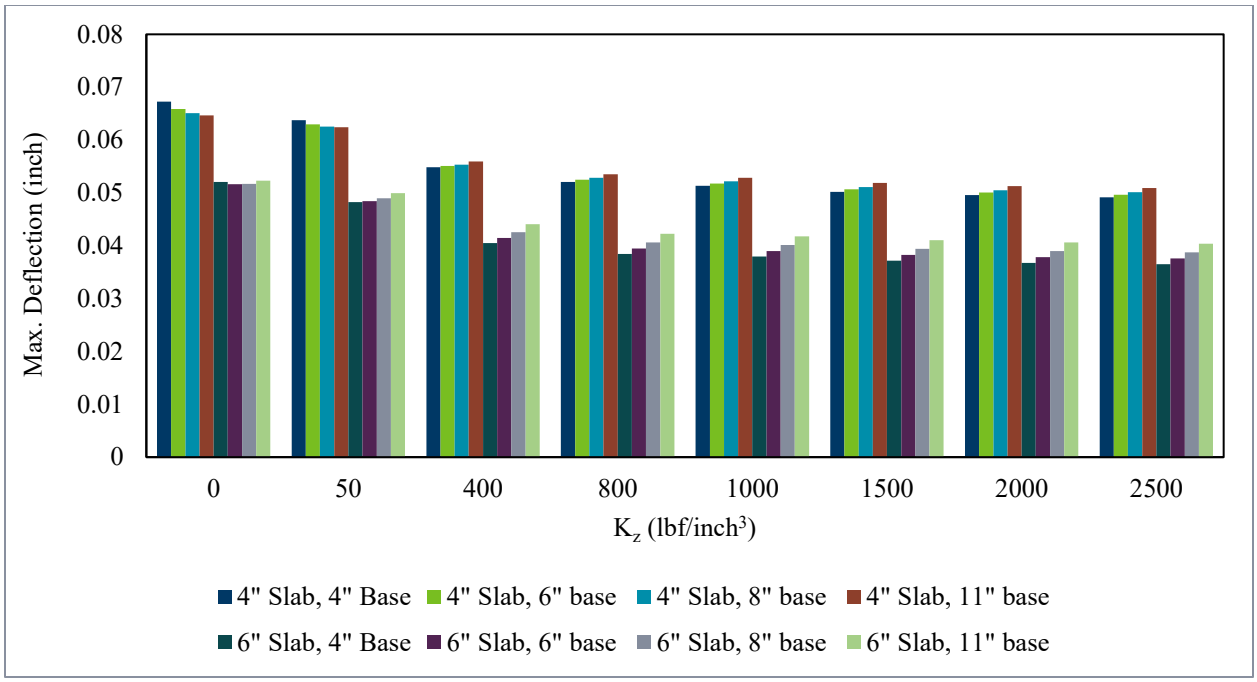

Figure A-7: Maximum displacement vs pavement structure over various values of Kz (early spring).

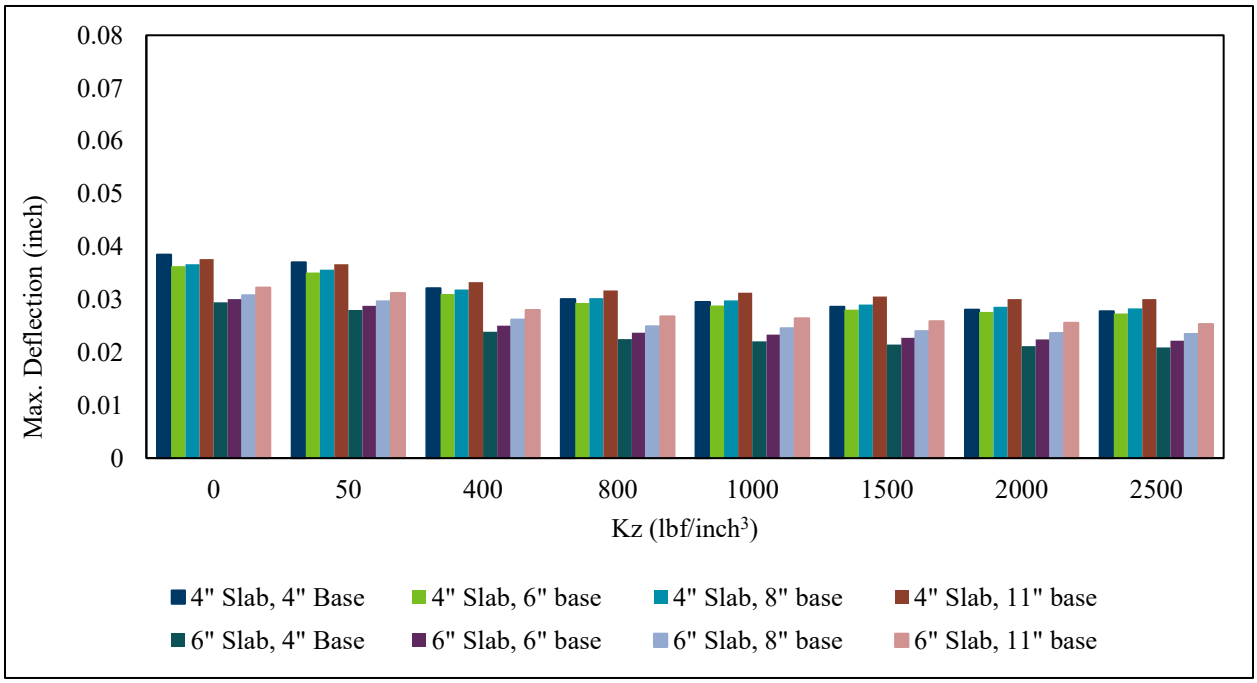

Figure A-8: Maximum displacement vs pavement structure over various values of K_z (summer).

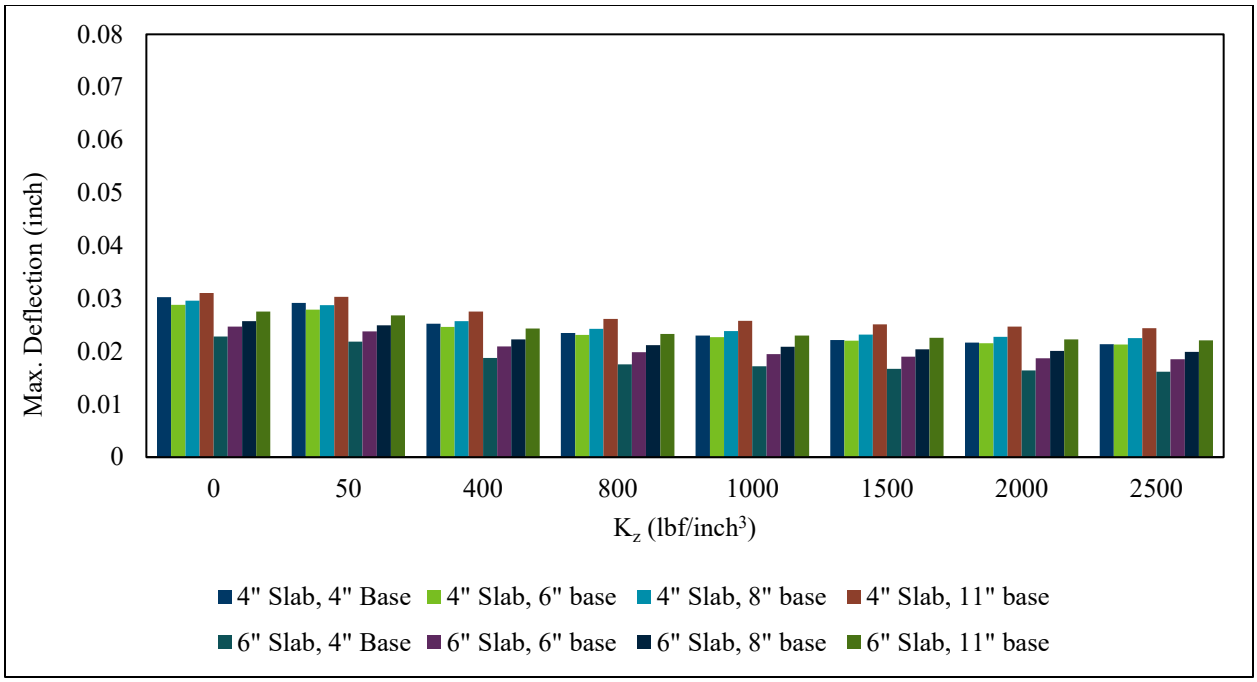

Figure A-9: Maximum displacement vs pavement structure over various values of K_z (winter).

Notes

- For early spring, the base layer elastic modulus = 9,000 psi, combined modulus of subgrade reaction = 138 pci, and temperature gradient = 5.35 ^{O}F/inch.
- For summer, the base layer elastic modulus = 30,000 psi, combined modulus of subgrade reaction = 461 pci, and temperature gradient = 4.71^{O}F/inch.
- For winter, the base layer elastic modulus = 50,000 psi, combined modulus of subgrade reaction = 786 pci, and temperature gradient = 4.48 ^{O}F/inch.

Materials used in fiber pullout testing

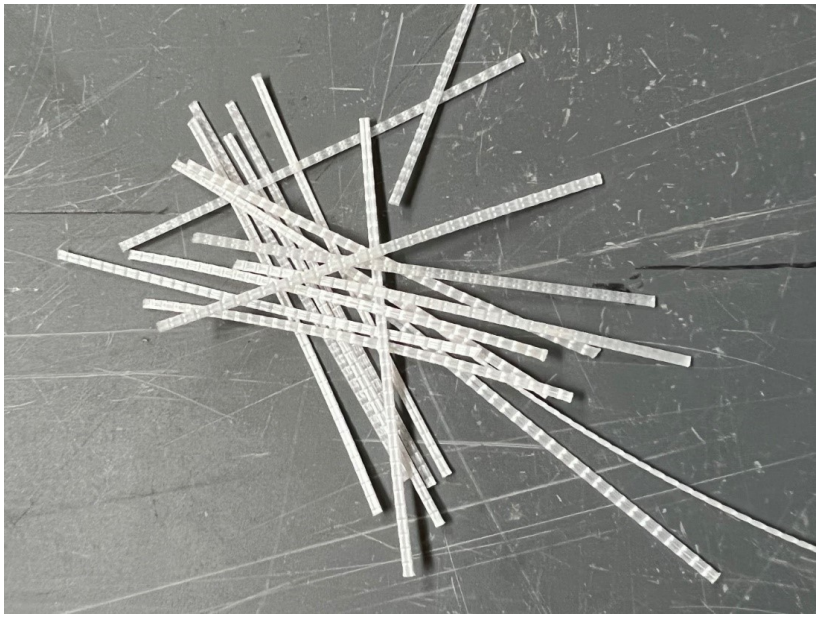

Figure A-10 Fiber 1

Figure A-11 Fiber 2

Figure A-12 Fiber 3

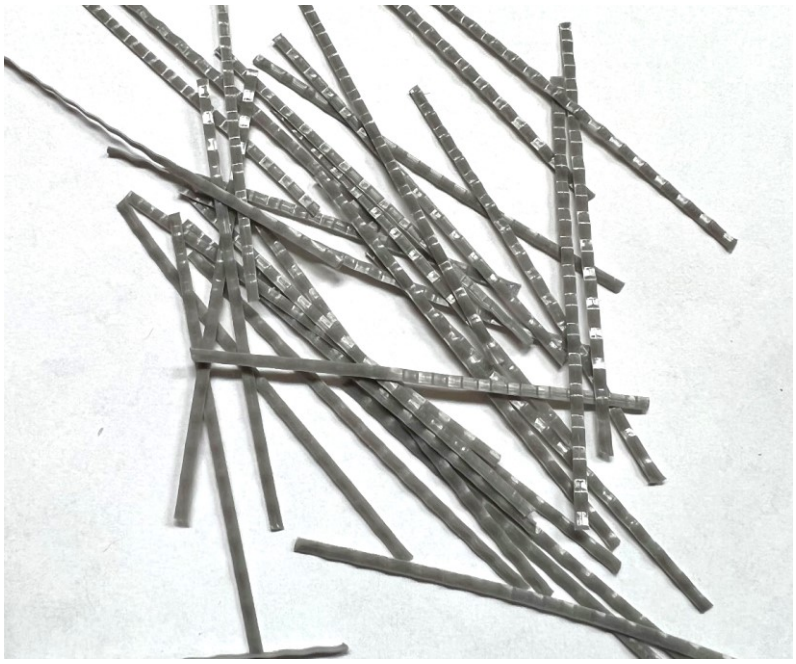

Figure A-13 Fiber 4

Table A-1 Fiber properties

Fiber Designation	Geometry	Length (inch)	Aspect Ratio*	Young's Modulus (ksi)	Tensile Strength (ksi)	Specific Gravity	Material
1	Embossed, Stiff	2.1	70	N/A	85	0.91	Polypropylene
2	Helical, Stiff, Brittle	1.7	57	6092	145	2	Alkali Resistant Glass
3	Straight, Smooth, Clear	1.89 - 2.28	52	1233	89	0.91	Polypropylene
4	Continuously Crimped, Stiff	2.4	74	N/A	N/A	N/A	Polypropylene

**Aspect ratio = length of the fiber/effective diameter of the fiber.*

Aggregates

Three different classes of coarse aggregates and one fine aggregate have been used for this study. The coarse aggregates are granite (Class A), limestone (Class B), and gravel (Class C) according to the MnDOT Standard Specifications for Construction (MnDOT, 2020). There were two different sizes of each aggregate type. Class A (Figure A-14) and Class B (Figure A-15) aggregates were mined and then crushed down to the desired sizes. They are rough-textured and have an angular shape. Class C aggregate (Figure A-16), gravel, was mined out of the ground as is. It is much rounder in shape. The fine aggregate is river sand (Figure A-17). Absorption and bulk specific gravity tests were carried out for all aggregates in accordance with the ASTM C127 and ASTM C128 procedures. The results are shown in Table A-2. Sieve analysis was also performed to determine the particle size distribution of each aggregate class. A blend was then created for each aggregate class so that the mix would achieve the required workability and strength requirements according to the PEM design method, which recommends the use of Tarantula Gradation. The sieve analysis results for different aggregate types and blends are shown in Figure A-18. Subsequently, Figure A-19 shows the Tarantula curve for each blend.

Table A-2 Bulk specific gravity and water absorption results of the coarse and fine aggregates

Coarse aggregate	Absorption	Bulk specific gravity
Granite 3/4" Class A	0.35%	2.70
Granite 1.5" Class A	0.25%	2.70
Limestone 3/4" Class B	0.83%	2.74
Limestone 1.5" Class B	1.08%	2.73
Gravel 3/4" Class C	1.47%	2.67
Gravel 1.5" Class C	1.34%	2.70
Fine Aggregate		
River Sand	1.70%	2.68

Figure A-14 Class A aggregate (3/4” on left, 1.5” on right)

Figure A-15 Class B aggregate (3/4” on left, 1.5” on right)

Figure A-16 Class C aggregate (3/4” on left, 1.5” on right)

Figure A-17 River sand (fine aggregate)

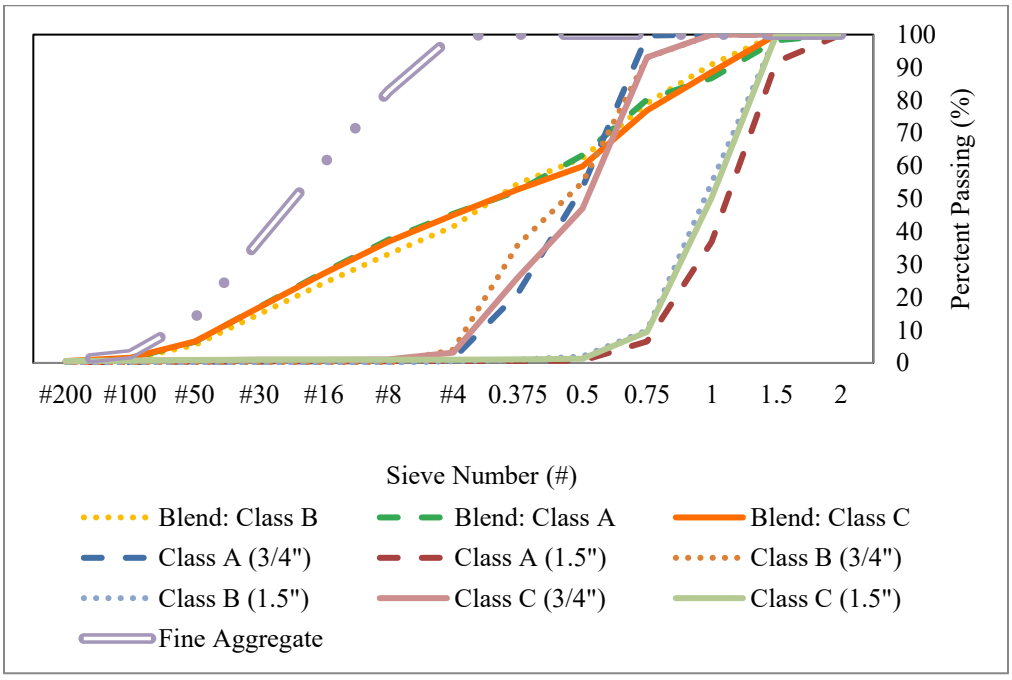

Figure A-18 Aggregate sieve analysis

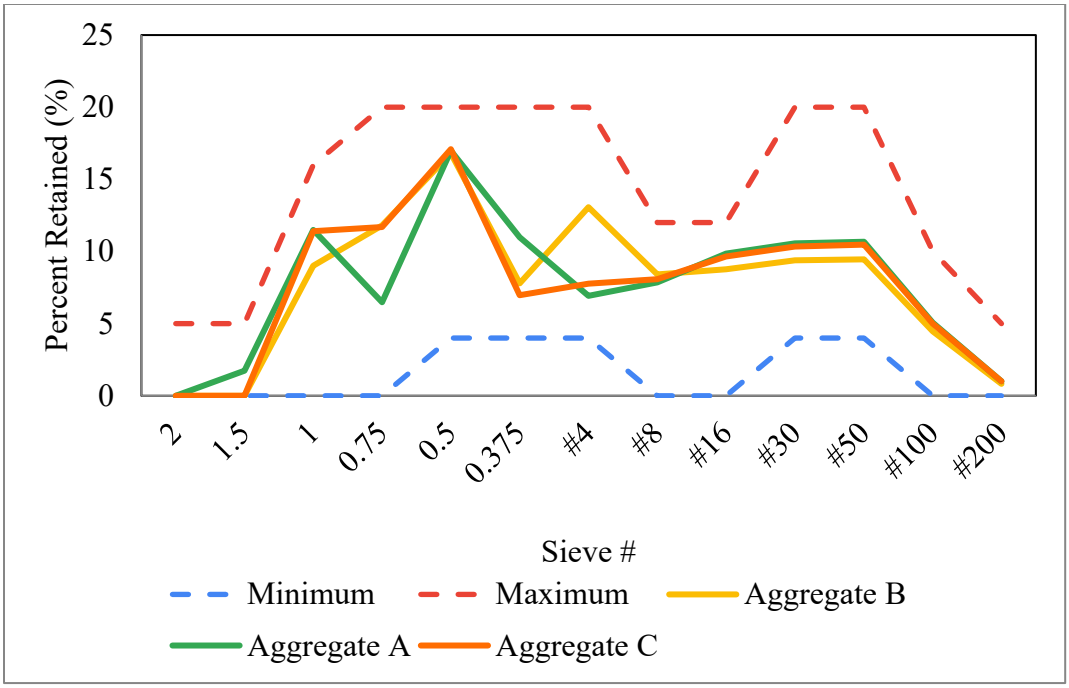

Figure A-19 Tarantula gradations of the three aggregate blends

Cementitious Materials

ASTM C150 Type-I cement was used for all concrete mixes for the fiber pullout tests. Fly ash is often used in cement as a partial cement replacement to mitigate the threat of ASR, improve workability, and increase concrete strength. The concrete mixes were designed in accordance with MnDOT mix design requirements (estimated concrete contract quantity >3500 cubic yards). ASTM C618 Class-F fly ash was used at a 20% replacement rate of cement for all mixes.

Mixture Design

Three different classes of aggregates were used as discussed above and the w/c was kept at 0.42. The design air void was 6% in every mix. The total cementitious material was varied between 480, 550, and 620 pcy. This correlates to paste contents of 27%, 30%, and 33%, respectively. The cementitious material was varied to check whether there was a correlation between paste content and fiber pullout toughness or peak load. Fibers will bind only to the paste and not the aggregates within the concrete.

Mid-range water reducer and air entrainer were added to make sure each mix met the requirements for slump and air content. A sample mix design for aggregate Class B, with 480 pcy of cementitious materials content is given below in Table A-3.

Table A-3 Mixture design for aggregate Class B (480 pcy)

Ingredients	Volume (%)	Mass (lb/yd^3)	Aggregates proportion by volume (%)
Cement (Type I)	7.24	384	-
Class B (¾")	29.20	1343	40%
Class B (1.5")	14.60	674	20%
Fine Aggregate	29.20	1318	40%
Potable Water	13.71	201.6	-
Fly Ash	1.81	96	-
BASF MasterAir 400 (fl. Oz)	-	1.20	-
MasterPolyheed 1020 (fl. Oz)	-	8.80	-
Air	6	-	-
Paste	27.01	681.6	-